DISSERTATION

Tuning of the PYTHIA 6.4 Multiple Parton Interaction model to Minimum Bias and Underlying Event data

by

Nameeqa Firdoua

A thesis submitted in partial fulfilment of
the requirements for the degree of

Doctor of Natural Sciences

supervised by

Univ.-Prof. Dr. Gerald Rudolph

Institute for Astro and Particle Physics,

University of Innsbruck, Austria
September 30, 2013

Declarations

I declare that this thesis is my own work and most of the material has been taken from my own published work. This work was done wholly or mainly while in candidature for a research degree at this university and has not been submitted in any form for another degree or diploma at any university or other institute of tertiary education. Information derived from the published and unpublished work of others has been acknowledged in the text, and a list of references is given.

Innsbruck, Austria
September 30, 2013, Nameeqa Firdous

Acknowledgements

First of all, I am thankful to Almighty Allah for His blessed knowledge and power which enabled me to achieve the milestone of my Doctoral Thesis.

Lastly, I want to thank and offer my regards to all of those who supported me in any respect during the completion of the thesis.

Innsbruck, Austria *Nameeqa Firdous*
September 30, 2013.

All that I am, or hope to be, I owe to my Mother

Abstract

QCD has been quite successful in describing hadronic interactions at large transfer momenta, also known as hard interactions. However high energy pp and $p\bar{p}$ collisions are dominated by soft partonic collisions. Different phenomenological models are implemented in several Monte Carlo (MC) event generators such as PYTHIA, PHOJET and HERWIG etc., which attempt to simulate these interactions. These MC event generators have free parameters which need to be tuned to improve the agreement with the data.

In this thesis the MC event generator PYTHIA6.424 is considered and the optimization of its model parameters have been presented. This work mainly focuses on tuning of multiple parton interaction parameters to Minimum Bias and Underlying event published data from ATLAS at 0.9 and 7TeV and from CDF II at 1.96 TeV. The method employed to tune the parameters is based on a linear and iterative approach and allows the simultaneous variation of many parameters. Six parameters are tuned, which are found to be very sensitive to the chosen data distributions using nine PDF sets of three different types: Leading order, MC adapted and Next-to-leading order. A significant connection is observed between the PDF being used and the parameter values obtained. The overall fit quality is reasonably good for all the PDF sets.

Contents

List of Figures

List of Tables

Chapter 1

Introduction

The Large Hadron Collider provides a valuable opportunity in testing of the Standard Model of particle physics. The principal physics goals are the search for the Higgs boson and for new physics beyond the Standard Model in a new energy regime, which is expected in rare high momentum transfer processes with small cross sections of typically 1 pb or less. There are four major experiments at the LHC: ALICE, ATLAS, CMS, and LHCb. The ATLAS and CMS are general purpose detectors, designed to investigate the largest range of physics possible. Having two independently designed detectors is vital for cross-confirmation of any new discoveries made. On the other hand ALICE and LHCb, have specialized detectors for analyzing the LHC collisions in relation to specific phenomena such that LHCb is a specialized b-physics experiment and ALICE is designed for heavy-ion collisions.

Most of the hadron hadron interactions at high energy are inelastic and predominantly soft ($p_t < 2GeV$) interactions, commonly called Minimum Bias (MB) processes or events, which however is an experimental definition depending on the trigger and the offline cuts to select events. Minimum Bias (MB) events have a large cross section of about 50 mb at 7TeV. The physics of the minimum bias events is not easy to understand, yet they are important for understanding of high energy reactions in contemporary collider experiments. For example at LHC, at each bunch crossing at nominal energy and luminosity about 20 minimum bias interactions are expected to take place [33, 2], which is already exceeded and varied between 20 and 30.

The understanding of softer physics is interesting not only in its own right, but is also important for precision measurements of hard interactions in which soft effects need to be accounted for. Current QCD models typically use perturbative QCD to explain parton interactions where it is applicable and an alternative phenomenological approach to describe low p_t or non perturbative QCD processes. These models have free parameters which needed to be tuned to describe the experimental data. The tool used to make predictions for collision experiments taking into account all aspects of QCD are Monte Carlo (MC) event generators. The most important feature of these generator is the ability to generate results at hadron level by the simulation of full events as they are observed by a detector in reality.

To describe hadron collisions, it is inevitable to select a set of parton density functions that describes the momentum distribution of the partons within a hadron. These parton density functions (PDFs) are usually derived from fits to various data collected in deep inelastic scattering experiments. Traditionally, LO PDFs are supposed to be the best choice for use with LO MEs as implemented in most Monte Carlo programs. However, another interesting view point has been put forward, which has been suggested that NLO PDFs may be more appropriate even for MEs at LO [31]. Recently another approach has been proposed which combines the advantages of both the LO and NLO PDFs. These are called MC-adapted PDFs (LO* and LO**) [62]. Here PYTHIA6 parameters optimization is presented with nine different PDF sets using three above mentioned approaches.

1.1 Motivation

The most general and obvious motivation behind tuning of Monte Carlo event generators can be described as the MC event generators use physics approximations so there are many free parameters which must be tuned to describe experimental data. Tuning of free parameters of these QCD models has started in the early 1980's at PETRA and PEP using e+e- annihilations into hadrons. A genuine multiparameter fitting method has been developed and applied within the TASSO experiment [17]. The ALEPH and DELPHI experiments at LEP [30, 23, 13] also developed similar methods for tuning during the 1990's. Since about 2002, a simple manual parameter adjustment has been done by R.Field [43] using underlying event data from ppbar interactions at the Tevatron. In 2008 pre LHC tunes [57] are developed using general purpose event generator PYTHIA6 [67]. Around this time, two program packages namely Rivet and Professor have been developed by people from MCnet in order to facilitate MC/data comparisons using Rivet and to perform multi-parameter optimizations using Professor [29]. The fitting method employs 2nd order polynomials to parametrize the MC, similar to [17]. This package is the main tuning tool used in the ATLAS experiment.

With the advent of LHC data at the highest energy, 7 TeV, the theoretical understanding of minimum bias events and the tuning procedure turned out to be more complicated than originally thought. A first PYTHIA6 tuning called AMBT1 [3] to preliminary ATLAS minimum bias and underlying event data collected at 0.9 and 7 TeV was unable to describe selected experimental data which led to two separate tunes for MB and UE data later on.

In this situation and in view of the size of the ATLAS collaboration, another and independent tuning activity is considered meaningful. We already started tuning PYTHIA6 with multi parameter fitting procedure [23] using linear approach which is iterative with the ability to vary many more parameters simultaneously than the Professor method.

The main objective of the current project is to investigate how the QCD Monte Carlo event generator PYTHIA6 predictions agree with data after optimization of its free parameters. Special emphasis is given to the Multiply Parton Interactions (MPI) parameters of the PYTHIA6. PYTHIA is highly successful and well established program. It has been developed over the past decades alongside experimental discoveries and most of the features visible in past and present experiments can be described by it. Variations on the main components of this model (e.g. MPI, parton shower, treatment of beam remnants and color reconnection) and their respective tuning to data have been developed and are available for different series of PYTHIA releases as can be seen in references [57, 71, 21, 36, 34]. There are, of course, other QCD MC generators like PHOJET, HERWIG, SHERPA and also PYTHIA 8 which is a C++ code. Considering these would go beyond the scope of the present thesis project. So we will restrict our description to PYTHIA6 only.

1.2 Structure of the Thesis

This thesis provides best fit results of PYTHIA6 to MB and UE data published by CDF II and ATLAS experiments at three center of mass energies, 1.96TeV, 0.9TeV and 7TeV respectively, using nine different Parton Density Functions (PDFs) from different groups. Other data from CMS and CDFI is also used for different studies. In particular, the MPI parameters of PYTHIA6 with early collision data from LHC is studied.

Chapter 2 provides brief introduction to the theoretical background relevant to the current study. The relevant aspects of QCD, Deep Inelastic scattering, Hard Interaction along with Parton Density Distributions (PDFs), are summarized in this chapter. Chapter 3 introduces main physics aspects of general purpose Monte Carlo (MC) event generators including Parton Showers, MPI, and Hadronization. Chapter 4 provides brief discussion about the selected detectors, ATLAS and CMS. Chapter 5 provides tuning method and tuning procedure. This chapter contains discussion about all the models/switches and parameters used in this tuning. Data sets used for current tunes are also discussed in this chapter. Chapter 6 gives a detailed parameters and model study. Chapter 7 gives final tuning results and comparison to different data sets. Chapter 8 provides separate tunes for MB and UE data. Chapter 9 concludes the current research work.

Chapter 2

Theoretical Background

In this chapter the theoretical background is summarized on which current study is based on, beginning with a brief introduction to the Standard Model (SM). Then some basic facts about Quantum Chromodynamics (QCD), which is part of the SM, and its application to lepton-hadron and hadron-hadron interactions are presented. More detailed description can be found in [26, 56, 48].

2.1 Standard Model of Particle Physics

Particle Physics attempts to describe the most elementary entities and deals with the science of the fundamental components of matter and the interactions between them. Nearly all known particle physics measurements are described by The Standard Model (SM) of particle physics quite successfully. The SM describes the fundamental constituents of matter as twelve different types of particles called fermions with spin 1/2. The interactions between the fermions are described by fundamental gauge interactions, mediated by gauge vector bosons, namely electromagnetic interactions, weak interactions and strong interactions. The fundamental forces and their charge carriers are shown in Table 2.1.

Fermions can be categorized further into quarks and leptons. The six fermions, which interact through strong interactions, are referred to as quarks. They form color neutral composite particles: mesons (bound state of quark and antiquark) and baryons (bound state of three quarks). Quarks also carry electric charge and weak isospin so they participate in the electromagnetic and weak interactions. The remaining fermions are referred to as leptons. Electrically charged leptons are: electron (e), muon (μ), and tau (τ). Each of

Interactions	strong	electroweak	gravity
Theory	QCD	GSW	general relativity
Symmetry Group	$SU(3)_C$	$SU(2)_L x U(1)_Y$	-
Gauge Bosons	g1...g8	$\gamma, W\pm, Z^0$	graviton
Charge	color	weak isospin , weak hypercharge	mass
Coupling	α_s	$\alpha, sin^2\theta_W$	G
Strength	0.2	0.03	10^{-40}

TABLE 2.1: The fundamental force carriers and properties

Fermions	*Generations* 1.	2.	3.	*QuantumNumbers* Q/e	I_3
Leptons	$\begin{pmatrix}\nu_e \\ e\end{pmatrix}$	$\begin{pmatrix}\nu_\mu \\ \mu\end{pmatrix}$	$\begin{pmatrix}\nu_\tau \\ \tau\end{pmatrix}$	0 -1	$+1/2$ $-1/2$
Quarks	$\begin{pmatrix}u \\ d\end{pmatrix}$	$\begin{pmatrix}c \\ s\end{pmatrix}$	$\begin{pmatrix}t \\ b\end{pmatrix}$	$+2/3$ $-1/3$	$+1/2$ $-1/2$

TABLE 2.2: The three generations of left handed fermions, divided into quarks and leptons with their corresponding Quantum numbers

them have an electrically neutral counterpart, called the neutrino. Neutrinos participate only in weak interactions. All the fermions are arranged into the three generations as it is shown in Table 2.2. Each generation consists of two quarks, one charged lepton, and one neutrino. The first generation is the set of lightest particles, all of which are also stable. The second generation is made of the heavier analogs of particles from the first generation. The muon neutrino ($\nu\mu$) is the only stable particle of the second generation. The same pattern repeats itself in the third generation, which consists of the heaviest unstable particles (except for the tau neutrino, which is stable).The Standard Model is formulated in terms of the gauge field Lagrangian being invariant under transformation of the $SU(3)_C \times SU(2)_L \times U(1)_Y$ symmetry group, where C indicates three color charges(r, g and b), L stands for left handed fermions and Y is a hyper charge defined through:

$$Q = I_3 + Y/2 \tag{2.1}$$

The Standard Model Lagrangian can be written as:

$$\mathcal{L} = \mathcal{L}_{strong} + \mathcal{L}_{electroweak} + \mathcal{L}_{higgs} \tag{2.2}$$

2.1.1 Higgs Mechanism

It is defined as a process which gives mass to elementary particles through spontaneous symmetry breaking, specifically it refers to the mass generation of W and Z gauge bosons through electroweak symmetry breaking in the Standard Model. This mechanism requires an elementary spin zero particle, known as Higgs[1] boson. According to this theory, the Higgs field pervades all space and when particles interact with this field they gain mass. Though the Standard Model of Particle Physics is proved to be a most accurate and a best understood model yet some deficiencies still exist. These deficiencies include the neutrino oscillations, matter antimatter asymmetry in the universe, and the nature of dark matter and dark energy.

2.2 Brief Overview of QCD

Quantum chromodynamics (QCD) is the theory of the strong interactions. It describes the interactions of the quarks and gluons, using the $SU(3)_C$ non-Abelian gauge theory of color charges, where C indicates the three color charges namely r, g, b. The Lagrangian of QCD is given by

$$\mathcal{L}_{QCD} = \sum_{f}^{N_F} \overline{q}_f (i\gamma^\mu D_\mu - m_f) q_f - \frac{1}{4} G_a^{\mu\nu} G_{\mu\nu}^a \tag{2.3}$$

where $D_\mu = \partial_\mu - i g_s T^a G_\mu(x)^a$, repeated indices are summed over and m_f is the mass of each quark and f denotes the six quark flavors. $G_a^{\mu\nu}$ is the field strength tensor for the strong field given by

$$G_a^{\mu\nu} = \partial^\mu G_a^\nu - \partial^\nu G_a^\mu + g_s f_{abc} G_b^\mu, G_c^\nu \tag{2.4}$$

[1]The Large Hadron Collider confirmed the existence of a Higgs boson on 14 March 2013.

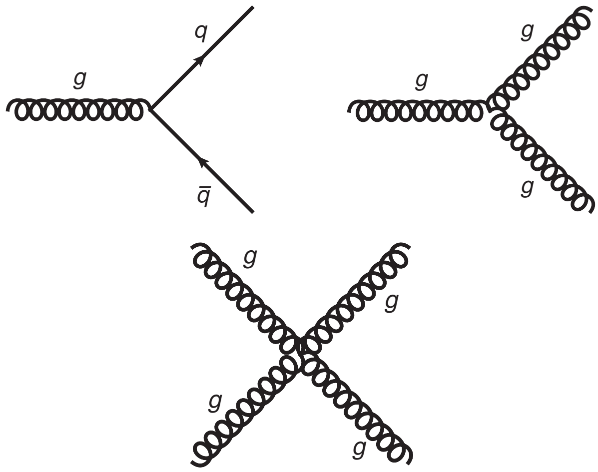

FIGURE 2.1: Interactions between strongly interacting particles including self interaction of gluon; quarks are denoted with q and gluons with g.

To leading order the strong coupling constant $\alpha_s = \frac{g_s^2}{4\pi}$ depends on the energy scale Q like

$$\alpha_s(Q^2) = \left(b_0 ln \frac{Q^2}{\Lambda^2}\right)^{-1} \tag{2.5}$$

The indices a, b and c run over the eight degrees of freedom of the gluon field. Unlike the photon in QED, the carrier of the color force is itself colored, so they can interact with each other by a three and four gluon vertex, as seen in Figure 2.1. This feature leads to two important physical consequences, Asymptotic freedom and Confinement. The first is asymptotic freedom, in which interactions become weak at large momenta or short distances. An important consequence of this fact is that it is possible to analyze QCD processes (e.g. scattering cross sections) by treating partons (i.e., quarks and gluons) as free particles independent from others in the event. The second is color confinement: quarks cannot exist singly, but must always be bound into color neutral hadrons, either as three quarks in a baryon, or one quark and one antiquark in a meson. Attempting to separate the quarks in a hadron will simply result in more quarks being created from the vacuum, resulting in the production of more hadrons.

In other words, QCD is an asymptotically free theory which is strongly coupling at low energy scales and weakly coupling at high energy scales, Figure 2.2. At high energies, perturbation theory in α_s can be used. But at low energies other methods such as lattice gauge theory are needed. The fact that the coupling constant of QCD diverges for small momentum transfers Q^2 leads to the non observability of free quarks; at low energies the

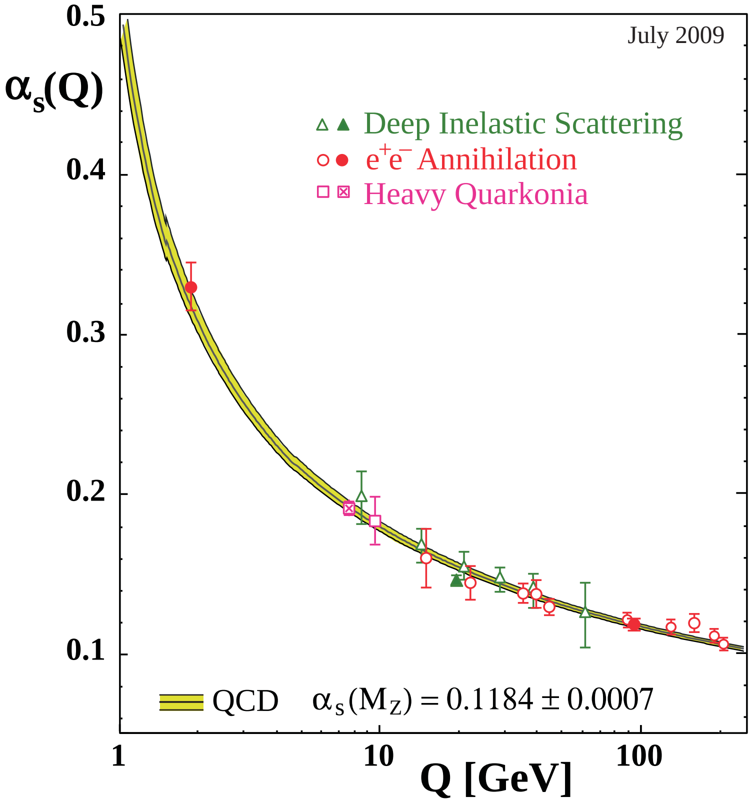

FIGURE 2.2: Summary of measurements of α_s as a function of the respective energy scale Q. The curves are QCD predictions for the combined world average value of $\alpha_s(M_Z)$ [25]

quarks and gluons are confined to SU(3) colour singlets called hadrons which are bound states of the quarks.

2.3 The Parton Model and Deep Inelastic Scattering

The deep inelastic scattering is defined as a collision process between a lepton from an ep collision and a quark from the proton, Figure 2.3. If the interacting quark carries a fraction, x of the protons 4-momentum, p, then the cross-section in the high energy limit for this process is given by

$$\frac{d^2\sigma}{dQ^2dx} = \frac{4\pi\alpha^2}{Q^4}\left[(1-y)\frac{F_2(x,Q^2)}{x} + y^2F_1(x,Q^2)\right] \tag{2.6}$$

Feynman and Bjorken introduced the parton model in the late 60s to describe the new data on deep inelastic scattering of electrons on nucleons. In this model the proton is a bound state of partons, called fermions (quarks or antiquarks) carrying electric charge. This model provides a very simple framework for calculating scattering cross sections as well as structure functions for the nucleons. The basic idea of the model is that every object with a finite size must have a form factor and therefore experience a dependence on the 4-momentum transfer (Q^2 dependence) from the scattered particle.

This prediction, that the structure functions, $F_1(x, Q^2)$ and $F_2(x, Q^2)$, should be approximately independent of Q^2, was experimentally verified and known as scale invariance or Bjorken scaling. The ep collider HERA provided a large amount of data on the inelastic scattering cross section at various x values shown in Figure 2.4. Bjorken scaling implies that the proton, when viewed at high Q^2 ($> 2GeV^2$), consists of quasi-free and point like partons. More detailed investigation showed that at low $x, F_2(x, Q^2)$ rises with increasing Q^2, while at high $x, F_2(x, Q^2)$ falls with increasing Q^2. It is nevertheless true that the structure functions depend more strongly on x, a dimensionless kinematic quantity, than on Q^2, related to the energy of the collision. In addition, it is observed that $F_1(x, Q^2)$ and $F_2(x, Q^2)$ are not independent, but satisfy the Callan-Gross relation:

$$F_2(x) = 2xF_1(x) \tag{2.7}$$

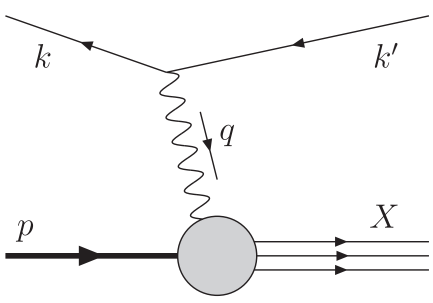

$$\begin{aligned} q^2 &= -Q^2 < 0 \\ s &= (p+k)^2 \\ W^2 &= (p+q)^2 \\ \nu &= p.q \\ x &= \frac{Q^2}{2\nu} \\ y &= \frac{p.q}{p.k} \end{aligned}$$

FIGURE 2.3: Deep Inelastic Scattering. An electron (or electroweak boson) with momentum k kicks a parton out of a proton with momentum p.

By analogy with $e^-\mu^- \to e^-\mu^-$ scattering, the differential cross section for elastic scattering between an electron and a quark with electric charge, $q_i = \pm 2/3, \pm 1/3$, and carrying a fraction, x, of the protons 4-momentum, can be expressed as

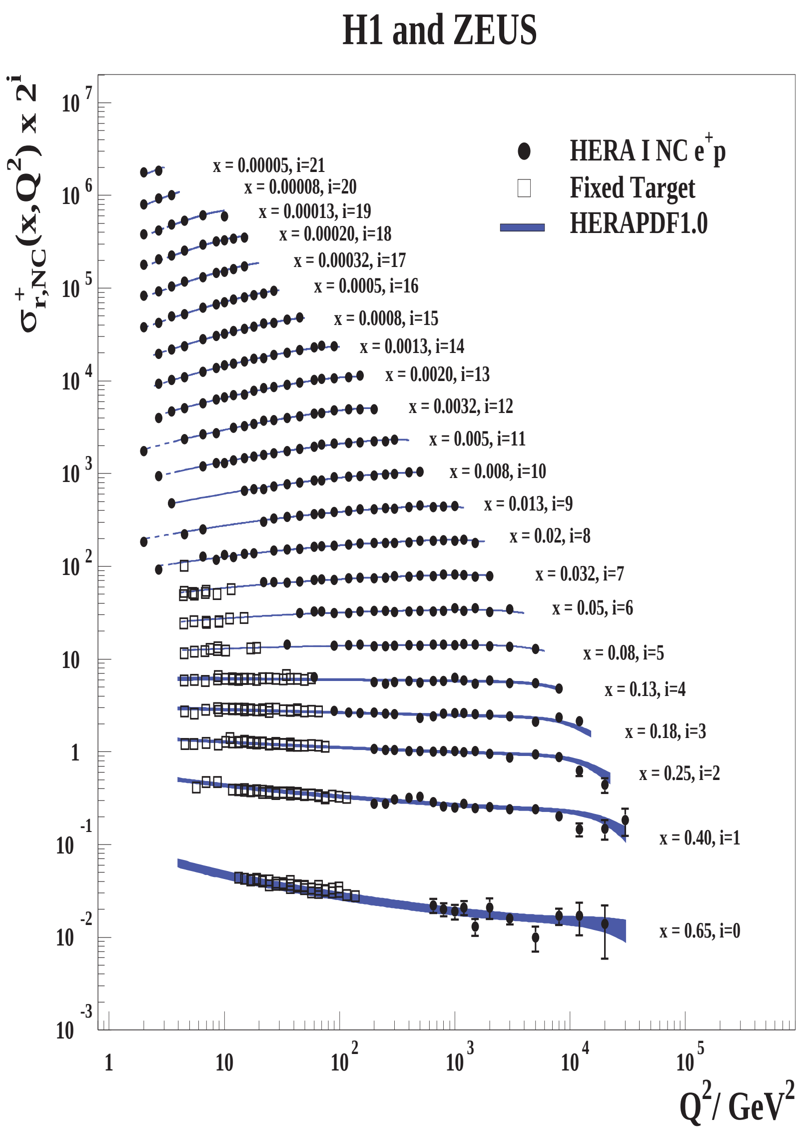

FIGURE 2.4: Combined data from H1 and ZEUS of structure function over a wide range of values of x as a function of Q^2 [10]

$$\frac{d\sigma}{dQ^2} = \frac{2\pi\alpha^2 q_i^2}{Q^4}\left[1+(1-y)^2\right] = \frac{4\pi^2\alpha^2 q_i^2}{Q^2}\left[(1-y)+\frac{y^2}{2}\right] \tag{2.8}$$

In the proton, the fraction of quarks having x in the range between x_0 and $x_0 + \delta x$ is $f_q(x_0, Q^2)\delta x$ where f_q is the parton distribution functions (PDF) for the quark concerned. Taking the distribution of quark momenta in this way, the cross-section for scattering from a particular quark type within the proton is

$$\frac{4\pi\alpha^2}{Q^4}\left[(1-y)+\frac{y^2}{2}\right] q_i^2 f_{q_i}(x, Q^2)\delta x \tag{2.9}$$

summing over all quarks and anti-quarks in the proton, since the gauge boson interacts equally with both, gives the expression

$$\frac{d^2\sigma}{dQ^2dx} = \frac{4\pi\alpha^2}{Q^4}\left[(1-y)+\frac{y^2}{2}\right]\sum_i q_i^2 f_{q_i}(x,Q^2) \tag{2.10}$$

Comparing Equation **2.6** and Equation **2.10** yields the parton model prediction for the proton structure functions:

$$F_2(x,Q^2) = 2xF_1(x,Q^2) = \sum_i \overbrace{xq_i^2 f_{qi}(x,Q^2)}^{quark} + \overbrace{xq_i^2\overline{f_{qi}}(x,Q^2)}^{anti-quark} \tag{2.11}$$

In the proton, quarks, anti-quarks and gluons each have non zero PDFs. At present the f_q cannot be analytically calculated within QCD. The perturbation theory predicts the scale dependence of $F(x,Q^2)$ through DGLAP evolution equations but does not accurately predict the x-dependence which has non perturbative origin. The x-dependence is parameterised at a fixed scale Q_0^2 then $F(x,Q^2)$ is evolved from Q_0^2 to any other Q^2 by numerically solving the DGLAP equations to various orders (LO,NLO, NNLO).

2.4 Hard Interactions of Quarks and Gluons

Quantum Chromodynamics (QCD) is the underlying theory of hard and soft high energy hadron collisions. In spite of the fact that perturbation theory predicts rates of hard processes and event properties to good precision, it fails to predict soft process rates and event properties. So phenomenological models with parameters adjusted to existing data are employed.

The perturbative framework for the calculation of hard scattering processes has been reviewed in [31] and is summarized here.

The QCD factorization theorem can be used to calculate a wide variety of hard scattering cross sections in hadron-hadron collisions. It rests on the concept that parton model ideas (originally developed in the context of deep inelastic scattering) could be extended to hadron hadron collisions. It was first pointed out by Drell and Yan [40] more than 30 years ago.The QCD factorization theorem states that the hadronic cross section $\sigma(AB \to \mu^+\mu^- + X)$ is a convolution of the partonic cross section $\hat{\sigma} for\ q\bar{q} \to \mu^+\mu^-$

with the parton distribution functions $f_{q/A}(x)$ extracted from deep inelastic scattering processes, corresponding to the structure depicted in Figure 2.5

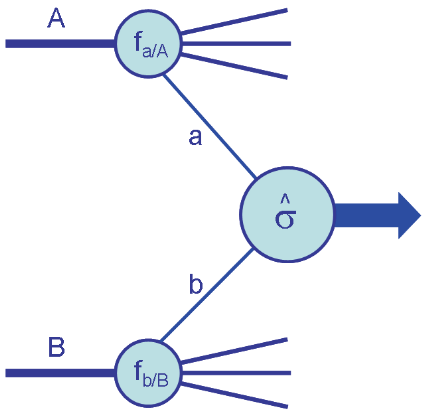

FIGURE 2.5: Diagrammatic structure of a generic hard scattering process [31]

$$\sigma_{AB} = \sum_{i,j} \int dx_a dx_b f_{a/A}(x_a, \mu_F^2) f_{b/B}(x_b, \mu_F^2) \hat{\sigma}_{i,j}(\mu_R^2, \mu_F^2) \tag{2.12}$$

Here μ_F is the factorization scale, which can be thought of as the scale that separates the long and short distance physics, and μ_R is the renormalization scale for the QCD running coupling. The scale dependence of all coefficients is compensated by the scale dependence of the parton distributions when calculating the cross section to all orders in perturbation theory. If higher order corrections have not been calculated, the cross section prediction depends on the specific choices of μ_F and μ_R . Typically, the scales are chosen at the order of magnitude of momentum scales of the hard process. Often, both scales are even assumed to be equal, e.g. the standard scale choice for the Drell-Yan process is $\mu_F = \mu_R = M$, the muon pair invariant mass . Similarly, appropriate scale choices to predict the production cross sections for Z-bosons, top quarks and large ET jets are the invariant masses of Z-boson and top quark or the jet transverse energy [31].

The parton distributions used in these hard-scattering calculations are solutions of the DGLAP equations

$$\frac{\partial q_i(x,\mu^2)}{\partial log\mu^2} = \frac{\alpha_S}{2\pi} \int_x^1 \frac{dz}{z} \left\{ P_{q_i q_j}(z,\alpha_S) q_j(\frac{x}{z},\mu^2) + P_{q_i g}(z,\alpha_S) g(\frac{x}{z},\mu^2) \right\} \tag{2.13}$$

$$\frac{\partial g(x,\mu^2)}{\partial log\mu^2} = \frac{\alpha_S}{2\pi} \int_x^1 \frac{dz}{z} \left\{ P_{g q_j}(z,\alpha_S) q_j(\frac{x}{z},\mu^2) + P_{gg}(z,\alpha_S) g(\frac{x}{z},\mu^2) \right\} \tag{2.14}$$

where the splitting functions have perturbative expansions:

$$P_{ab}(x, \alpha_S) = P_{ab}^{(0)}(x) + \frac{\alpha_S}{2\pi} P_{ab}^{(1)}(x) + \cdots \quad \textbf{(2.15)}$$

Figure 2.6 shows the predictions for some important Standard Model cross sections at pp and $p\bar{p}$ colliders, calculated using the above formalism (at next-to-leading order in perturbation theory).

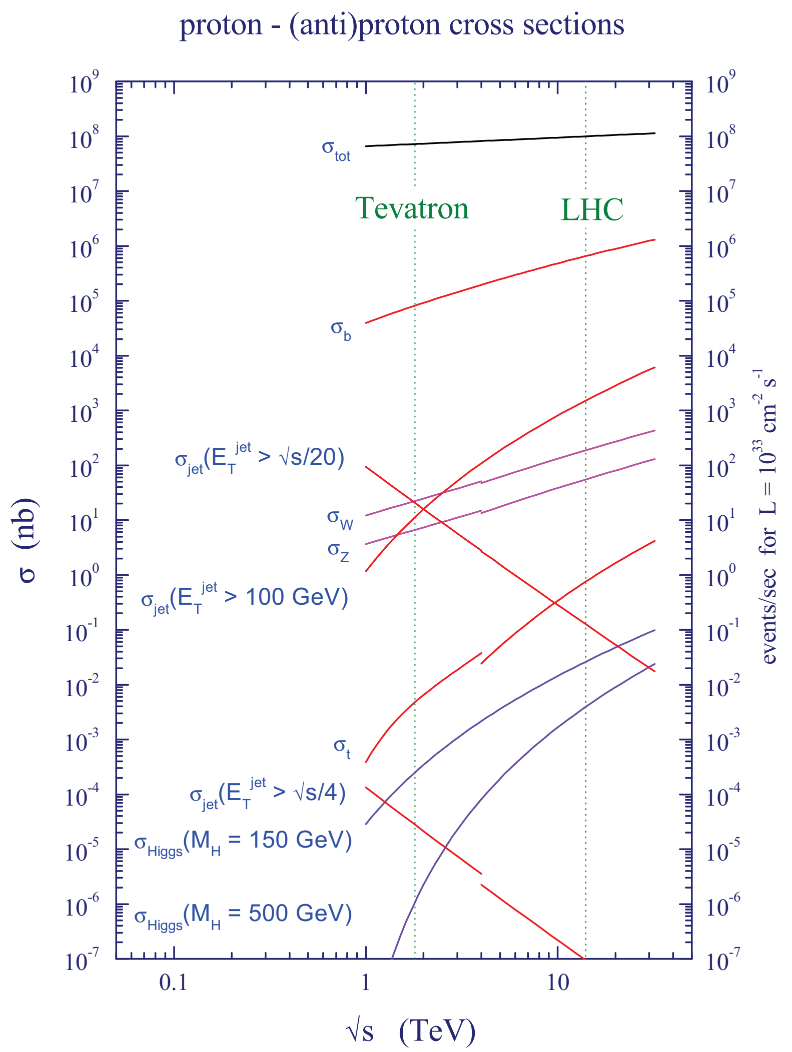

FIGURE 2.6: Standard Model cross sections at the Tevatron and LHC colliders [31]

2.5 Parton Distribution Functions (PDF)

Parton distribution functions (PDFs) are parameterizations of the partonic content of the proton. The calculation of the production cross sections at hadron colliders for both interesting physics processes and their backgrounds relies upon a knowledge of the distribution of the momentum fraction x of the partons (quarks and gluons) in a proton in the relevant kinematic range [31]. Parton distribution functions play a central role in event generators, for the simulation of hard processes, parton showers and multiple parton interactions. The choice of PDF set therefore influence both cross sections and event shapes [27]. To lowest order the function $f_i(x, Q^2)$ describes the probability to find a parton of species i with a momentum fraction x when a proton is probed at a scale Q^2 . This distribution cannot be predicted from first principles, since it depends on the non-perturbative physics of the proton wave function.

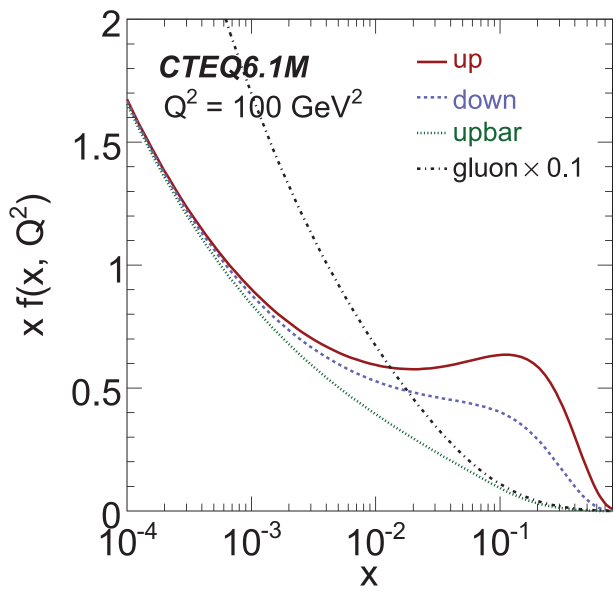

Figure 2.7: CTEQ6.1 Parton distribution functions parametrization at NLO at $Q^2 = 100GeV^2$ [31] The gluon distribution has been scaled down by a factor of 10.

With an ansatz for the initial distributions at some low scale Q_0, the evolution towards larger scales is predicted by the DGLAP equations [45],[39],[16]. Figure 2.7 shows at low x the gluons g/10 dominate, the distributions of the u and d quarks at high x are higher than the distributions of their corresponding antiparticles due to the valence quarks in the proton. Different tunes have been made, by comparing an evolved ansatz with relevant data, e.g. from Deeply Inelastic Scattering. Over the years global QCD analysis (or fits) of hard scattering data have been presented, with increasing accuracy as newer data have been added. Also the theoretical framework has seen some improvements. The CTEQ [54] and MRST/MSTW [55] collaborations have been especially diligent in regularly presenting updated tunes. These and others are available in the LHAPDF library [73].

2.5.1 MC-adapted PDFs

These PDFs [62, 61] are a relatively new concept which provide PDF's especially designed for LO generators. The idea is to obtain the behavior of an LO PDF, in particular the LO gluon distribution, in the phase space relevant for the soft QCD models, while at the same time modifying the high-x PDFs such that the predictions of the LO MC generator for hard processes closely resemble the full NLO predictions, i.e. using NLO PDFs in NLO ME calculations. ATLAS was the first experiment to use these mLO PDFs in MC production campaigns [34].

Chapter 3

Monte Carlo Event Generators

The Monte Carlo method refers to any procedure that makes use of random numbers and probabilistic statistics to solve problems. These methods are used extensively in numerical analysis and simulation of natural phenomena. In the context of particle physics, Monte Carlo generators are used to produce theoretical simulations of real events. They use both the perturbation theory of QCD to predict the behavior of the hard scattering interactions (characterized by large momentum transfer) and phenomenological models to describe the soft proton proton interactions. Different Monte Carlo generators often simulate different physics models, using matrix elements, PDFs, evolution equations, parton showers or hadronisation models. Because of this, comparing a variety of Monte Carlo models to data provides a test of the compatibility of different theories with experimental results. The number of event generators is increasing. The few major general purpose and specialized event generators used by current experiments are given below

- PYTHIA (General purpose)
- HERWIG(General purpose)
- SHERPA(General purpose)
- ISAJET(General purpose)
- ALPGEN(Specialized)
- MC@NLO (Next to Leading Order)
- CompHEP(Specialized)

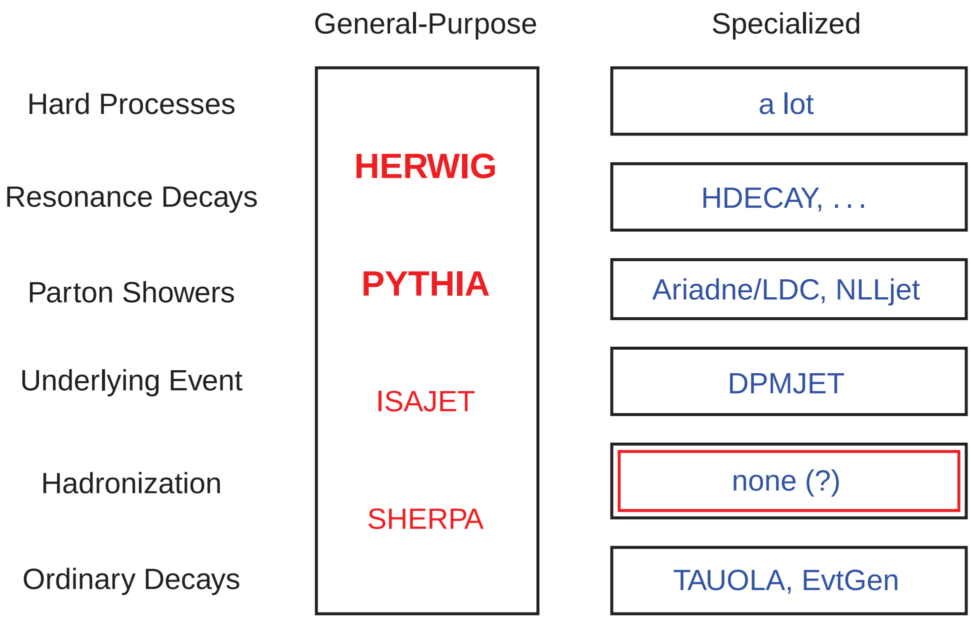

FIGURE 3.1: General landscape of different MC event generators showing general purpose and specialized MC event generators.Many of the specialized event generators include code only for the core calculations, and use general purpose event generators like PYTHIA and HERWIG as a user interface.

In the current study PYTHIA 6.4 has been used for tuning. A detailed description can be found in[67]. Event generators can be used in many different ways. The five main applications are probably that they provide

- a feeling for the kind of events one may expect/hope to find, and at what rates
- a help in the planning of a new detector, so that detector performance is optimized, within other constraints, for the study of interesting physics scenarios.
- a help for devising the analysis strategies that should be used with real data, to optimize signal-to-background conditions
- a method for estimating detector acceptance corrections that have to be applied to raw data
- a convenient framework within which to interpret the observed phenomena in terms of a more fundamental underlying theory

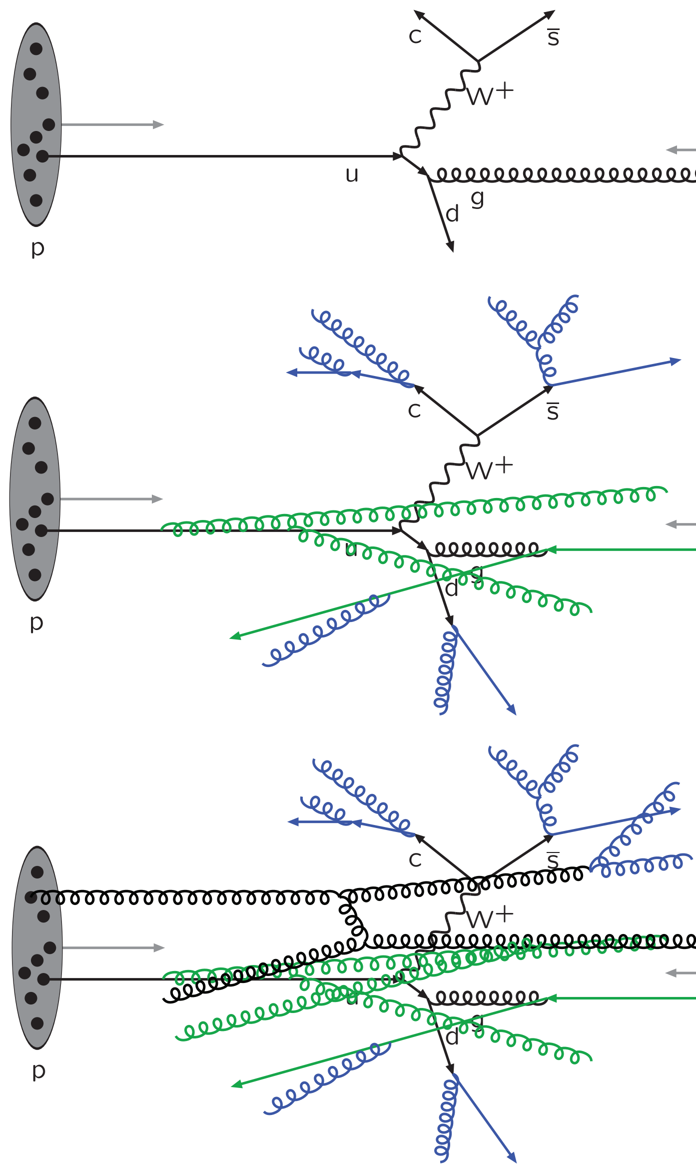

FIGURE 3.2: Sketch of a proton proton collision at high energies [66]

3.1 Main Physics aspects of MC Event Generator

In this section brief overview of the steps by which event generators build up the structure of a hadron-hadron collision involving a hard process is given. The processes involved in an event are complex, including many physical aspects which can be either strong interaction or electroweak. Therefore, a description of a typical high energy physics process should simulate several subprocesses. Figure 3.2 illustrates the complex variety of processes taking place in a single proton proton collision. The different stages that a full hadron level Monte Carlo event generator has to simulate consist of the following:

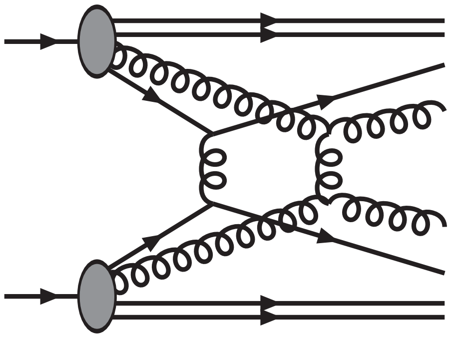

FIGURE 3.3: Schematic illustration of an event with two $2 \to 2$ perturbative interactions [68]

- **Hard Process**

  Hadrons are composite objects made up of partons(quarks and gluons).Initially one parton from each hadron undergo a hard collision. Short lived resonances such as the top, $W^{\pm}$, Z^0 are produced in the hard process which subsequently decay into their decays products [65]. The hard process is already described in Section 2.4 in detail.

- **Initial State Radiations (ISR)**

  A collision implies accelerated color (and often electromagnetic) charges, and thereby bremsstrahlung can occur. Emissions that are associated with the two incoming colliding partons are called Initial State Radiation (ISR). Such emissions can be modeled by so called space like parton showers. Section 3.2 contains more details.

- **Final State Radiations (FSR)**

  Detailed description is given in section 3.2. Emissions that can be associated with outgoing partons are instead called Final State Radiation (FSR), and can be approximated by time like parton showers. The distinction between a hard process and ISR and FSR is ambiguous.

- **Multiple Parton Interactions (MPI)**

  So far only one parton is extracted from each incoming hadron to undergo a hard collision. But the hadron is a composite object and has more than one parton. So, further parton pairs from each hadron may collide within one single hadron hadron collision, Figure 3.3. This is called multiple parton interactions (MPI). Detail can be found in section 3.3.

- **Beam Remnants (BR)**

  Part of the incoming beam which does not take active part in the initial-state radiation or hard-scattering process is called beam remnant, these remnants then colour connected to the rest of the event [65]. They carry much of the energy of incoming beam and only fraction of the energy is taken by the colliding partons. These remnants also carry colors that compensate the color taken away by the colliding partons.

- **Hadronisation**
  The confinement forces become significant as the partons created recede from each other. The structure and evolution of these force fields cannot currently be described from first principles, so models have to be introduced. At the end all the outgoing partons end up confined inside hadrons.This process is called hadronization [65]. The hadronization step is not shown in the Figure 3.2 but will be described in detail in section 3.4

3.2 Parton Shower (PS)

When a quark emits a gluon in hard collision processes, perturbation theory fails to describe the process in the collinear region or when the gluon energy vanishes, because higher order terms occur in processes where a soft gluon is emitted or when a gluon or light quark splits into two almost collinear partons. Parton branching is the common name for these soft and collinear configurations. In collision processes, parton branching typically happens for the ingoing and outgoing quarks and gluons of the hard interaction. The incoming quark carrying a fraction x of the hadron momentum initially has low virtual mass squared. It undergoes the hard scattering which happens at a scale Q after getting more virtual masses and lower momentum fractions by successive small angle emissions. After the collision, the outgoing parton of the hard scattering process has initially a large positive mass squared, which then gradually decreases by consecutive parton emissions.

Figure 3.4 shows schematically a hard hadron collision. Two hadrons (A and B) are coming in and one incoming parton in each hadron undergoes a hard scattering, resulting in outgoing partons. The hard scattering of the incoming partons at a scale Q, can be calculated using perturbative QCD. But all incoming and outgoing partons undergo branchings as well, giving rise to the parton showers (and to scale dependent PDFs). A lower order perturbative calculation fails to describe the shower behavior, where perturbative QCD calculations become too complicated at higher orders to be used. But

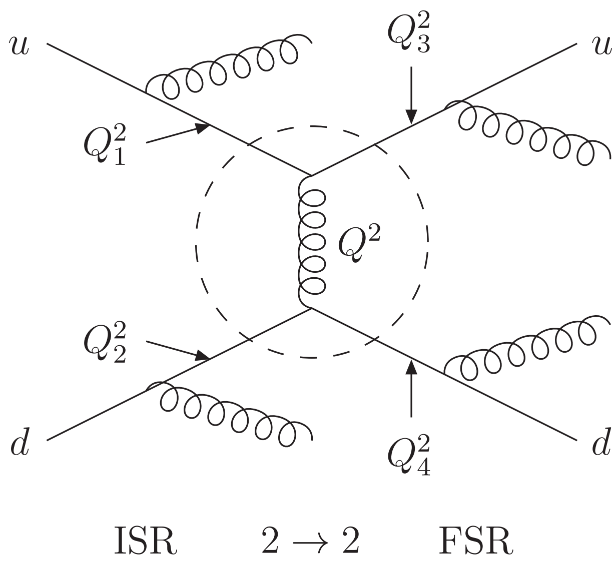

FIGURE 3.4: The factorization of a 2→n process

an approximate perturbative treatment of QCD to all orders is adequate at describing the branching physics.

An incoming parton has a negative (virtual) mass squared. Therefore its branching process is called spacelike, giving rise to initial state showers. The opposite is true for outgoing branching partons. These partons have a positive mass squared and their branching is called as timelike. They give rise to final state showers. A process $a \to bc$ can be understood as a branching, where a is called the mother and b and c are called daughters. Each daughter is free to branch as well, so that a shower like structure can evolve. For a timelike branching, it is assumed that the mass of the mother is much higher than the masses of the daughters. For a spacelike branching, the assumption is that daughter which takes part in the hard interaction has a much larger virtuality than the other partons. In PYTHIA6 p_t-ordered approach [69] is used where all emissions are ordered in a sequence $p_{\perp max} > p_{\perp 1} > p_{\perp 2} > ...... > p_{\perp min}$, which means that each initial parton is evolved from the $p_{\perp max}$ scale downwards. The one with the largest $p_\perp$ undergoes the first branching. Consequently, all partons now existing are evolved from $p_{\perp 1}$ downwards, and a $p_{\perp 2}$ is chosen, this continues until $p_{\perp min}$ is reached. The $p_\perp$ is defined as: $p^2_{\perp evol} = z(1-z)(M^2 - m_0^2)$ [64],

where $p_{\perp evol}$ is the evolution variable, z gives energy sharing in the branching, M is the off shell mass of the branching parton and m_0 is its on shell value. The evolution variable is approximately the $p_\perp^2$ of a branching, where $p_\perp$ is the transverse momentum for each of the two daughters with respect to the direction of the mother.

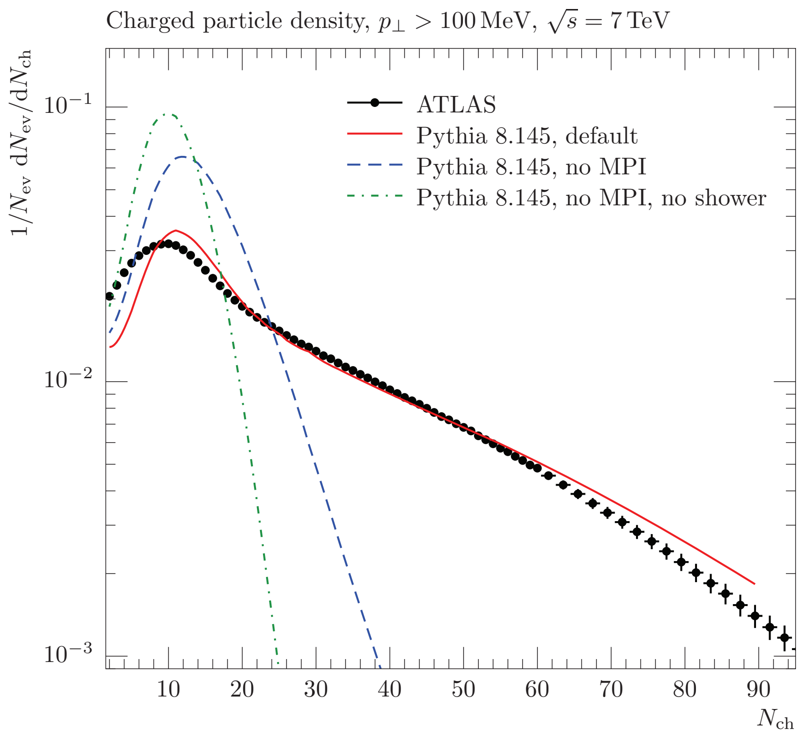

FIGURE 3.5: Description of the charged particle multiplicity measured by the ATLAS experiment with/without MPI and parton showers [3], for particles with p_t >100 MeV, $|\eta| < 2.5$. [22]

3.3 Multiple Parton Interactions (MPI)

As the hadron is a composite object, it is possible that more than one pair of partons may interact in a hadron hadron collision. This leads to the possibility of multiple interaction within a single hadron hadron collision.Figure 3.5 shows the comparison of the ATLAS minimum bias charged track multiplicity to a Monte Carlo model with and without MPI. It is clearly seen that the multiplicity distribution can not be predicted without MPI. This behavior is independent of whether parton showers are included or not. Description of multiplicity distribution is a strongest argument that MPI must be included in realistic models of soft physics. Many calculations of the total hadron hadron cross section [22] [44] also support the presence of MPI.

Sjostrand and van Zijl in [70] proposed first detailed Monte Carlo model for perturbative MPI , still a similar physical picture is used in most modern implementations. Useful additional references can be found in [24, 47, 68].

The basic concepts of this approach can be found [70]. The cross section for QCD hard 2→2 processes, as a function of the $p_\perp^2$ scale, is given by

$$\frac{d\sigma_{int}}{dp_t^2} = \sum_{i,j,k} \int dx_1 \int dx_2 \int d\hat{t} f_i(x_1, Q^2) f_j(x_2, Q^2) \frac{d\hat{\sigma}_{ij\to kl}}{d\hat{t}} \delta\left(p_t^2 - \frac{\hat{t}\hat{u}}{\hat{s}}\right) \quad \textbf{(3.1)}$$

Where x_1, x_2 are momentum fraction of partons and $f_i(x, Q^2)$ are the structure functions, defined as the probability of finding a parton i carrying a fraction x of the energy of the incoming hadron, when hadron is probed at a scale Q^2. It is assumed that the hardness of processes is given by the p_t scale of the interaction, i.e. $Q^2 = p_t^2$. $\hat{s}, \hat{u}, \hat{t}$ are Mandelstam variables such that

$$\hat{s} = (p_1 + p_2)^2 = (p_3 + p_4)^2 = x_1 x_2 s, \quad \textbf{(3.2)}$$

$$\hat{t} = (p_1 - p_3)^2 = (p_2 - p_4)^2, \quad \textbf{(3.3)}$$

$$\hat{u} = (p_1 - p_4)^2 = (p_2 - p_3)^2 \quad \textbf{(3.4)}$$

For massless partons, the three Mandelstam variables are related by

$$\hat{s} + \hat{u} + \hat{t} = 0, \quad \textbf{(3.5)}$$

The cross section for QCD $2 \to 2$ processes is dominated by t-channel gluon exchange contributions. In the $\hat{t} \ll \hat{s}$ limit, where $p_t^2 = \hat{t}\hat{u}/\hat{s} \approx \mid \hat{t} \mid$, quark and gluon interactions just differ by the color factors, so approximately

$$\frac{d\sigma_{int}}{dp_t^2} \approx \int\int \frac{\mathrm{dx}_1}{x_1}\frac{\mathrm{dx}_2}{x_2} F(x_1, P_t^2) F(x_2, P_t^2) \frac{d\hat{\sigma}}{dp_t^2}, \quad \textbf{(3.6)}$$

where

$$\frac{d\hat{\sigma}}{dp_t^2} = \frac{8\pi\alpha_s^2\,(p_t^2)}{9p_t^4} \quad \textbf{(3.7)}$$

It is derived from leading order pQCD matrix element, and

$$F(x, Q^2) = \sum_q (xq(x, Q^2) + x\overline{q}(x, Q^2)) + \frac{9}{4} xg(x, Q^2) \quad \textbf{(3.8)}$$

For constant α_s and neglecting the x integrals,

$$\sigma_{int}(p_{tmin}) = \int_{p_{tmin}}^{\sqrt{s}/2} \frac{d\sigma}{dp_t} dp_t \alpha \frac{1}{p_{tmin}^2} \tag{3.9}$$

In the limit $p_{tmin} \to 0$, the integrated cross section above a minimal p_t diverges and exceeds the total proton proton cross section illustrated in Figure 3.6.

This phenomenon,$\sigma_{int} > \sigma_{tot}$, can be explained in two ways: Firstly the interaction cross section σ_{int} counts interactions, but total cross section σ_{tot} counts events.An event containing two interactions counts twice in the interaction cross section but only once in the total cross section. Hence, the ratio between interaction cross section and total cross section is a measure of the average number of interactions per event which is perfectly allowed to be larger than unity. The actual number is assumed to be Poisson-distributed.

Secondly, the suppression of number of interaction at low $p_\perp$ is because of color screening/saturation effect. A first estimate of an effective lower cutoff due to color screening would be the proton size [27].

$$p_{tmin} \simeq \frac{h}{r_p} \approx \frac{0.2GeV \cdot fm}{0.7fm} \approx 0.3GeV \simeq \Lambda_{QCD}, \tag{3.10}$$

but this appears to be too low. Alternatively, it should be noted that the 2x2 cross section is divergent like $\frac{\alpha_s^2(p_t^2)}{p_t^4}$ therefore it is replaced by $\frac{\alpha_s^2(p_t^2+p_{t0}^2)}{(p_t^2+p_{t0}^2)^2}$, which regularizes the divergences smoothly, where p_{t0}^2 is a free parameter to be tuned to data. It is convenient to order all interactions occurring in same event in p_t, as discussed in previous Section 3.2. More realistically, varying impact parameter approach should be used so that each collision could be characterized by a varying impact parameter b. Within the classical framework used here, b is a distance of closest approach. A small b value corresponds to a large overlap between the two colliding hadrons, increasing the probability for multiple interactions. On the other hand, a large b,corresponds to a grazing collision, with less probability for multiple interactions or with a large probability that no parton parton interactions take place [69].

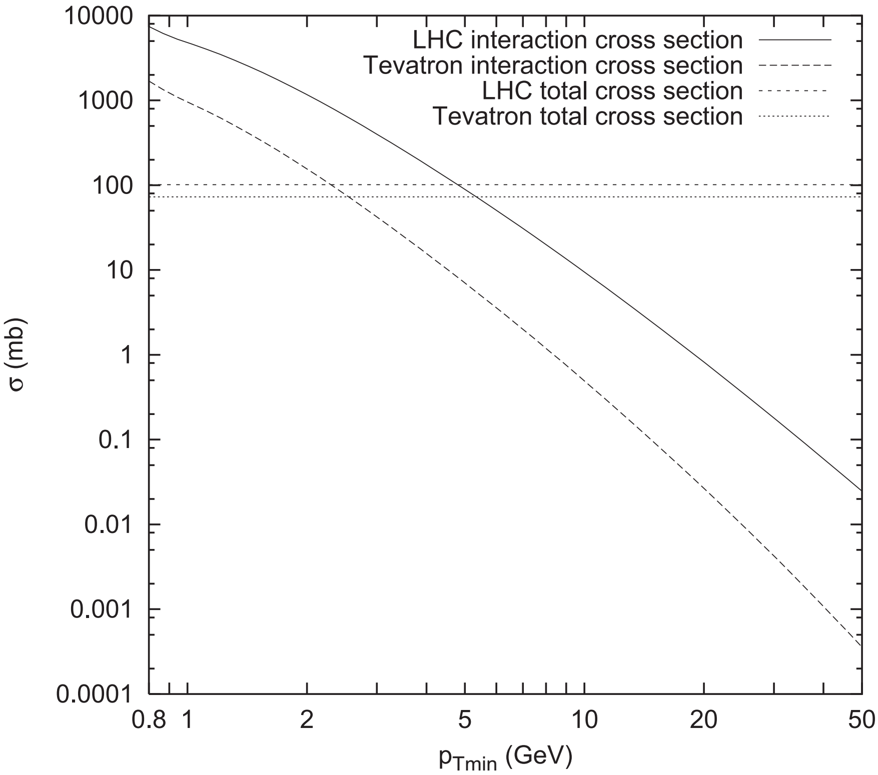

FIGURE 3.6: The integrated interaction cross section σ_{int} above $p_{t\,\mathrm{min}}$ for the Tevatron, with 1.8 TeV pp collisions, and the LHC, with 14 TeV pp ones,the respective total cross section is represented by the flat lines[68]

3.4 Hadronisation

PYTHIA uses the Lund model [19] to describe the hadronization process. The Lund model calculates the transition from a multi-parton system to final state hadrons with a string fragmentation model. Details can be found in [27, 65, 59], brief overview is given below.

A starting point for the string model is an expected linear confinement at large distances in QCD. It can be easily illustrated for the production of a back to back $q\overline{q}$ pair, e.g. in e^+e^- annihilation events. As the partons move apart, the color flux tube being stretched between q and $\overline{q}$ shown in Figure 3.7, with a rising potential $V(r) = \kappa$r. κ is a string constant $\sim 1GeV/fm \sim 0.2GeV^2$.

The string between a $q\overline{q}$ pair gains potential energy by the movement of the quarks. This potential energy increases as quark antiquark pair move apart, and at some point string breaks by the production of new quark antiquark pair. In other words, Inside the string field quark antiquark fluctuations absorb energy from the string to become real particles.In the Lund model, the string breaks proceed with the outermost hadrons, containing the

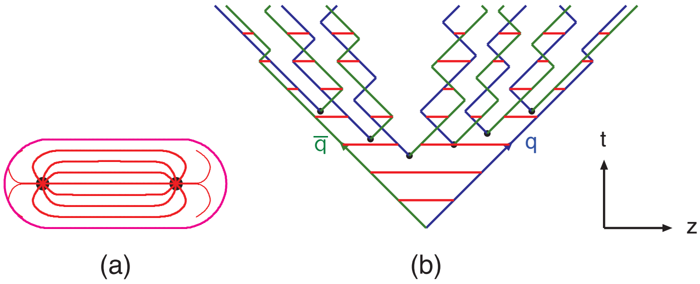

FIGURE 3.7: (a) A flux tube spanned between a quark and an antiquark. (b) The motion and breakup of a string system [27]

endpoint quarks, towards the center of the string. This process proceeds until only on mass shell hadrons remain, each hadron corresponding to a small piece of string.

In order to provide details of the individual string breaks, the Lund model invokes the idea of quantum mechanical tunneling. This leads to a flavor- independent Gaussian spectrum for the transverse momentum of produced quark antiquark pairs and a suppression of heavy quark production($u : d : s : c \approx 1 : 1 : 0.3 : 10^{-11}$):

$$Prob(m_q^2, p_\perp^2) \propto exp(\frac{-\pi m_q^2}{\kappa})exp(\frac{-\pi p_{\perp q}^2}{\kappa}) \quad \textbf{(3.11)}$$

where m_q is the mass and $p_\perp$ is the transverse momentum of the quark produced in the breakup process.

Baryon production is still poorly understood but can be described by diquark-antidiquark creation.

The fragmenting parton may combine with the other parton from a newly created break-up to form either a vector or a pseudoscalar meson. In case of baryons, to form either a spin 1/2 or a spin 3/2 baryon. Hadronisation proceeds through a iterative process where the longitudinal momentum fraction, z, of each hadron is generated via the Lund symmetric fragmentation function, having parameters a and b, see Figure 3.8. The Lund string model has many free parameters which have to be determined from data. Finally, unstable particles and resonances are decayed using known decay tables.

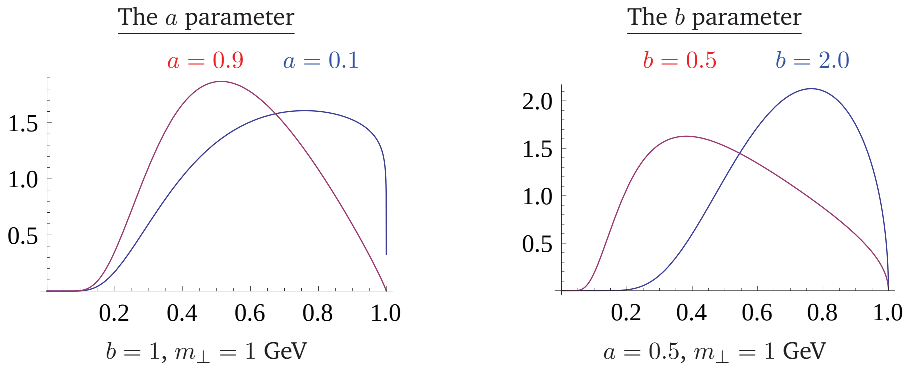

FIGURE 3.8: Parameters a and b of the Lund symmetric fragmentation function. Variation of the a parameter is made with fixed b=1 GeV^{-2} while variation of the b parameter is made with fixed a=0.5 [59]

3.5 Diffraction

The total proton proton cross section is the sum of the elastic and inelastic cross sections. In elastic scattering both protons emerge intact and no other particles are produced as shown in Figure 3.9 . The LHC cross section (at 14TeV) for elastic scattering is $\sim$ 30mb [72, 58]. In elastic scattering, the final state and initial state particles are identical. Inelastic events can be diffractive or non diffractive (ND). A diffractive reaction is one in which no internal quantum numbers are exchanged between the colliding particles. Diffraction occurs when the exchanged Pomeron interacts with the proton to produce a system of particles called as the diffractive system. In diffractive scattering, the energy transfer between the two interacting protons remains small, but one or both protons break into multi particle final states with the same internal quantum numbers of the colliding protons. In ND events, there is an exchange of quantum numbers between the two interacting systems, while in diffractive events, a colour singlet called a Pomeron is exchanged. In QCD, the Pomeron is regarded as a colorless and flavorless multiple gluon [1] or a glueball exchange. The emitted Pomeron can interact with the proton, breaking it up into a group of final state hadrons. If one of the incoming protons breaks up, the event is single diffractive (SD) shown in Figure 3.10. The LHC cross section (at

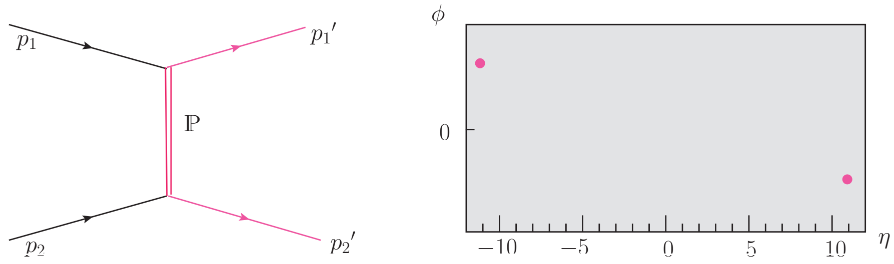

FIGURE 3.9: Diagram for elastic scattering and ϕ vs η plot showing the distribution of products after the interaction [58]

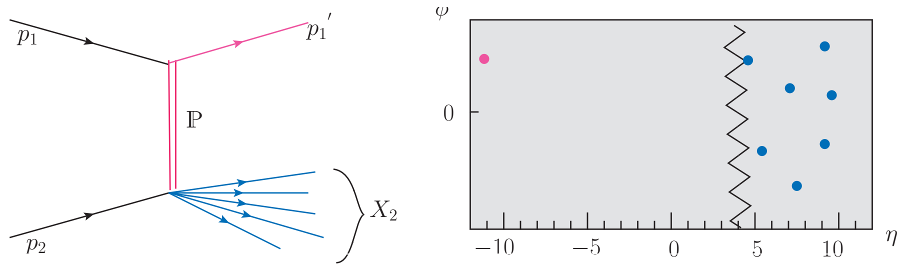

FIGURE 3.10: Diagram for single diffraction and a window showing a rapidity gap between $-10 < \eta <3.5$ [58]

14TeV) for SD is $\sim$ 10mb . If both the incoming protons break up, the event is double diffractive (DD) shown in Figure 3.11. The LHC cross section (at 14TeV) for DD is $\sim$ 7mb [72]. A different topology becomes possible with two Pomerons exchanged, namely Central Diffraction or Double Pomeron Exchange. In this process, both the protons are intact and are seen in the final state as shown in Figure 3.12 . The LHC cross-section for CD is $\sim$ 1mb [72]. In Non diffractive (ND) interactions there is an exchange of colour charge and subsequently more hadrons are produced. This is shown in Figure 3.13. ND interactions are the dominant process in pp interactions and are expected to be $\sim$60% of all interactions at the LHC with a cross section of $\sim$ 65mb (at 14TeV) [72]. A consequence of a colorless Pomeron exchange is that the two final state hadrons or diffractive masses have a large rapidity gap (LRG) between them. The characteristic appearance of rapidity gaps in diffractive events is something experimentalists can exploit.

There are several possible descriptions of diffraction, allowing several alternative approaches. Diffraction in PYTHIA6, as described in [67], is based on a Regge theory. It uses pomeron model to generate the cross section and the diffractive mass and momentum transfer [60]. Empirical corrections are introduced to make Regge model to cover the full phase space [67]. These corrections enhance the production of small masses and suppress the production near the kinematic limit. Particle production M_X from low mass states ($< 1GeV$) is

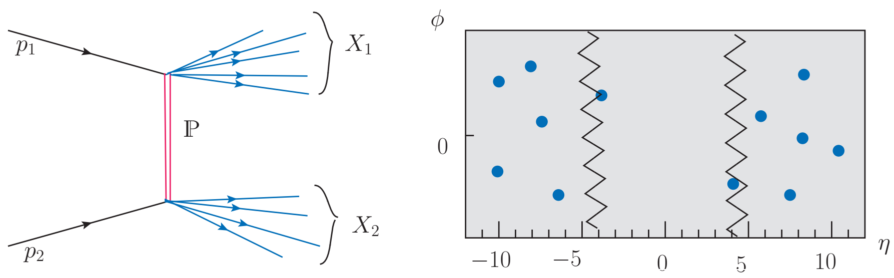

FIGURE 3.11: Diagram for double diffraction and ϕ vs η plot showing the distribution of products after the interaction [58]

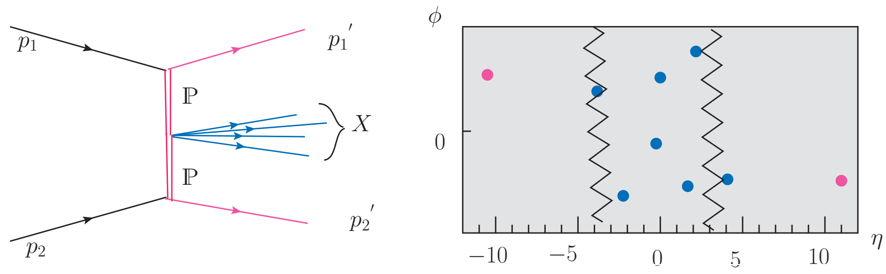

FIGURE 3.12: Diagram for central diffraction and two windows showing a rapidity gap [58]

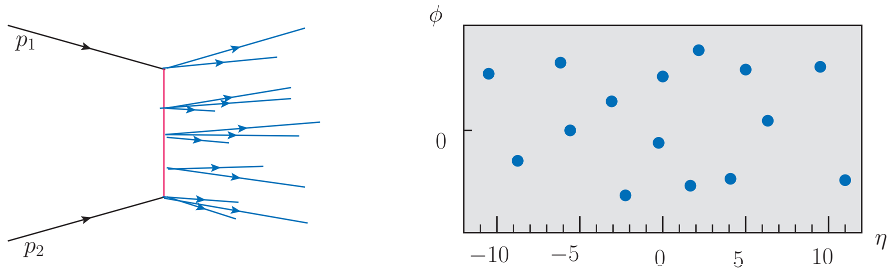

FIGURE 3.13: Diagram for non-diffraction [58]

treated as an isotropic two body decay. Particle production from high mass states is based on the string model. Two string configurations are possible depending on whether the pomeron couples to a quark or gluon [67] .

Chapter 4

Collider Experiments

The present work is based on the published data from ATLAS experiment at 0.9 TeV and 7TeV and CDF II at 1.9TeV. The following sections provides a brief overview of these particle detectors. The detailed description of these experiments can be found in [2, 8, 33, 42, 1].

4.1 Coordinate System

The experiments mentioned above use a right handed coordinate system, the z-axis is along the axis of the experiment (in the direction of the colliding beams). In the transverse plane, the x-axis is horizontal and the y-axis is vertical. Because of the cylindrical symmetry, it is sometimes more convenient to use a spherical (R, ϕ, θ) or cylindrical (r, ϕ, z) coordinate system instead of the Cartesian coordinate system. To describe the kinematics of particles used in this thesis in a more intuitive way, cylindrical coordinates p_t , θ and ϕ are introduced, where p_t is the transverse momentum and defined as

$$p_t = \sqrt{p_x^2 + p_y^2} \tag{4.1}$$

and θ and ϕ are angular coordinates in the r-z and x-y plane respectively. where θ is

$$\theta = tan^{-1}(\frac{\sqrt{p_x^2 + p_y^2}}{p_z}) \tag{4.2}$$

the convention is to count ϕ angle from the x-axis, so

$$tan\phi = \frac{p_y}{p_x} \tag{4.3}$$

The pseudo rapidity η is used instead of the polar angle θ because the number of particles produced in rapidity intervals of the same size is roughly constant over wide range and defined as

$$\eta = -logtan\frac{\theta}{2} = -\frac{1}{2}ln\frac{P - p_z}{P + p_z} \tag{4.4}$$

The quantity Δ R is often used to measure distances in $\eta - \phi$ space;

$$\Delta R = \sqrt{\Delta\eta^2 + \Delta\phi^2} \tag{4.5}$$

4.2 The Large Hadron Collider(LHC)

The Large Hadron Collider (LHC) [42] at CERN has been designed and constructed to collide proton beams with center of mass energies of 14 TeV and a luminosity of $10^{34}cm^{-2}s^{-1}$. LHC is a towering superconducting hadron accelerator and collider in a 26.7 km long tunnel. It has eight arcs and eight straight sections, the basic layout is shown in Figure 4.1.

Peak performance at 8TeV pp running was reached towards end of 2012, with differential luminosity $L = 7 \times 10^{33}/(cm^2 s)$ and 50 ns time between bunch crossings. The average number of interactions per bunch crossing already exceeded design values and varied between 20 and 30. Altogether about 25 fb^{-1} integrated luminosity was collected by each of the experiments ATLAS and CMS, at 7 and 8 TeV during run 1. The 7 TeV data used for this thesis were collected during low-luminosity running at the start-up phase in April 2010.

The LHC can also collide heavy ions with an energy of 2.8 TeV per nucleon and a peak luminosity of $10^{27}cm^{-2}s^{-1}$. There are two general purpose detectors at the LHC, ATLAS (A Toroidal LHC Apparatus) [1] and CMS (Compact Muon Solenoid) [32] . These detectors surround the interaction region as fully as possible and have been designed and built to discover manifestations of new physics. In addition to these, there are two specialized experiments namely, LHCb (Large Hadron Collider Beauty Experiment) [18]

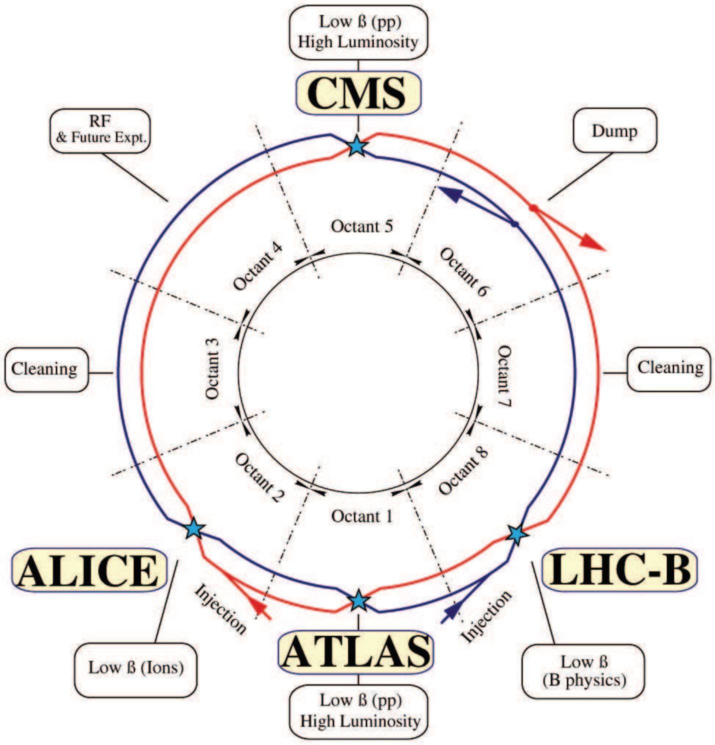

FIGURE 4.1: Schematic layout of the Large Hadron Collider (LHC)

and ALICE (A Large Ion Collider Experiment) [9]. LHCb has been specially designed to study B-physics whilst ALICE is dedicated to investigating heavy ion physics when the LHC is colliding lead ions rather than protons. In this study we used data from ATLAS detector, a brief description of the detector is given below.

4.2.1 The ATLAS Detector

ATLAS is the multi-purpose detector and biggest of the four LHC detectors. It consists of many sub detectors to cover the wide range of high energy physics measurements. It can be divided into four main subsystems: two tracking detectors (inner detector and muon system) and two calorimeters (electromagnetic and hadron calorimeter). The detailed description about the ATLAS detector can be found in many documents [1], [2] and [33]. In the following section atlas subdetectors will be described briefly, while trying to focus on relevant subdetector (inner detector) for the presented work.

4.2.1.1 Inner detector(ID)

The ATLAS inner detector is a tracking detector designed to track charged particles produced in proton-proton collisions at the LHC at an energy of 14 TeV. It has been constructed to measure momentum, direction and impact parameters of charge particles. It also provides some particle identification. The detector is also needed to resolve multiple vertices from the overlap of 23 collisions per bunch crossing expected at design luminosity and the measurement of secondary vertices. It covers the pseudorapidity range $|\eta| \leq 2.5$ and immersed in a 2T axial magnetic field.

The ID consists of the following parts:

- The Pixel detector, closest to the interaction point
- The Semiconductor Tracker (SCT), surrounds the pixel detector
- The Transition Radiation Tracker (TRT), outer most detector of the ID

Each subdetector is divided into one central barrel region and two end cap regions. Each particle produces an average of 3 pixel, 8 SCT and 36 TRT hits.

4.2.1.2 The Pixel Detector

The pixel detector is designed to provide a very high-granularity with a high precision set of measurements as close to the interaction point as possible. It covers a sensitive radial distance from the interaction point of 50.5-150 mm. The system consists of three barrels at average radii of$\sim$4 cm, 11 cm, and 14 cm, and four disks on each side, between radii of 11 and 20 cm, which complete the angular coverage. The system is designed to be highly modular containing approximately 1500 identical barrel modules and 1000 identical disk modules and uses only one type of support structure in the barrel and one type in the disks [2]. Charged tracks are detected because they create elctron hole pairs by ionisation in the silicon material the created charge then is collected in the pixels due to the applied voltage.

4.2.1.3 The Semiconductor Tracker (SCT)

It is similar to the Pixel Detector, designed to provide a very high-granularity but segmented in strips rather than pixels. The detection principle is also similar to the

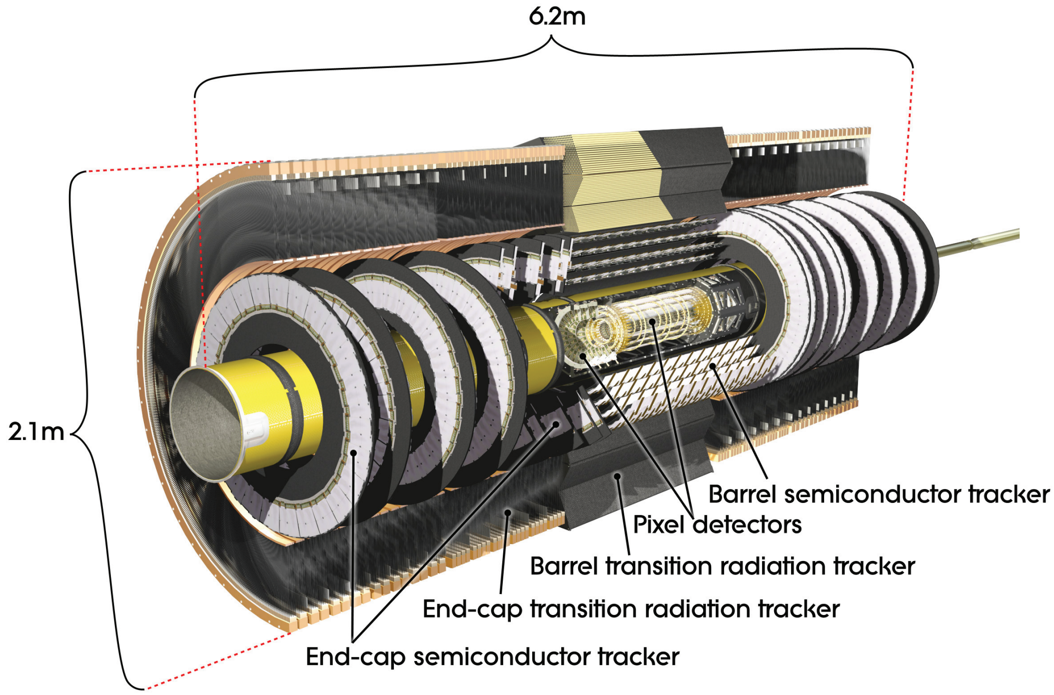

FIGURE 4.2: Atlas Detector

Pixel Detector: electron hole pairs are created by charged particles and then charges are collected in one end of a strip. It covers a sensitive radial distance from the interaction point of 299-560 mm. The SCT system is designed to provide four precision measurements per track in the intermediate radial range contributing to the measurement of momentum, impact parameter and vertex position [2]. Because of high granularity it provides good pattern recognition.

4.2.1.4 The Transition Radiation Tracker (TRT)

TRT is a straw detector that is mainly designed to provide many measurements aimed at increasing the momentum resolution and providing additional particle identification potential via the transition radiation probability. The Transition Radiation Tracker (TRT) consists of three parts, a barrel and two endcaps. Its basic elements are thin walled proportional drift tubes, hereafter called strawtube or simply straws. Each straw is 4 mm in diameter giving a fast response and good mechanical properties for a maximum straw length of 150 cm. Straw tubes were chosen as detecting elements as they offer a high degree of modularity of the detector and also they can easily be integrated into a

Item		**Radial extension**	**Length (mm)**
Pixel	Overall envelope	45.5<R<242	0 <| z | <3092
3 cylindrical layers	Sensitive barrel	50.5<R<122.5	0 <| z | <400.5
2 × 3 disks	Sensitive end-cap	88.8<R<149.6	495 <| z | <650
SCT	Overall envelope	255<R<549 (barrel)	0 <| z | <805
		251 <R <610 (end-cap)	810 <| z | <2797
4 cylindrical layers	Sensitive barrel	299 <R<514	0 <| z | <749
2 × 9 disks	Sensitive end-cap	275 <R <560	839 <| z | <2735
TRT	Overall envelope	554 <R <1082 (barrel)	0 <| z | <780
		617 <R <1106 (end-cap)	827 <| z | <2744
73 straw planes	Sensitive barrel	563 <R <1066	0 <| z | <712
160 straw planes	Sensitive end-cap	644 <R <1004	848 <| z | <2710

TABLE 4.1: Main parameters of Inner detector [2]

medium producing transition radiation without compromising the continuous tracking concept. The barrel part is comprised of 52544 straws 144cm in length oriented parallel to the beam. The two end caps each contain 122880 straws 37cm in length radially aligned to the beam axis. The detector geometry guarantees that particles cross 35 –40 straws in a pseudorapidity interval from 0 to 2, providing continuous tracking at larger radii of the Inner Detector while enhancing its pattern recognition ability. The operating conditions in the ATLAS experiment at the Large Hadron Collider (LHC) impose stringent requirements on the straw properties. All choices of materials, the straw design, the active gas, and the operating point were made to ensure safe, and efficient operation in the high radiation environment [11].

4.2.1.5 Trigger System

The ATLAS trigger system consists of three levels of event selection: L1, L2, and event filter. The L2 and event filter together form the High-Level Trigger (HLT). The Minimum Bias Trigger Scintillators (MBTS) are designed to trigger Minimum Bias event and function only during initial data taking at low luminosities. After some months of higher luminosity operation the scintillators will yellow due to radiation damage. The two sets of sixteen scintillator counters are installed on the inner face of the end cap calorimeter cryostats and are used to trigger on minimum bias events. A minimum bias trigger should select inelastic collisions with as little bias as possible, precluding the use of the standard high p_T triggers. Ideally, the L1 random trigger with beam pickup is to be used to accept

Criteria	Full Tracks
pt >100 or 500 MeV	YES
$\mid \eta \mid$<2.5	YES
Layer-0 hit if expected	YES
> 1 Pixel hit	YES
> 2, 4 or 6 SCT hits for tracks*	YES
$\mid d_0 \mid$<1.5 mm and $\mid z_0 \mid .sin\theta$ <1.5 mm	YES
χ^2 probability >0.01 for pt>10 GeV	YES

Table 4.2: Selection criteria for the full reconstruction of tracks. Full Tracks refers to the algorithms used at 0.9 and 7 TeV. The transverse momentum cut applied depends on the selected phase space region. *The SCT hit selection are for $p_t < 200$, $200 < p_t < 300$ or $p_t > 300$ MeV, respectively.

events with zero bias and then inelastic collisions were selected offine. Events which pass the L1 trigger are then transferred to the L2 and EF trigger systems (HLT), seeded from a specific lower level trigger and is able to examine relevant features of the event in greater detail in order to make an overall trigger decision. The events used to make the minimum bias measurements are collected with the MBTS. The distributions must therefore be corrected for trigger inefficiencies that can potentially cause a bias.

4.2.1.6 Track Reconstruction

Tracks are reconstructed offline within the full acceptance range $\mid \eta \mid< 2.5$ of the ID [37, 38] by requiring a minimum number of silicon hits and then extrapolated to include measurements in the TRT [3]. Tracks are required to pass the selection criteria shown in Table 4.2. The impact parameters d_0 and z_0 are calculated with respect to the event primary vertex. The layer-0 selection requires a hit in the inner most layer of the Pixel detector if a hit is expected. The track fit probabilityχ^2 cut is applied to remove tracks with mis-measured p_t due to misalignment or nuclear interactions. These tracks are used to produce the corrected distributions and are referred as selected tracks [3].

4.2.1.7 Event Selection

To reduce the contribution from background events and non-primary tracks, also to minimise the systematic uncertainties, the events are required to satisfy the following criteria:

- at least one hit in the Minimum Bias Trigger Scintillators (MBTS);
- a reconstructed primary vertex with at least two tracks;
- no further primary vertex composed of 4 or more tracks (to veto pile-up events);
- at least 1, 2 or 6 good tracks depending on the phase-space used. The good track definition is given by:
- $\mid \eta \mid < 2.5$ and $p_t > 100$ MeV or $p_t > 500$ depending on the phase-space considered;
- Pixel and SCT hits requirements;
- transverse and longitudinal impact parameters calculated with respect to the event primary vertex $\mid d_0 \mid < 1.5$ mm and $\mid z_0 \mid sin\theta <$1.5 mm, respectively. The distribution at the particle level within the chosen kinematic range, starting from the one reconstructed, can be obtained with the knowledge of the trigger, vertex and tracking efficiencies.

4.2.1.8 Corrected Data

The effect of events lost due to the trigger and vertex requirements is corrected using an event by event weight whereas p_t and η distributions of selected tracks are corrected for using a track by track weight. For all distributions in all phase space regions considered, closure tests are carried out. These tests are carried out on MC where the reconstructed samples are corrected according to the same procedure as used on the data [3].

4.3 CDF Experiment at the Tevatron

The Collider Detector at Fermilab (CDF) is a general purpose particle detector at the Tevatron $p\overline{p}$ collider [41]. Here we briefly describe the component of this detector.

4.3.1 The Tracking System

There is a tracking system outside the beam pipe and is composed of an inner set of silicon microstrip detectors and an outer drift chamber (COT). The silicon detectors are located between radii of $1.5 < r < 29.0$ cm, and provide precision measurements of the impact

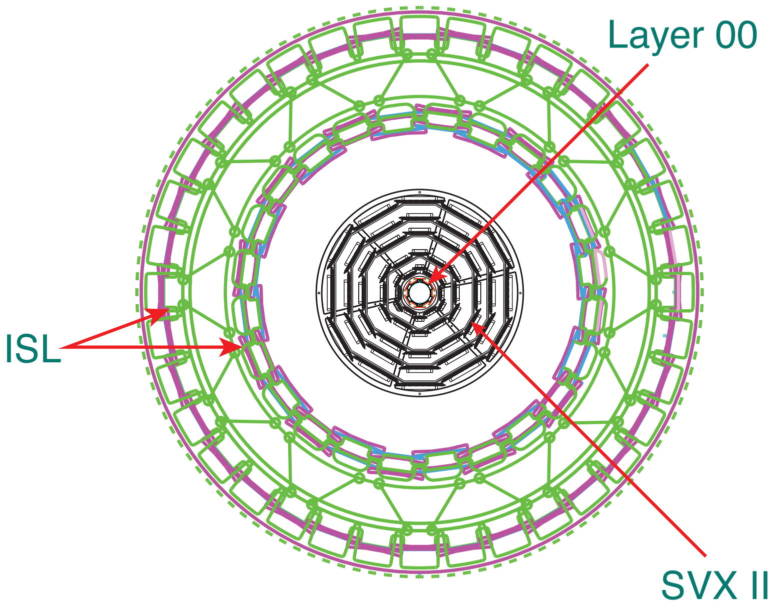

FIGURE 4.3: A cross-sectional view in the plane of the locations of the three components of the silicon detector, Layer 00, SVXII, and ISL

parameter of track with respect to the primary vertex. The innermost layer, known as L00 [49], is single sided layer and is attached directly on the beam pipe. Five layers of double sided silicon microstrips, SVX-II [63], cover the pseudorapidity $\eta < 2$ region: in each layer one side is oriented at a stereo angle with respect to the beam axis to provide three dimensional measurements. The last layer , known as ISL [15], is located outside silicon microstrips.

It consists of one layer of silicon microstrips covering the region $\eta < 1$ and of two layers at $1 < \eta < 2$ where the COT coverage is incomplete or missing. The COT is a cylindrical open cell drift chamber with 96 sense wire layers grouped into eight alternating superlayers of stereo and axial wires. Its active volume covers $40 < r < 137$ cm and $z < 155$ cm, thus providing full coverage up to $\eta < 1$ to tracks originating within η 60 cm. Outside the COT, a solenoid provides a 1.4 T magnetic field that allows the particle momenta to be computed from the trajectory curvature [8].

4.3.2 Trigger System

CDF uses a three level trigger system that selects events to be recorded to tape at 75 Hz from the bunch crossing rate of approximately 2.5 MHz. Level 1 trigger is also termed as minimum bias trigger that operates as follows. An antiproton proton bunch crossing, signaled by the Tevatron radio frequency, is defined to contain at least one ppbar interaction if there is a coincidence in time of signals in both forward and backward CLC modules. This required coincidence is the start gate of the first level CDF trigger called Level 1 . The minimum bias trigger is rate limited at Level 1 in order to keep the Level 3 output at 1 Hz. A total of about 16 million bunch crossings was recorded [8].

4.3.3 Event Selection

Reconstructed tracks are accepted if they comply with a minimal set of quality selections including a minimum number of hits, both in axial and stereo layers of the COT. All tracks are required to originate in a fiducial region in the plane (d_0; Δz) A similar selection criterion is used along the beam axis: Δz $<$ 1 cm for tracks with silicon information and Δz $<$ 2 cm for the remaining tracks primary charged particles must have a transverse momentum greater than 0.4 GeV/c and pseudorapidity $|\eta| \leq 1$ in order to optimize the efficiency and acceptance conditions [8].

4.4 Phenomenology of Hadron-Hadron Collisions

The total proton proton cross section can be split into two terms:

$$\sigma_{total} = \sigma_{elastic} + \sigma_{inelastic} \quad \textbf{(4.6)}$$

The first term is elastic scattering; the situation when colliding protons deflect through a small angle without breaking up. The second inelastic term describes multi-particle production. The inelastic scattering accounts for $\sim$ 80% of all the proton-proton collisions. The total proton proton cross section (elastic + inelastic) is 65 mb at 900 GeV collision energy ($\sigma_{inelastic}$ for pp has been measured by ATLAS at 7TeV [7] to be 60 ± 2 mb).

The inelastic processes are categorized as follows:

$$\sigma_{inelastic} = \sigma_{SD} + \sigma_{DD} + \sigma_{ND} \quad \textbf{(4.7)}$$

- Single Diffraction (SD): one of the two protons softly breaks up into other particles, $\sim$ 15–18% of the σ_{total}.

- Double Diffraction (DD): both protons break up, 10% of the σ_{total},
- Non Diffraction (ND): the protons break up and produce lots of soft particles uniformly distributed in pseudorapidity, 50% of σ_{total}. It also includes hard scattering between parton constituents of the protons.

If the partons from the colliding protons scatter with high momentum transfer, $> 2GeV$, they are likely to produce several particles with significant p_t . This process (also referred to as the hard scattering process) is a part of the hard core component. The hard scattering of the two partons is accompanied by the scattering of the other partons (multiple parton interactions), initial and final state radiation, and beam remnants. These processes are referred to as the underlying event. At high luminosity (high collision rate) each event may yield several proton collisions in the same proton bunch crossing. In such cases the rare hard scattering collisions are usually superimposed on multiple diffractive and hard core low p_t collisions. This low p_t background is referred to as the pile up. The expected pile up for the LHC design luminosity is 20 collisions per beam crossing. These particles are accounted for by soft QCD physics models, which are fit to the data.

4.5 Soft QCD Physics Studies

Minimum Bias (MB) and Underlying Event(UE) data are considered as an excellent probe of soft QCD physics. Same phenomenological models are used to describe both, underlying events in hard $2 \rightarrow 2$ scattering process and soft MB collisions.

4.5.1 MB Events

Minimum Bias is an experimental definition and defined through the experimental apparatus that triggers the collection of the data. A trigger is set up so as to collect, with uniform acceptance, events from all possible inelastic interactions. Altough it is designed to avoid bias in the sample some bias is usually introduced due to the minimum energy threshold or limited geometrical acceptance of the trigger[3]. Generically it refers to events selected with a loose trigger that accepts a large fraction of the inelastic cross section. However, slightly different definitions are made by each experiment. Minimum bias events are usually associated with the non-single-diffractive (NSD) inelastic portion of the total cross section. This is mostly for historical reasons, since the trigger used to select inelastic events in previous hadron collider experiments typically required a forward-backward coincidence, thus suppressing single-diffractive interactions. Elastic scattering was not included since the trigger only accepted events with activity in the central region.

Three slightly different definition of minimum bias used in this dissertation because the data used is from three different detectors. Minimum bias events are dominated by soft interactions, with low transverse momentum and low particle multiplicity. This type of data are collected with a loose trigger requirement. The requirement is designed to minimize trigger bias towards some specific event signatures. Ideally, the min bias data should contain all the physics processes proportional to their production rates. It is dominated by the events with soft QCD collisions.

4.5.2 MB Observables

Distributions of charged particles in hadron collisions have been measured by many experiments previously in both ppbar as well as pp collisions [12], [20]. In the present study minimum bias measurements from ATLAS and CDF II [3, 8] have been used:

- Distribution of the multiplicity of charged particles per event (N_{ch})
- Pseudorapidity distribution of charged particles normalized by the number of events.
- Charged particle distribution in bins of p_t where each entry is weighted by $\frac{1}{p_t}$ and the distribution is normalized by the number of events.
- Average p_t as a function of Nch

The average charged particle multiplicity per event followed by the charged particle pseudorapidity density is the simplest minimum bias measurement. The pseudorapidity distribution of particles produced in pp collisions is strongly correlated with the rate of parton parton scattering. As the collision energy increases, the rate of multiple parton interactions also increases, producing a rise in the central pseudorapidity density. An accurate event generator model should take into account the expected variation of multiple parton scattering with the collision energy.

4.5.3 Underlying Event(UE)

Those aspects of hadronic interaction which are attributed not to hard scattering process, but to the accompanying interactions of the remnants of the proton is defined as the Underlying Event(UE) [4] .The UE may have contributions from both hard and soft physics (low p_t transfer) Much of the complexity involved in describing proton proton scatterings derives from the composite nature of hadrons. The underlying event in hadron hadron collisions is only weakly constrained by existing data and comprises many aspects not describable by perturbative QCD. Traditionally, measurements of minimum bias events were used to parametrize the underlying event.

4.5.4 UE Observables

ATLAS detector has measured charged particle distributions, which are sensitive to the underlying event, in addition to the charged multiplicity measurements described above. These measurements are based on data collected using a minimum bias trigger to select proton proton collisions at center of mass energies of 900 GeV and 7 TeV. Charged particles in each event are measured for different regions in terms of azimuthal angle with respect to the track with maximum transverse momentum referred to as leading track. Since a hard scattering should be selected, $p_{t,lead}$ is required to be$>$ 1 GeV, for example. The direction of the leading track is used to define regions of the η–ϕ plane which have different sensitivities to the UE. The azimuthal angular difference between charged tracks and the leading track is defined as $\mid \triangle\phi \mid = \mid \phi - \phi_{leadingtrack} \mid$. The following three azimuthal regions are defined as shown in Figure 4.4.

- Toward Region: $\mid \triangle\phi \mid < 60°$
- Transverse Region: $60 < \mid \triangle\phi \mid < 120°$,
- Away Region: $\mid \triangle\phi \mid > 120°$

The transverse region is most sensitive to the underlying event [4]. The observables examined in this analysis are described in Table 5.7.

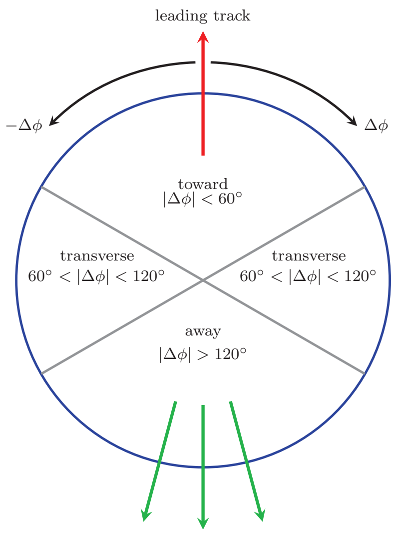

FIGURE 4.4: Three regions in the azimuthal angle with respect to the leading track [4]

Chapter 5

Tuning Setup

This section contains a discussion of the switches and parameters of the PYTHIA6 program considered in this thesis. Also described are the tuning method, the tuning strategy and the data used.

5.1 Tuning method

The method used in this study is based on the linear parametrization of the observables with the possibility of iteration. The increasing accuracy of experimental data and the demands of physics analyses require many parameters to be fitted simultaneously. This is possible with the method used. In practice, 2nd or higher order approach is limited to n$\leq$ 6 parameters [23] because of the rapid (quadratic) rise of computer time with the number of parameters.

The tuning method used is summarized here but details can be found somewhere else [23]. A measurable quantity (e.g. the contents of interval j of a distribution) is denoted by M_j and the set of model parameters to be determined by $x_k; k = 1....n$. For a given set of central values x_{k0}, 2N Monte Carlo events are generated and the histograms of various distributions are filled. For each parameter, four more points in the parameter space are considered, situated at distances

$-\Delta x_{left}, -\Delta x_{left}/2, \Delta x_{right}/2, \Delta x_{right}$

from the central value x_{k0}. At each of these four points and for each parameter, N Monte Carlo events are generated and again the histograms filled and stored.

A linear expression

$$M_j(x_k) = m_j^k + a_j^k(x_k - x_{k,0}) \tag{5.1}$$

is fitted for each measured quantity M_j and each parameter x_k, yielding a slope a_j^k and offset m_j^k . If the fit is not acceptable (χ^2 probability less than 10%) a quadratic expression is tried and used to monitor the parameter region for which the linear expression is acceptable. The actual parameter fit is always performed using the linear terms only. The entire process of Monte Carlo event generation is then repeated, moving the central values $x_{k,0}$ accordingly, until the final fitted values of the parameters all remain within the linear ranges and change by less than their errors. The model parameters are fitted by minimizing the χ^2 function, using the program MINUIT [50]:

$$\chi^2 = \sum_j \left(\frac{M_j^{data} - M_j^{MC}(\overrightarrow{x})}{\sigma_j^{data}} \right)^2 .w_j \tag{5.2}$$

w.r.t the parameters $\overrightarrow{x}$, where the sum runs over all of the measured quantities. The errors $\sigma_j^{data}$are taken to be the quadratic sums of statistical and systematic uncertainties; Monte Carlo errors are small compared to these and are neglected. By using above Equation **5.2**. it is implicitly assumed that the experimental data points are uncorrelated. This is not true in general, however, since there are both intrinsic correlations between variables as well as systematic errors from the correction procedure which introduce correlations between neighboring bins. As a result, the errors on the fitted parameters and the corresponding χ^2 values should only be regarded as giving a rough measure of statistical uncertainty and relative goodness-of-fit. As an option de-weighting of selected distributions can be used, described in Section 5.5.

5.2 Fragmentation Tuning

In order to keep number of parameters manageable, a 2- step strategy has been followed. This strategy is based on the assumption that the parameters related to the MPI's can be decoupled from the fragmentation parameters. In this first step, the fragmentation parameters were determined from fits to ALEPH $e^+e^- \rightarrow$ *hadrons* data taken at Z^0 pole. The procedure and the results are very similar to those published earlier [23], except that

Switch	Value	Description
MSTP(3)	1	Λ_{QCD} in different parts of event generation
MSTP(51)	LHAPDF code	
MSTP(52)	2	External PDF sets can be selected from LHAPDF
MSTP(70)	2	Model for smooth ISR cut off($p_{\perp}^{0}$)
MSTP(72)	2	model for final state radiation off ISR partons
MSTP(81)	21	turn on multiple parton interactions (New Scenario)
MSTP(82)	5	Hadronic matter overlap function
MSTP(88)	0	quark junctions $\rightarrow$ diquark/ Baryon mode
MSTP(95)	6	Colour Reconnection (Annealing model)
MSTU(112)	5	number of flavours considered in α_s expression

TABLE 5.1: Switches/models of PYTHIA6 used in the final tune

now the p_t-ordered parton shower for FSR and the Lund-Bowler scheme for heavy quarks were used, and that updated measurements were included. The resulting numbers [46] are listed in Table 5.4.

5.3 Parameters and switches for pp interactions

In the 2nd step, the parameters pertaining to hadron hadron interactions were tuned, using the optimized fragmentation parameters obtained in first step. The main focus of the thesis is to investigate how well the PYTHIA model describes measured particle densities from inelastic pp collisions at high energy. In the following section the implementation of the above method is given. The main aspects of the procedure are the selection of model parameters and the data to which the selected parameters to be fitted. Relevant switches may also be found in Table 5.1 . If a certain switch is not cited, it means that it is left at its default value. In the following section the selected switches and parameters used for the current study are described. The section 5.4 contains discussion about selected data.

5.3.1 Λ_{QCD} Treatment

PYTHIA provides two possibilities, either to use same Λ_{QCD} in the running of α_s for ISR, matrix element(ME) and FSR or alternatively three different values. The switch MSTP(3) gives the control over the selection of Λ values. For MSTP(3)=1, PARP(1)=PARU(112) provides Λ value for hard interactions, PARP(61) provides Λ value for ISR and PARP(72)

PDF type	PDF set	LHAPDF code
Leading order (LO)	CTEQ6LL	10042
	CTEQ5L	19070
	MSTW08LO	21000
Modified leading order (mLO)	MRSTMCal(LO**)	20651
	MRST2007 (LO*)	20650
	CT09MC2	10772
Next-to Leading order (NLO)	CTEQ6.6	10550
	CT10	10800
	MSTW08NLO	21100

Table 5.2: PDF sets used in final tune with corresponding LHAPDF codes

provides Λ value final state radiations. For the default option MSTP(3)=2, Λ value is chosen according to the parton distribution functions parameterizations. This Λ value which is provided by the selected PDF is used both for the hard scattering, ISR and FSR. We studied both options in detail, discussed in Chapter 6 and have chosen MSTP(3)=1 for final tune because it leaves more freedom.

5.3.2 Parton Density Functions (PDF)

PDFs are parametrization of partonic content in a hadron, already discussed in Chapter 2. PYTHIA has leading order (LO) PDF set as a default, called CTEQ5L [53]. It has been selected by setting MSTP(51)=7 with MSTP(52)=1. PYTHIA also offers an interface to LHAPDF (the Les Houches Accord PDF Interface) [73], a software tool that allows access to the latest (Leading order, modified leading order and next to leading order etc.) PDF sets. This is done by setting MSTP(52)=2 along with MSTP(51)= LHAPDF code of selected PDF set. All the used PDF sets in the final tune and their corresponding codes are given in Table 5.2.

5.3.3 Multiple Parton Interactions: Switches and Parameters

Section 3.3 contains a detailed discussion about multiple parton interactions, so it should be obvious that MPI have to be switched on in order to get a reasonable description of the data. The so called new scenario of interleaved ISR/MPI and beam remnants is switched on with MSTP(81)= 21. For purpose of studies, the MPI's can be switched off with MSTP(81)=20. The amount of the MPI component is regulated by a single cut off parameter, p_{t0}, for the p_t of 2→2 scattering processes, which is assumed to scale with E_{cm} according to a power law:

$$p_{t0} = PARP(82)(\frac{E}{7TeV})^{PARP(90)} \quad \textbf{(5.3)}$$

Both PARP(82) and PARP(90) are considered as tuning parameters, with PARP(89)= 7TeV chosen as the reference energy.

5.3.3.1 Hadronic Matter overlap and Parameters

Several methods for the generation of a varying impact parameter are included in PYTHIA. They are all based on the assumed matter distribution of the hadrons which have partly been explored in elastic electron proton scattering experiments. PYTHIA offers double exponential as well as double Gaussian matter distribution models parameterized by two parameters PARP(83) and PARP(84) , or a matter distribution that is a continuous interpolation between exponential and Gaussian , parameterized by a single parameter PARP(83). These scenarios can be chosen by setting MSTP(82)=4 or 5 respectively. PARP(83) has different meaning in both options. We have chosen MSTP(82)=5 for final tune.

5.3.4 Initial State Radiation (ISR)

PYTHIA provides possibilities to change both Λ_{QCD} in the definition of the α_s evolution for ISR and the allowed phase space for ISR radiation [36, 67]. The strong coupling in the ISR shower is defined as $\alpha_s(kQ^2, \Lambda^2_{ISR})$ where the multiplicative factor k corresponds to PARP(64) parameter and the QCD scale Λ_{ISR} is given by PARP(61). The other ISR parameter is PARP(67), which is a multiplicative scale factor applied to the maximum scale at which the shower begins its evolution [36]. For this tune we investigated all these parameters, PARP(61), PARP(64) and PARP(67). As these parameters have little effects on data (MB and UE), so we fixed them at best values found in preliminary tunes. These values are found consistent with data , even if default. Parameter values used in final tunes for these parameters can be found in Table 5.5.

5.3.5 Final State Radiation (FSR)

We considered two parameters related to FSR for tuning, maximum virtuality scale factor for FSR is given by PARP(71) and Λ_{FSR} given by PARP(72). In principle Λ_{FSR} should be determined from the structure of high-p_t jets. However, it is found that this parameter is also very sensitive to minimum bias p_t. So we treated this parameter as an adjustable parameter in final tunes. Whereas PARP(71) showed weak sensitivity to the data in the preliminary tunes. So we fixed this parameter at best value found in preliminary tunes, same for all PDF sets used in this study.

5.3.6 Primordial k_T

In PYTHIA6, as in all other current event generators, the distribution of primordial k_T inside the hadron is modeled by a Gaussian distribution with the energy independent width σ = PARP(91) as a tunable parameter. But this variable mostly effects the low p_t part of well defined hard process, e.g. the position of the peak of the Z^0 boson p_t spectrum in Drell-Yan events [36]. We studied this parameter for the selected data and found that it has weak impact on selected distributions, and fits give values around 2GeV. So we fixed it at same value for all PDF sets. The value for this parameter and other fixed parameters used in final tunes can be found in Table 5.5.

5.3.7 Beam Remnants Parameters

We also considered beam remnant parameters for tuning by checking their sensitivity to the selected data. PARP(79) is an enhancement factor applied when assigning x to composite systems (e.g. diquarks) in the beam remnant in the new model and PARP(80) gives a probability. When colors of partons kicked out from a beam remnant are to be attached to the remnant, PARP(80) gives a suppression for the probability of attaching those partons to the colour line between two partons which themselves both lie in the remnant [67]. These two parameters are treated as adjustable parameters in the preliminary tunes and fixed at best fit values in the final tunes, values can be found in Table 5.5

5.3.8 Color Reconnection and Parameters

The mechanism of colour reconnection is implemented in PYTHIA in such a way that the overall string length is reduced as much as possible. Which means the partons tend to be colour connected to the partons closest to them in momentum space, hence minimizing the total string length. This is done by an iterative procedure, i.e, colors are reconnected between final state partons again and again to achieve the shortest string length. The switch MSTP(95) controls the choice of colour reconnection model. We used MSTP(95)=6 in the final tune. The total probability for a string piece to survive the annealing and preserve its original colour connections is

$$P_{keep} = (1 - \xi P_{78})^{n_{int}} \quad \textbf{(5.4)}$$

where $\xi = \frac{1}{1+P_{77}^2 <p_\perp>^2}$, P_{78} is the parameter PARP(78) in the code and sets the overall colour reconnection strength, n_{int} is the number of parton parton interactions in the selected event, giving a rough first estimate of the number of strings spanned between the remnants. ξ was introduced together with the Perugia tunes and gives a possibility to suppress reconnection among high p_t string pieces, with P_{77} corresponding to PARP(77) in the code and $< p_\perp >$ being a measure of the average transverse momentum per pion that the string piece would produce [71].

5.3.9 Diffraction and Parameters

A detailed description of diffraction modeling is given in Section 3.5. PYTHIA6 offers the controls over the selection of diffraction types already discussed in Section 3.5. By selecting different options of switch MSEL user can get full control or can have some preprogrammed alternatives:

MSEL= 1, non diffractive (semi)hard QCD processes

MSEL= 2, diffractive (SD+DD) + Elastic are added

Choices for MSEL also depends on experimental data definition:

For ATLAS, MSEL= 2 and

For CDF II MSEL=1 is used. In the current work we used default settings for diffraction.

ISUB code	Processes Description
11	$f_i f_j \to f_i f_j (QCD)$
12	$f_i f_i \to f_k f_k (QCD)$
13	$f_i f_i \to gg$
28	$f_i g \to f_i g$
53	$gg \to f_k \overline{f_k}$
68	$gg \to f_k \overline{g} g$
91	elastic scattering
92	Single diffraction ($AB \to XB$)
93	Single diffraction ($AB \to AX$)
94	double diffraction
95	low p_T production

Table 5.3: The subprocess number or ISUB code given in PYTHIA6, and the description of these processes provided MSEL=1,2

5.4 Data Used

In this thesis we used mainly minimum bias and underlying event data from the ATLAS experiment at two center of mass energies 0.9TeV and 7TeV, along with CDF run II data at 1.96TeV and CMS data at 0.9 and 7TeV. The ATLAS data represents the most accurate and comprehensive measurement at the highest energy. The sensitivity of the observable to the PYTHIA6 model parameters is investigated in detail in Chapter 6.

5.4.1 ATLAS Minimum Bias Data

We used minimum bias data published by ATLAS Collaboration [3] at center of mass energies of 0.9 and 7TeV for charged particles using a single arm minimum bias trigger. Measurements in five separate phase space regions with varying contribution from diffractive events are considered:

- Phase space (PS) 1;

  at least one charged particle in the kinematic range $|\eta| < 2.5$ and $p_t > 500$ MeV

- Phase space (PS) 2;

  at least two charged particles in the kinematic range $|\eta| < 2.5$ and $p_t > 100$ MeV

- Phase space (PS) 3;

Parameter	default*	Final Tune	Description
MSTJ(41)	2	12	Use PYPTFS
MSTJ(11)	4	5	Lund-Bowler for HQ
PARJ(1)	0.1	0.128	diquark suppression
PARJ(2)	0.3	0.268	strange quark suppression
PARJ(3)	0.4	0.772	strange diquark suppression
PARJ(11)	0.5	0.549	spin-1 light meson
PARJ(12)	0.6	0.450	spin-1 strange meson
PARJ(13)	0.75	0.500	spin-1 heavy meson
PARJ(14)	0.	0.12	$P(L = 1, S = 0, J = 1)$
PARJ(15)	0.	0.04	$P(L = 1, S = 1, J = 0)$
PARJ(16)	0.	0.12	$P(L = 1, S = 1, J = 1)$
PARJ(17)	0.	0.20	$P(L = 1, S = 1, J = 2)$
PARJ(19)	1.0	0.402	end-point baryon suppression
PARJ(21)	0.36	0.329	σ_q
PARJ(26)	0.4	0.245	η' suppression
PARJ(41)	0.3	0.425	a
PARJ(42)	0.58	1.65	b
PARJ(46)	1.	1.42	r_c
PARJ(47)	1.	0.975	r_b
PARJ(81)	0.29	0.261	Λ_{QCD} in resonance decays
PARJ(82)	1.	0.90	shower cut-off

TABLE 5.4: Tuned flavor/fragmentation parameters used in final tunes and their default values in PYTHIA6

Parameter	default*	Selected	Description
PARP(64)	1.	1.	ISR Scale factor for α_S
PARP(71)	4.	1.	max. virtuality scale factor for FSR (non-s-channel)
PARP(67)	4.	1.	max.Q^2 scale factor for ISR
PARP(79)	2.	1.5	beam remnant x enhancement
PARP(80)	0.1	0.06	beam remnant break-up suppression
PARP(89)	1800.	7000.	reference $E_{cm}\ for\ p_{t0}$
PARP(91)	2.	2.	intrinsic $k_\perp$ width
PARP(93)	5.	10.	intrinsic $k_\perp cut - off$

TABLE 5.5: Selected values of parameters which were studied in Preliminary tunes, but kept fixed in final tunes

at least six charged particles in the kinematic range $|\eta| < 2.5$ and $p_t > 500$ MeV

- Phase space (PS) 4;

  at least twenty charged particles in the kinematic range $|\eta| < 2.5$ and $p_t > 100$ MeV

- Phase space (PS) 5;

  at least one charged particle in the kinematic range $|\eta| < 2.5$ and $p_t > 2.5$ GeV

The phase space 1 region is most inclusive for p_t >500MeV. The second measures the most inclusive charged particle spectra and is also used as the basis for the model dependent extrapolation to $p_t = 0$.

The phase space 3 region considered is similar to the first but with a higher cut on the number of charged particles, thus reducing the expected contribution from diffractive events in the sample. The phase space 4 region is also diffraction suppressed. The phase space 5 region is chosen to get data less influenced by non perturbative parts of the non diffractive modeling and to be useful for predicting high p_t particle rates and for trigger studies [3].

It can be seen from [3] that none of the MC generators is able to describe the p_t spectrum in the low-p_t region, 100< p_t <500 MeV. Therefore, PS1 and PS3 were selected for final tunes. The PS1 is included in order to see how well (or not) the MC describes the diffractive contribution. The tuning results of other phase spaces will be discussed in the Chapter 8. Table 5.6 shows the distributions used in the final tunes.

5.4.2 ATLAS Underlying Event Data

Measurements of charged particle distributions, sensitive to the underlying event, published by ATLAS Collaboration [4] at center of mass energies of 0.9 and 7TeV using a minimum bias trigger are used. Three regions are defined in azimuthal angle with respect to the highest transverse momentum charged particle in the event, required to satisfy $p_{t,lead} > 1$ GeV. The region transverse to the dominant momentum flow is most sensitive to the underlying event. The charged particles considered are in kinematic range $|\eta|$<2.5 and pt>500 MeV. Underlying event data analysis is already discussed in Section 4.5 and Table 5.7 shows distributions used in the final tunes.

Observable	$\sqrt{s}$
Track-based minimum bias at 900GeV and 7 TeV in ATLAS [3]	
N_{ch}, *track* $p_\perp > 500MeV, N_{ch,} \geq 6, \mid \eta \mid \leq 2.5$	7 TeV
$p_\perp$, *track* $p_\perp > 500\ MeV, N_{ch} \geq 6, \mid \eta \mid \leq 2.5$	7 TeV
η, *track* $p_\perp > 500\ MeV,\ N_{ch} \geq 6, \mid \eta \mid \leq 2.5$	7 TeV
$\langle p_\perp \rangle$ *vs.* $N_{ch}, trackp_\perp > 500\ MeV, N_{ch} \geq 1, \mid \eta \mid \leq 2.5$	7 TeV
N_{ch}, *track* $p_\perp > 500MeV, N_{ch,} \geq 1, \mid \eta \mid \leq 2.5$	7 TeV
$p_\perp$, *track* $p_\perp > 500\ MeV, N_{ch} \geq 1, \mid \eta \mid \leq 2.5$	7 TeV
η, *track* $p_\perp > 500\ MeV,\ N_{ch} \geq 1, \mid \eta \mid \leq 2.5$	7 TeV
N_{ch}, *track* $p_\perp > 500MeV,\ N_{ch,} \geq 6, \mid \eta \mid \leq 2.5$	0.9TeV
$p_\perp$, *track* $p_\perp > 500\ MeV,\ N_{ch} \geq 6, \mid \eta \mid \leq 2.5$	0.9TeV
η, *track* $p_\perp > 500\ MeV,\ N_{ch} \geq 6, \mid \eta \mid \leq 2.5$	0.9TeV
$\langle p_\perp \rangle$ *vs.* N_{ch}, *track* $p_\perp > 500\ MeV\ ,\ N_{ch} \geq 1, \mid \eta \mid \leq 2.5$	0.9TeV
N_{ch}, *track* $p_\perp > 500MeV,\ N_{ch,} \geq 1, \mid \eta \mid \leq 2.5$	0.9TeV
$p_\perp$, *track* $p_\perp > 500\ MeV,\ N_{ch} \geq 1, \mid \eta \mid \leq 2.5$	0.9TeV
η, *track* $p_\perp > 500\ MeV,\ N_{ch} \geq 1, \mid \eta \mid \leq 2.5$	0.9TeV
CDF Run II minimum bias [8]	
$\langle p_\perp \rangle$ *vs.* N_{ch}, *track* $p_\perp > 400MeV, \mid \eta \mid < 1$	1.96TeV

TABLE 5.6: Minimum Bias observables used in the final tuning

5.4.3 CDF run II Data

Minimum Bias data published by CDF at the Tevatron at 1.96 TeV [8] is also considered in this study. We select only average p_t vs N_{ch} for final tunes.

5.4.4 CMS Data

Data published by CMS experiment [51, 52] at two center of mass energies 0.9 TeV and 7TeV has also been studied in this work, Chapter 6.

5.5 Weights

A mechanism of weighting/deweighting is introduced for the observables used. So that to have a possibility to emphasize the importance of single observables or single data compared to others. This will be used in Chapter 8.

Observable	$\sqrt{s}$
Track-based underlying event at 0.9TeV and 7TeV in [4]	
$Transverse\ region\ N_{ch}\ density\ vs.\ p_{\perp}\ (leadingtrack)$	7TeV
$Toward\ region\ N_{ch}\ density\ vs.\ p_{\perp}\ (leadingtrack)$	7TeV
$Away\ region\ N_{ch}\ density\ vs.\ p_{\perp}\ (leadingtrack)$	7TeV
$Transverse\ region\ \sum p_{\perp}\ density\ vs.\ p_{\perp}\ (leadingtrack)$	7TeV
$Toward\ region\ \sum p_{\perp}\ density\ vs.\ p_{\perp}\ (leadingtrack)$	7TeV
$Away\ region\ \sum p_{\perp}\ density\ vs.\ p_{\perp}\ (leadingtrack)$	7TeV
$Transverse\ region\ \langle p_{\perp}\rangle\ vs.\ p_{\perp}\ (leadingtrack)$	7TeV
$Toward\ region\ \langle p_{\perp}\rangle\ vs.\ p_{\perp}\ (leadingtrack)$	7TeV
$Away\ region\ \langle p_{\perp}\rangle\ vs.\ p_{\perp}\ (leadingtrack)$	7TeV
$Transverse\ region\ \langle p_{\perp}\rangle\ vs.\ N_{ch}\ (transverse)$	7TeV
$Toward\ region\ \langle p_{\perp}\rangle\ vs.\ N_{ch}\ (toward)$	7TeV
$Away\ region\ \langle p_{\perp}\rangle\ vs.\ N_{ch}\ (away)$	7TeV
$Transverse\ region\ N_{ch}\ density\ vs.\ p_{\perp}\ (leadingtrack)$	0.9TeV
$Toward\ region\ N_{ch}\ density\ vs.\ p_{\perp}\ (leadingtrack)$	0.9TeV
$Away\ region\ N_{ch}\ density\ vs.\ p_{\perp}\ (leadingtrack)$	0.9TeV
$Transverse\ region\ \sum p_{\perp}\ density\ vs.\ p_{\perp}\ (leadingtrack)$	0.9TeV
$Toward\ region\ \sum p_{\perp}\ density\ vs.\ p_{\perp}\ (leadingtrack)$	0.9TeV
$Away\ region\ \sum p_{\perp}\ density\ vs.\ p_{\perp}\ (leadingtrack)$	0.9TeV
$Transverse\ region\ \langle p_{\perp}\rangle\ vs.\ p_{\perp}\ (leadingtrack)$	0.9TeV
$Toward\ region\ \langle p_{\perp}\rangle\ vs.\ p_{\perp}\ (leadingtrack)$	0.9TeV
$Away\ region\ \langle p_{\perp}\rangle\ vs.\ p_{\perp}\ (leadingtrack)$	0.9TeV
$Transverse\ region\ \langle p_{\perp}\rangle\ vs.\ N_{ch}\ (transverse)$	0.9TeV
$Toward\ region\ \langle p_{\perp}\rangle\ vs.\ N_{ch}\ (toward)$	0.9TeV
$Away\ region\ \langle p_{\perp}\rangle\ vs.\ N_{ch}\ (away)$	0.9TeV
Cluster based	[5]
$Transverse\ N\ density\ vs.\ p_{\perp}^{clus1}$	7TeV
$Transverse\ \sum p_{\perp} density\ vs.\ p_{\perp}^{clus1}$	7TeV
$Transverse\ N\ density\ vs.\ p_{\perp}^{clus1}$	0.9TeV
$Transverse\ \sum p_{\perp}\ density\ vs.\ p_{\perp}^{clus1}$	0.9TeV

TABLE 5.7: Underlying Event observables used in the final tuning

5.6 Monte Carlo Event Analysis and Statistics

For the MC generated events, the observables discussed above are computed using a private FORTRAN program. For a typical run, the number N (see Section 5.1) of MC events generated at each point and for each parameter was 0.68×10^6 and 1.3×10^6 at 0.9TeV and 7TeV respectively, such that 0.5×10^6 and 10^6 events are accepted in ATLAS PS1. The corresponding number was 0.5×10^6 for ND events at 1.96TeV. Depending on the PDF set, a run takes 3-4 days of computing time on a single 2.9Ghz intel Xeon X5570 processor with 8MB L2 Cache and 8GB of main memory.

Chapter 6

Preliminary Tunes

The major motivation behind the preliminary tunes presented in this chapter, is to study the selected models and their free parameters, mentioned in Chapter 5. This chapter is divided into two main parts. First part contains model study and in the second part we provide parameter study.

6.1 Model study

The models we selected for this work have already been described in Section 5.3. These are main models needed to describe multiple interactions in PYTHIA6 framework. These models are based on physics approximation so none of these given options can be considered as perfect or preferred one. Parameters relevant to the selected models are tuned to the minimum bias and underlying event data to find best models combination for final tunes. Figure 6.1 shows the flow diagram of the models we studied.

6.1.1 Multiple Parton Interactions

Since the proton or any other hadron is a composite object, in a head on collision of two hadrons there is a probability that more than one pair of partons undergo scatterings, resulting in a higher multiplicity compared to events with only one strong interaction. PYTHIA6 offer this model with the switch MSTP(81).

- Model option 1; MSTP(81)=0, MPI is switched off.

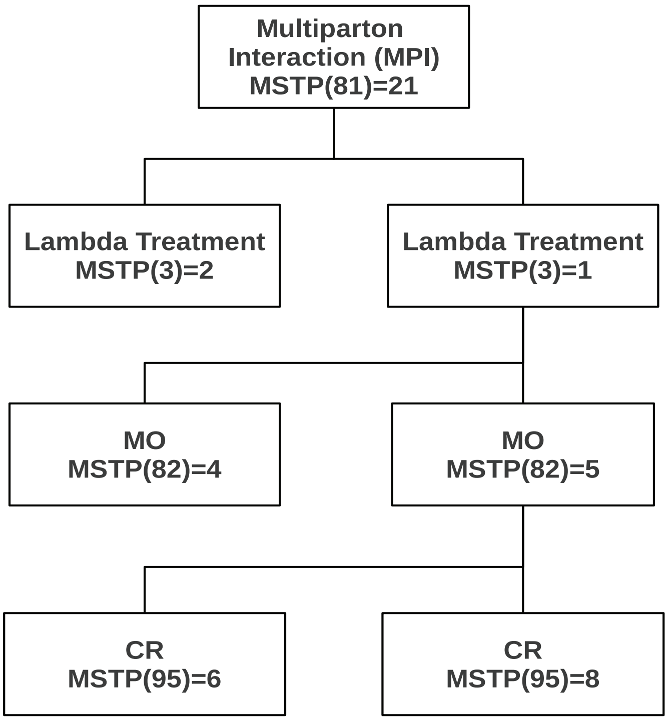

FIGURE 6.1: Different Physics models of Lambda QCD treatment, Matter distribution (MO) and Color reconnection (CR) selected by switches MSTP(3), MSTP(82) and MSTP(95) respectively provided by PYTHIA6 are investigated.

- Model option 2; MSTP(81)=21, MPI is switched on with new scenario of multiple parton interactions, interleaved with ISR, and p_t as ordering variable

An illustration of the effect of multiple parton interactions is Figure 6.2. The mean particle transverse momentum, p_t , as a function of the charged particle multiplicity demonstrates that models fail to describe the data if the possibility of multiple parton interactions is neglected. This observable is sensitive to the presence of MPI since a higher multiplicity, which is a result of MPI, result in a lower mean transverse momentum, p_t. If MPI's are enabled, the model describes the data convincingly well.

6.1.2 Matter Overlap

The amount of scatterings within the varying impact parameter approach is described by a matter overlap distribution between the two protons. We considered two models for this study given below:

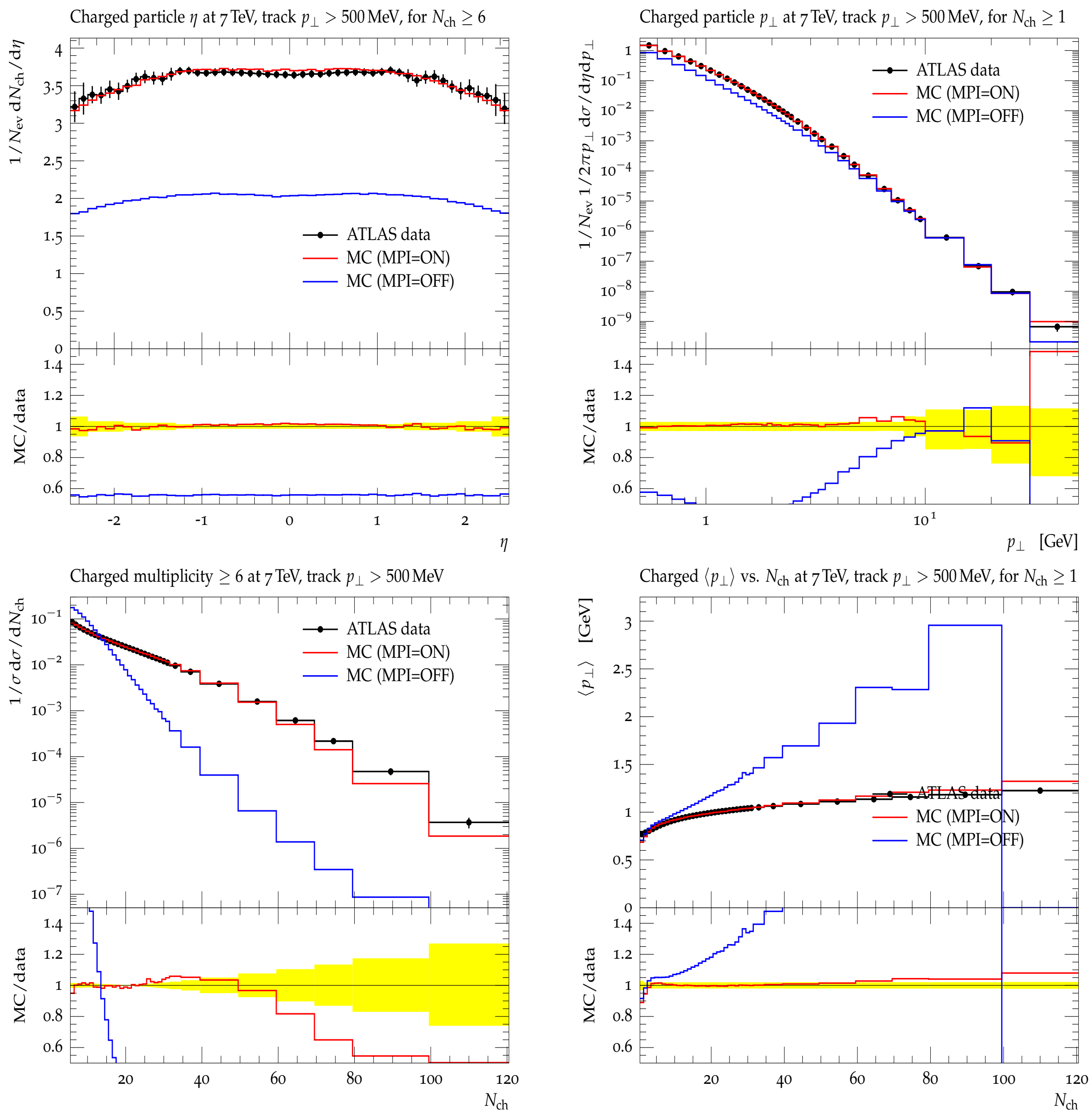

FIGURE 6.2: Comparison plots of tunes with MPI switched on/off to the ATLAS Minimum Bias data using CTEQ6LL (LO) PDF set.

- Model option 1; MSTP(82)=4, hadronic matter overlap using a double Gaussian matter distribution.
- Model option 2; MSTP(82)=5, hadronic matter overlap function which is an interpolation between a Gaussian and an exponential distribution.

The choice of matter overlap affects the shape of the multiplicity distribution. Some effects can be seen in η and p_t distribution as well. The approach which interpolates between Gaussian and exponential distribution looks favored by data as compared to double Gaussian approach, as is visible in Figure 6.3.

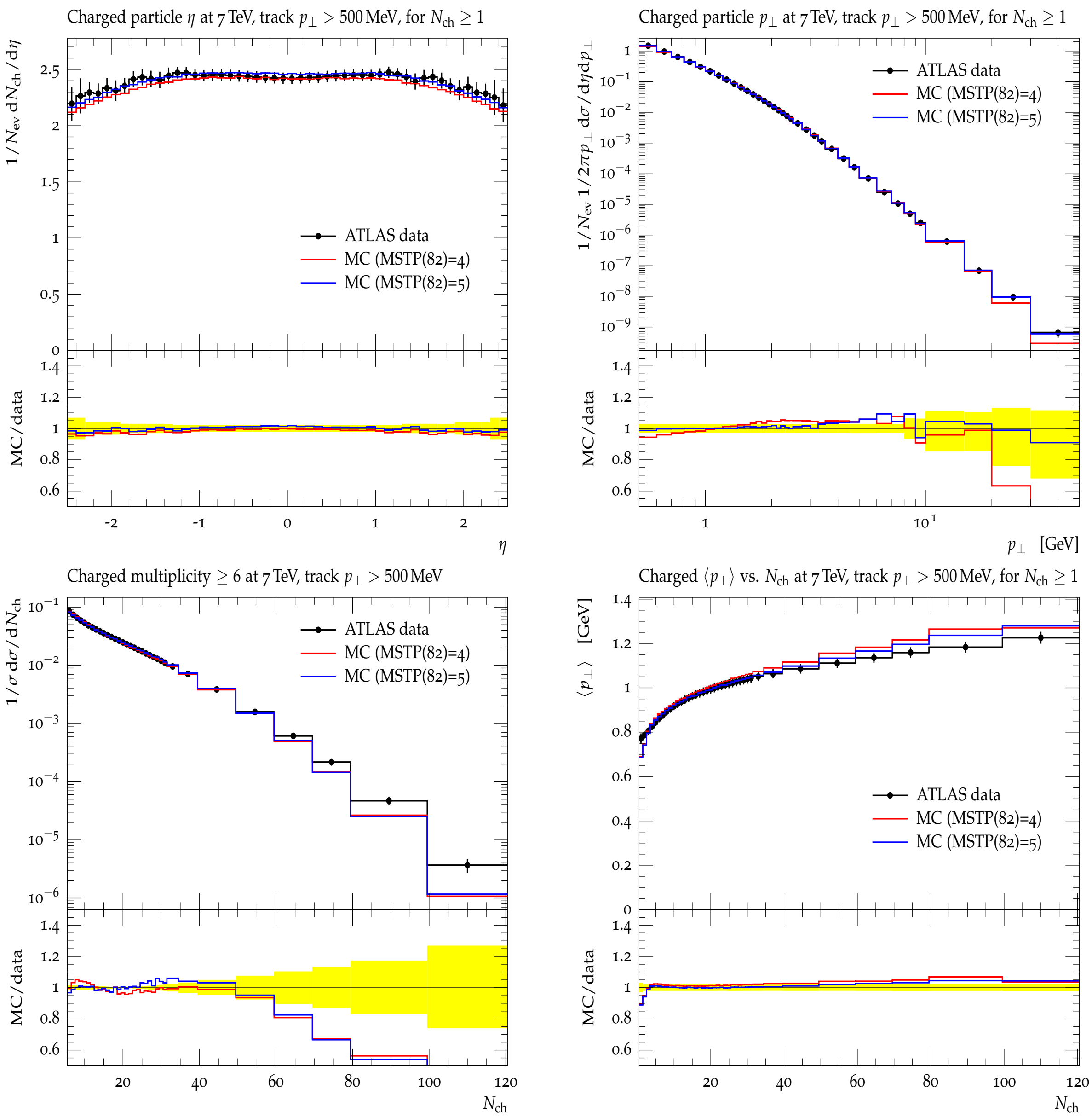

FIGURE 6.3: Comparison plots of tunes with two options for matter distribution to the ATLAS Minimum Bias data using CTEQ5L (LO) PDF set.

6.1.3 Color Reconnections

The switch MSTP(95) gives control over selection of method for color reconnection in the final state. Three choices are studied to see their impact on distributions.

- Model option 1; MSTP(95)=0, no color reconnection
- Model option 2; MSTP(95)=6, with a probability for a string piece to survive the annealing and preserve its original color connections.

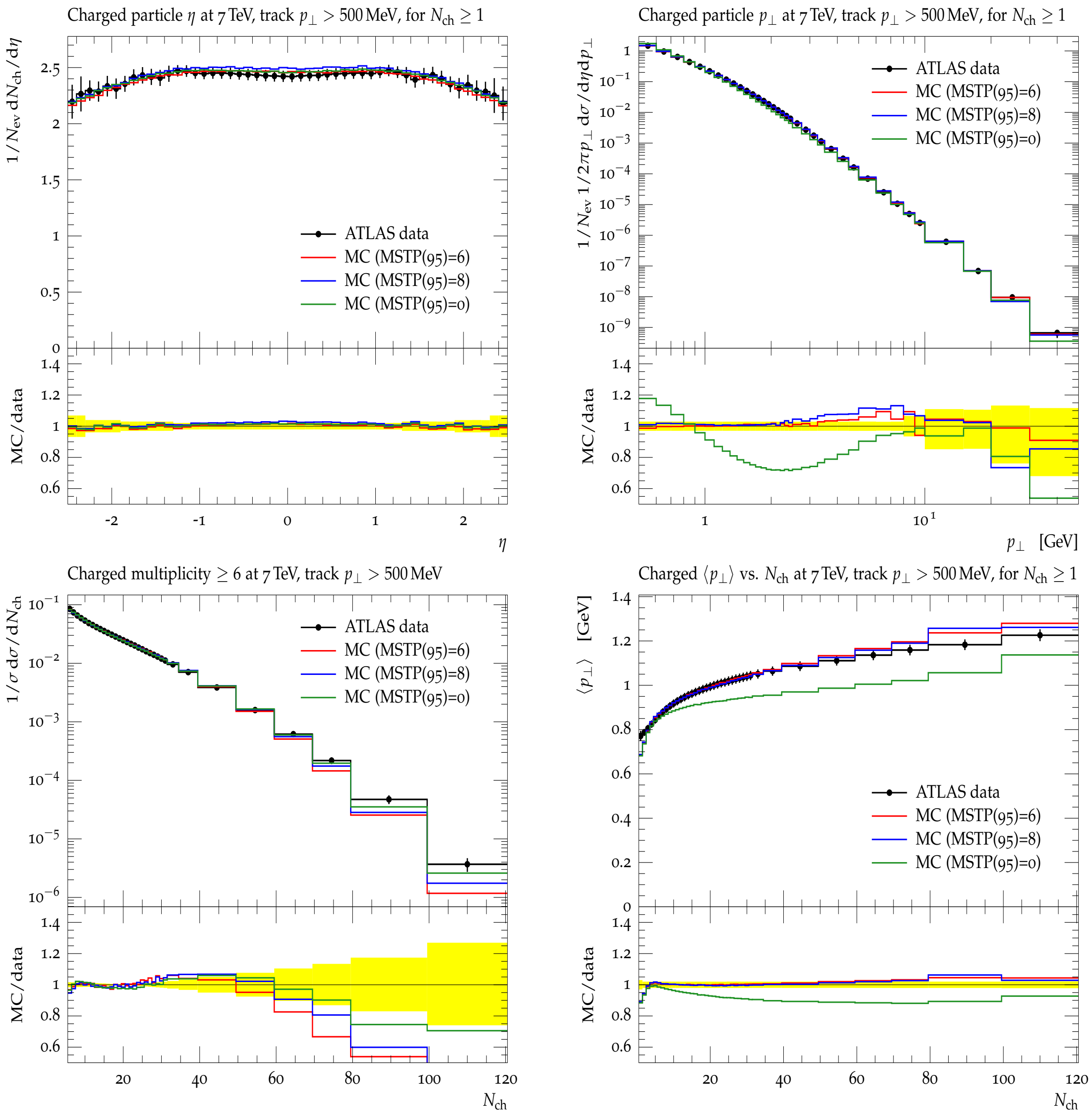

FIGURE 6.4: Comparison plots of tunes with three different option for color reconnections model to ATLAS Minimum Bais data using CTEQ5L (LO) PDF set.

- Model option 3; MSTP(95)=8, reconnection probability calculated for each individual string piece by using the average string density in the rapidity region spanned by that string piece.

The p_t distribution and average p_t vs multiplicity (N_{ch}) appear to be sensitive to the color structure in the final state, within the framework of the PYTHIA6 modeling. The p_t spectrum is too soft and the increase of $< p_t >$ with N_{ch} is too weak when CR is switched off. It is clear from the plots that to describe data CR should be switched on.

The remaining two model choices describe data equally well except at the higher p_t tail where the first choice MSTP(95)=6 seems better than other choice, Figure 6.4.

6.1.4 Λ_{QCD} Treatment

Because of approximations in the perturbative QCD calculations it is quite obvious to have three different Λ values for ME, ISR and FSR to describe data well. PYTHIA6 provides possibilities to select the same Λ_{QCD} in the α_s evolution for ISR, ME and FSR as well as three different values. The switch MSTP(3) gives the control over these possibilities.

- Model option 1; MSTP(3)=2, Λ_{QCD} value is chosen according to the parton distribution functions parameterizations. Then for hard scattering and the initial and final state radiations, the same Λ_{QCD} value is used.
- Model option 2; MSTP(3)=1, Λ_{QCD} values can be chosen by the user.

Figure 6.5 shows the comparison between the two MSTP(3) options. Multiplicity and p_t distributions show that the model with same value of Λ_{QCD} in all parts of event generation is unable to describe data. This fit is done using CTEQ5L PDF, so the value passed to all three Λ is 0.192 GeV. Fit results, Chapter 7, show that to describe data well Λ_{QCD} for FSR must be quite high around 0.5GeV, whereas Λ_{QCD} for ME is lower than 0.192 GeV. The Λ_{QCD} for ISR is not sensitive to the MB data. Because of physics approximations used in event generator like PYTHIA6, it is not possible to describe data with the same value of Λ_{QCD} at different parts of the program. So we used MSTP(3)=1 in the current tunes.

6.2 Parameter study

As the linear parametrization approach is used, the number of simultaneously varied parameters is not a problem. Therefore, thirteen parameters of different models were considered for tuning.

In the following section the parameter study is described to see the impact of these parameters on the observables.

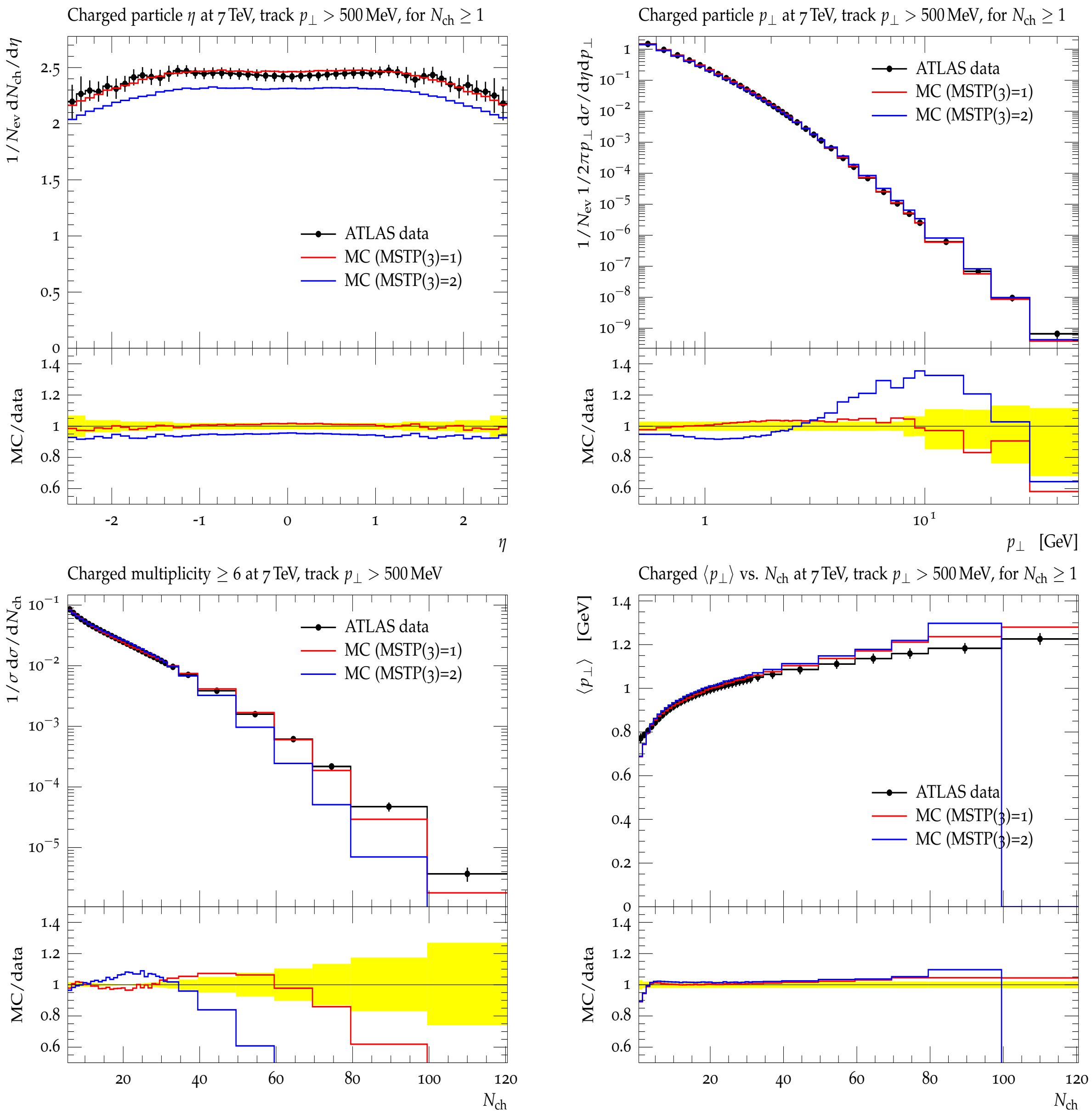

FIGURE 6.5: Comparison plots of tunes with two options for selection of Λ_{QCD} to the ATLAS Minimum Bias data using CTEQ5L(LO) PDF set.

6.2.1 Parameters Correlation

At the end of χ^2 minimization Minuit calculates the correlation between all the tuning parameters using the covariance matrix. Correlation coefficients are given in Table 6.1. The strongest correlation exists between p_{t0} (PARP(82)) and Λ_{ME}(PARP(1)). The next strong correlation is observed between color reconnection parameters, PARP(78) and PARP(77). Remaining parameters are less correlated. This type of study helps to understand the behavior of the free parameters. It has been observed that any strong correlation between parameters sometimes causes an instability.

PARP	82	83	78	77	1	72	90
82	1	-0.589	0.087	0.294	0.949	-0.030	-0.274
83		1	-0.010	-0.141	-0.446	-0.418	0.021
78			1	0.871	0.133	-0.203	-0.365
77				1	0.35	-0.081	-0.404
1					1	-0.167	-0.420
72						1	0.156
90							1

TABLE 6.1: Correlation coefficients for seven MPI parameters as calculated by Minuit

6.2.2 Relative Accuracy

Minuit provides error estimates for each fitted parameter, taking the correlation into account. The ratio of error divided by value (relative error) is an indication of the accuracy of the parameter determination.

Table 6.2 contains relative error of thirteen parameters. It is clear from the table that UE/MPI model parameters p_{t0} and energy evolution have small relative error which means they are well constrained/determined by the data used. The same is true for the matter overlap parameter. Λ_{QCD} parameters, PARP(72) and PARP(1), also have small relative error so treated as adjustable parameters. Λ_{QCD} parameter for ISR, PARP(61), has larger relative error as compared to other two Λ_{QCD} parameters. Color reconnection model parameters have large errors, but this is because of their strong positive correlation between them as listed in Table 6.1. Sensitivity study shows that these parameters are very sensitive to p_t and $< p_t > \ vs.\ Nch$ distributions. We treated only PARP(78) as an adjustable parameter in final tunes.

Parameters related to the beam remnant have much higher error as compared to other parameters, which means that these parameters can not be well constrained by the selected data. So these parameters are kept constant at best fit values obtained from preliminary tunes.

6.2.3 Stability of Parameters w.r.t Distributions

It is important to study the stability of the minimum found with respect to the distributions selected from different data sets from ATLAS, CDFII and CMS as discussed in Section 5.4. Altogether eight parameters are fitted using different combinations of the observables

Parameter	Type	Relative error%
PARP(82)	UE	0.41
PARP(90)	UE	0.25
PARP(83)	UE	0.33
PARP(72)	IFSR	1.1
PARP(71)	IFSR	13.0
PARP(1)	ME	1.5
PARP(61)	ISR	2.6
PARP(67)	ISR	15.0
PARP(91)	BR	2.1
PARP(79)	BR	6.3
PARP(80)	BR	9.7
PARP(78)	CR	2.7
PARP(77)	CR	2.5

TABLE 6.2: Relative error

at three different energies: 0.9TeV, 1.9TeV and 7TeV. While devising the combinations of observables we ensure that parameter sensitivity is not compromised. Figure 6.6 shows the fitted parameter values with respect to the χ^2 values obtained from different observable combinations. It can be seen that PARP(90) and PARP(83) are most stable parameters, whereas PARP(61) seems less stable as its values show more spread w.r.t different χ^2 values.

6.2.4 Λ_{FSR}

One of the key parameters of this tuning from the point of view of improvements in the minimum bias p_t distribution is Λ_{FSR} (PARP(72)). Its value to describe pp data is quite different from e^+e^- value. pp data prefer higher values of this parameter. Figure 6.7 shows both shape and normalization is better described by higher values of Λ_{FSR}. It is clear from the plots that the value obtained from e^+e^- data (= 0.26 GeV)is unable to describe p_t distribution in both low as well as high p_t region. The higher value of Λ_{FSR} also preferred by ATLAS and CDF jet shape data.

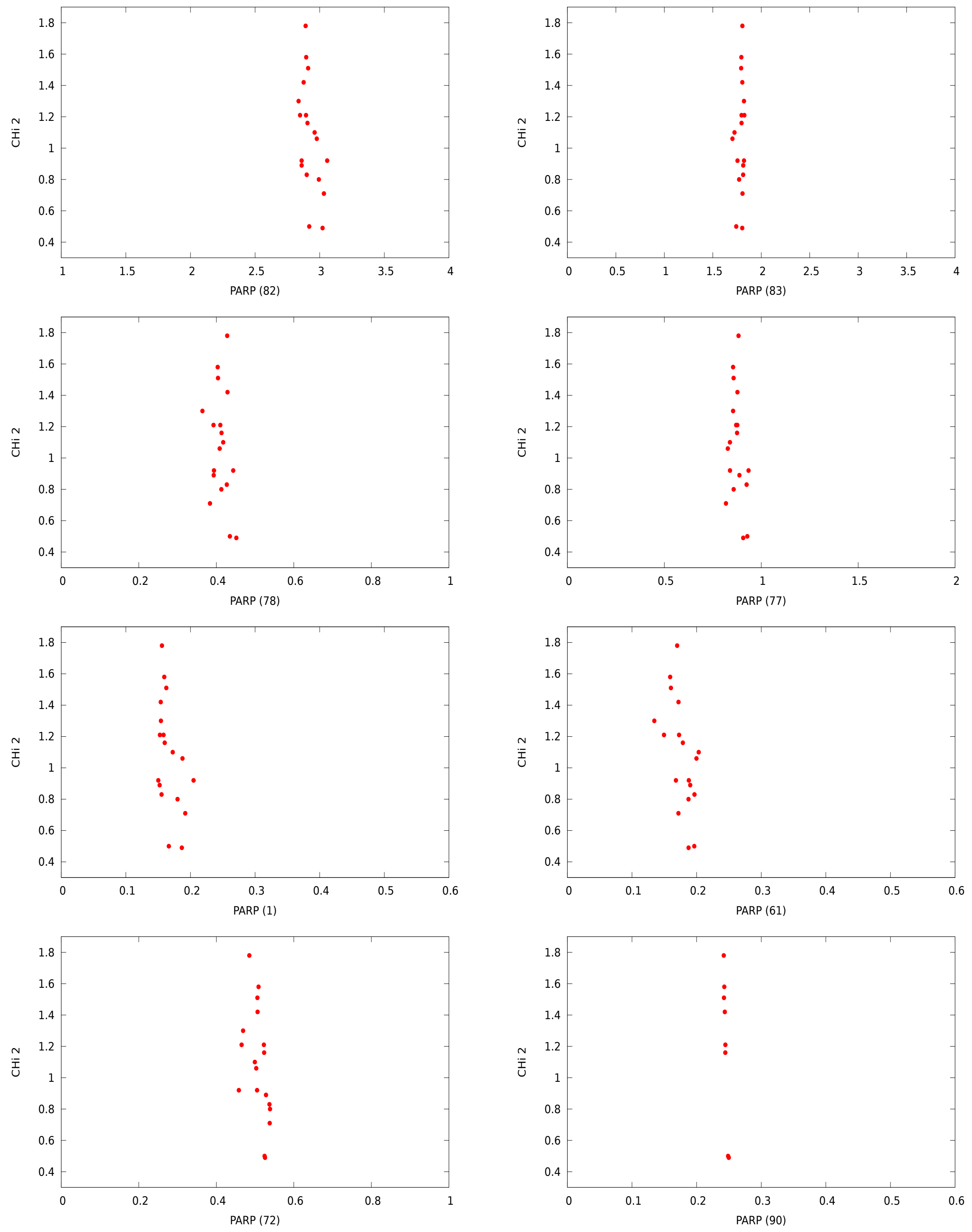

FIGURE 6.6: Stability plots of eight parameters w.r.t χ^2/N_{df} obtained from different distribution combinations

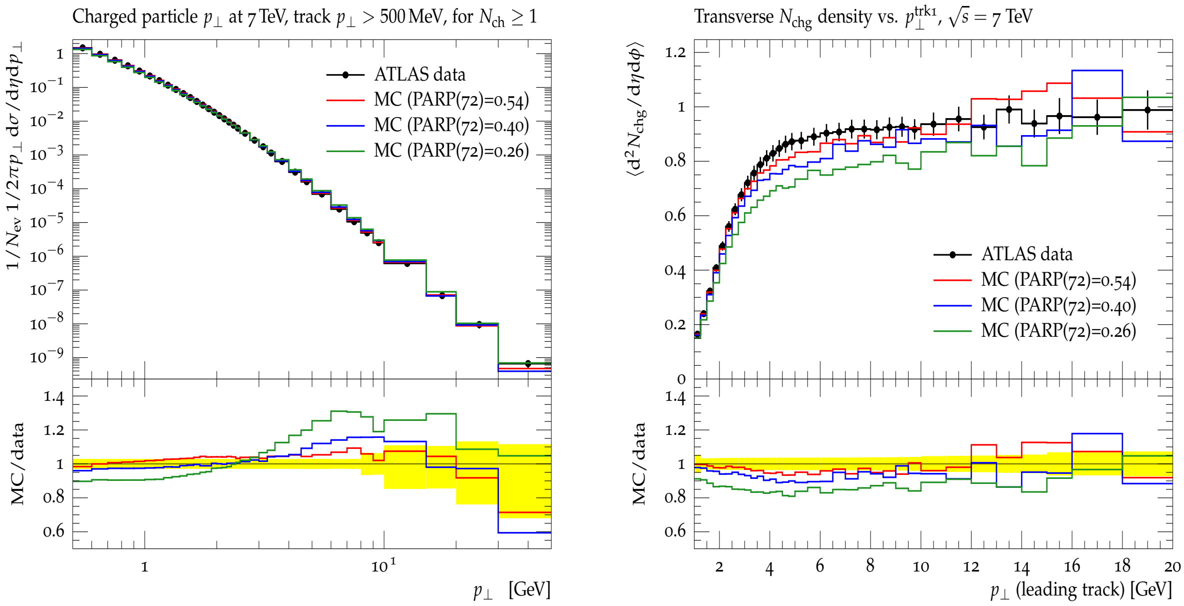

FIGURE 6.7: Effects of Λ_{FSR}

6.2.5 Sensitivity

It is desirable to tune those parameters which are sensitive to the selected observables. It is important that if a parameter has no effect on an observable at all then the minimizer very likely yields useless results. Sensitivity is defined as how strongly/weakly a parameter affects the observables. This study is done by fixing all parameters at best fit value and then each parameter is varied at a time.

- PARP(82):
  This is MPI cut off parameter described in Section 5.3.3. It is strongly constrained by the minimum bias and underlying event data having relative error of 0.41%. It affects average multiplicity, higher value results in lower multiplicity. It also affects the underlying event number densities in all three regions but transverse region is more sensitive as shown in Figure 6.8. It affects transverse $\sum p_t$ but there is very little or no effect observed in the two other regions, see Figure 6.9. It is strongly correlated $\sim 95\%$ with Λ_{ME}, PARP(1). The correlation between these parameters is positive. Because of its sensitivity, this parameters is treated as an adjustable parameter in the final tunes.

- PARP(90):
  It is described in Section 5.3.3, it gives energy evolution of PARP(82), and thus should be treated as an adjustable parameter when data at more than one energy

are used. It is also well constrained by the selected data with the relative error of 0.25%.

- PARP(83):
  It is described in Section 5.3.3.1. It influences the shape of the multiplicity distribution and is well constrained by minimum bias data with relative error of 0.33%. Because of its sensitivity we include PARP(83) in the list of adjustable parameters in the final tunes.

- PARP(1):
  It is very sensitive parameter and well constrained by the selected data having relative error of 1.5% given in Table 6.2. It has a strong positive correlation with PARP(82) as shown in Table 6.1. This parameter strongly affects the average multiplicity and p_t distribution. Preliminary tunes show that this parameter is very sensitive to the chosen PDF type so it is considered as an adjustable parameter for final tunes.

- PARP(72):
  This is one of the sensitive parameters we considered as tuneable parameters with relative error of 1.1% shown in Table 6.2. It is sensitive to p_t distribution and also affects underlying event number densities. Figure 6.7 shows that lower value of PARP(72) causes a decrease in p_t spectrum for $p_t < 3$GeV, above 3GeV MC overshoots the data for same value. Figure 6.7 also shows plot for underlying event density in the transverse region, it is seen MC undershoot the data with lower value of this parameter and vice versa. It has no significant correlation with other parameters but preliminary tunes show that it also very sensitive to the PDF type. So this parameter is treated as an adjustable parameter in final tunes.

- PARP(78):
  It is a color reconnection parameter and very sensitive to the average p_t vs N_{ch} distribution with relative error of 2.7%. This large error is a result of its strong correlation with PARP(77). These parameters have second strong correlation after PARP(82) and PARP(1). Its strong correlation with PARP(77) also causes instabilities in fit results, but because of its sensitivity to average p_t vs N_{ch} distribution we considered it as tuneable parameter in final fits.

- PARP(77):
  It is also a color reconnection parameter and strongly correlated with PARP(78) as described above, it affects p_t distribution. It has large relative error of 2.5%, shown

in Table 6.2, because of the same reason given above. Their strong correlation causes instability in the fit results so we fix this parameter at best value of 0.90 for all PDF sets in the final tune.

- PARP(61):
  It is weakly constrained by the selected data having relative error of 2.6% given in Table 6.2. It caused instability in the fit results so we fixed it at best fit value of 0.19 for all PDFs in the final tunes.

It can be seen in Table 6.2 that the parameters related to the beam remnant and ISR are not very well constrained by the observable tuned to. So these parameters are fixed at best values obtained from preliminary tunes. All MC sets generated for the final tunes have eight variable parameters. But for the reasons given above, two of them, PARP(61) and PARP(77), are held constant at 0.19 and 0.90, respectively, in the final tunes.

6.3 Diffraction Treatment

Since diffractive events have not been subtracted in the measurement, one cannot use the distributions for a direct comparison to theory predictions without a reliable diffractive model. Currently, there is no fully reliable model of diffractive events available in any Monte Carlo event generator including PYTHIA6. We consider two options to investigate the effects of diffractive scattering in PYTHIA6 framework. The switch MSEL provides options to select between full user control and some preprogrammed alternatives.

- MSEL=1 All processes are used mentioned in Table 5.3 other than diffractive scattering.
- MSEL=2 All processes are used mentioned in Table 5.3 including diffractive scattering.

To study the effects of two above mentioned options we used two data sets from ATLAS experiment

- Data including diffractive events, $N_{ch} \geq 1$ in the kinematic range $\mid \eta \mid < 2.5$ and $p_t > 500$ MeV

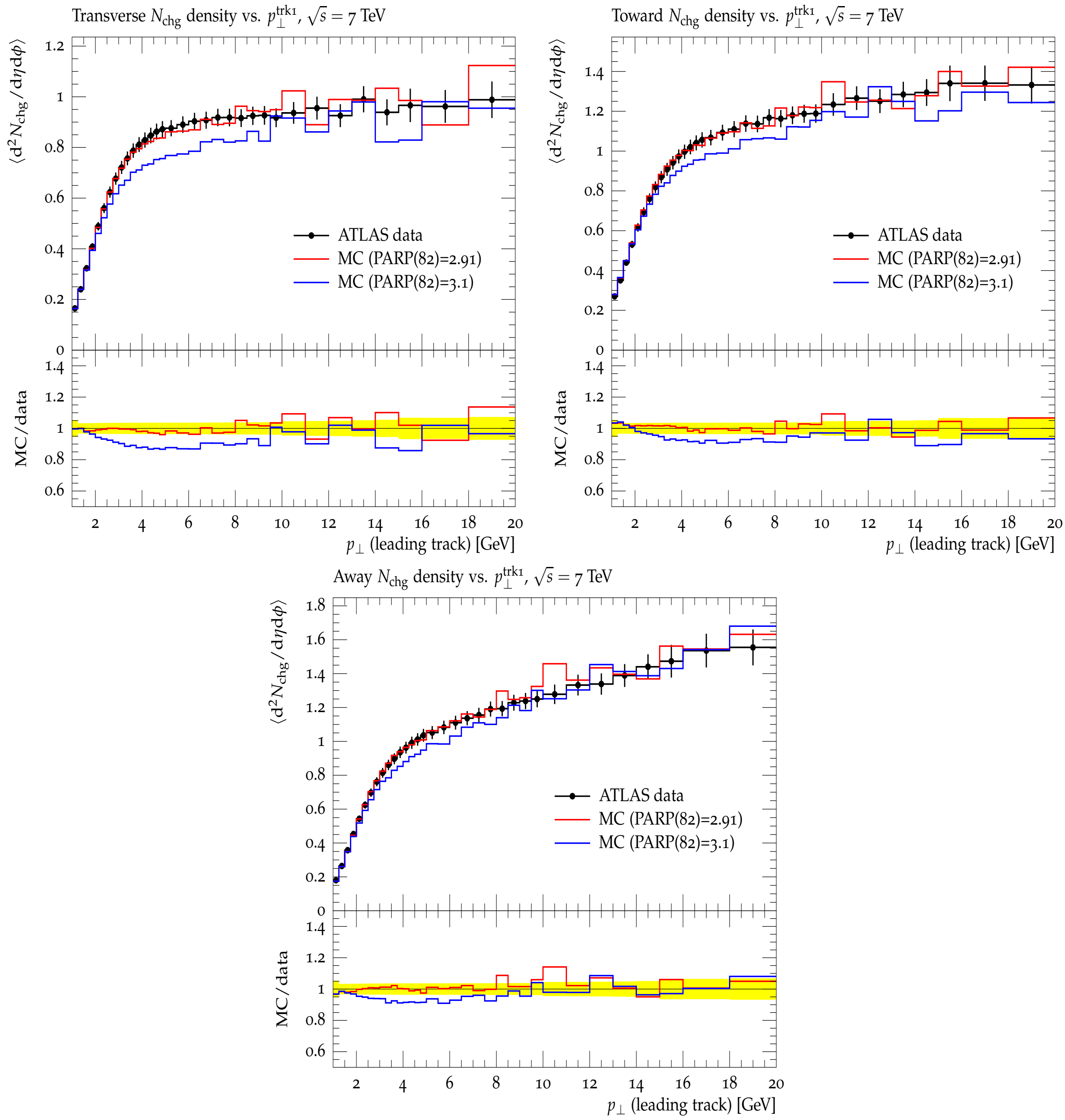

FIGURE 6.8: Comparison plots of PYTHIA6 tunes to the ATLAS UE distribution, charged particle densities vs $p_{t,lead}$ for three regions at $\sqrt{s} = 7TeV$ for two different values of PARP(82).

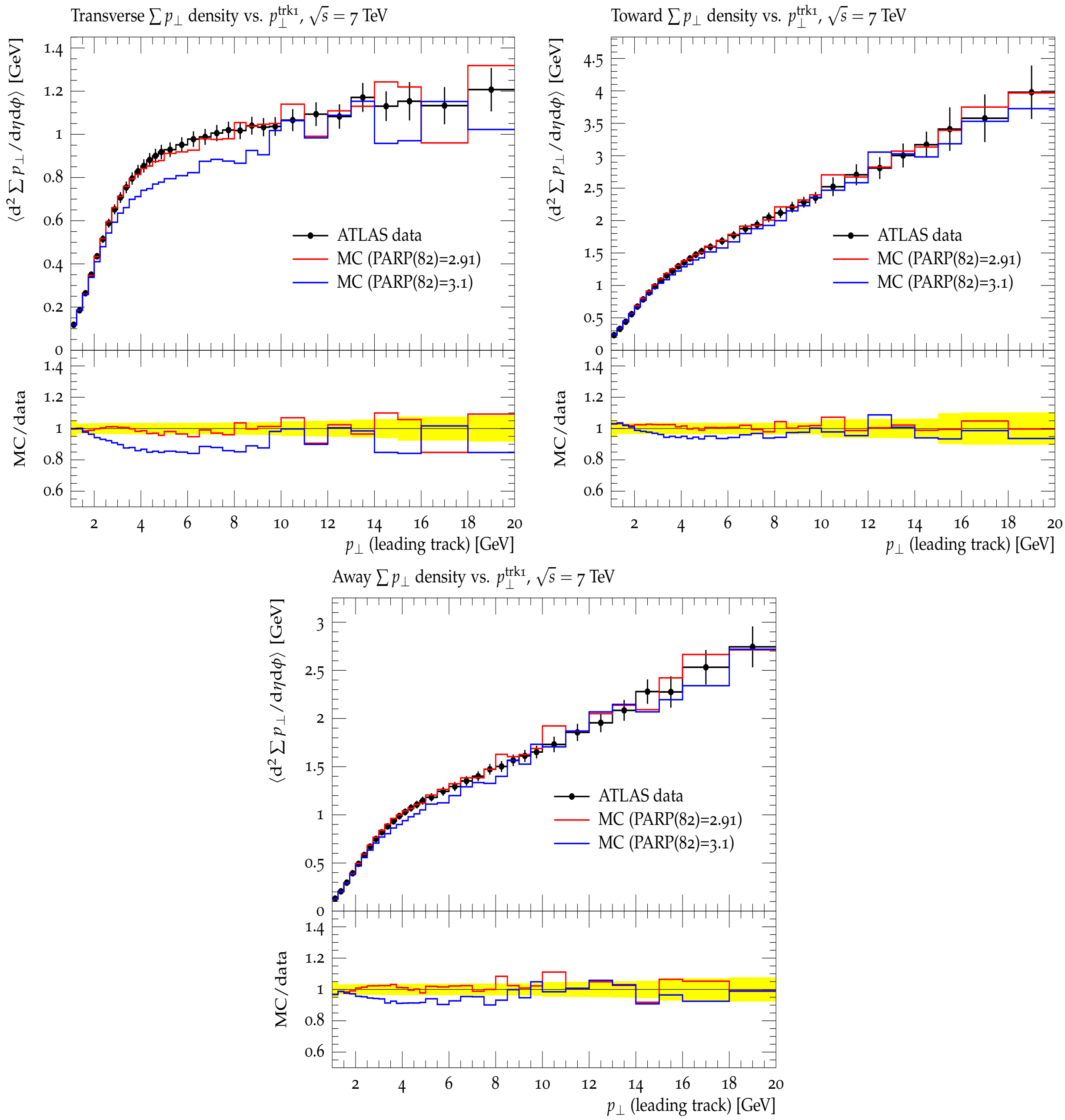

FIGURE 6.9: Comparison plots of PYTHIA6 tunes to the ATLAS UE distribution, sum p_t densities vs $p_{t,lead}$ for three regions at $\sqrt{s} = 7TeV$ for two different values of PARP(82).

- Data with suppressed diffractive events, $N_{ch} \geq 6$ in the kinematic range $\mid \eta \mid < 2.5$ and $p_t > 500$ MeV

Figures 6.10 and 6.11 show the two options for both data. It can be seen that diffraction suppressed data can be described without including diffractive scattering but when data used with diffraction MC predicts more activity than data requires. For average p_t vs N_{ch} distribution the difference can only be observed at low multiplicity where diffraction dominates $N_{ch} \leq 6$.

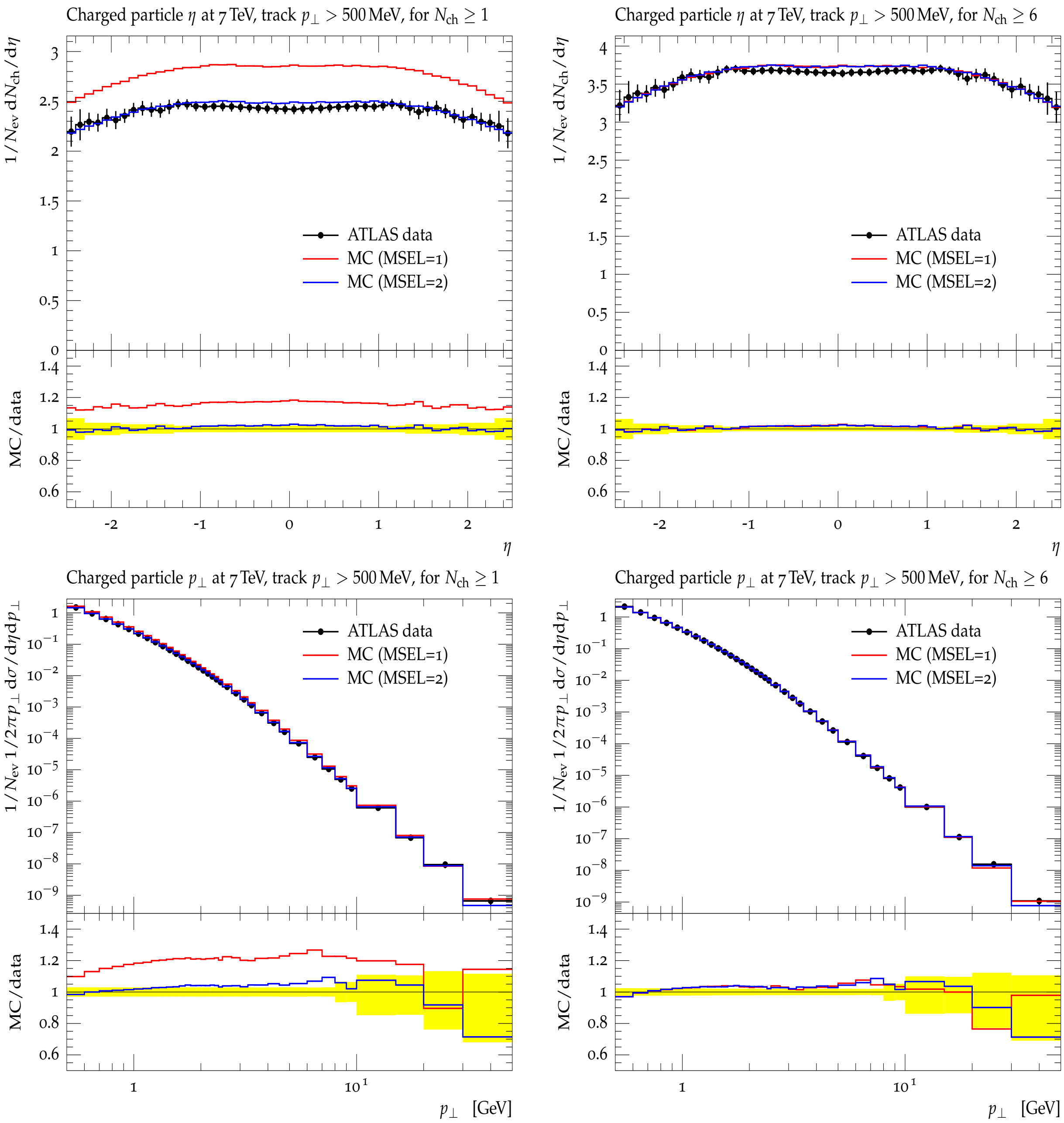

FIGURE 6.10: Comparison plots of tunes with two different options of MSEL to the ATLAS minimum bias data using CTEQ5L PDF set.

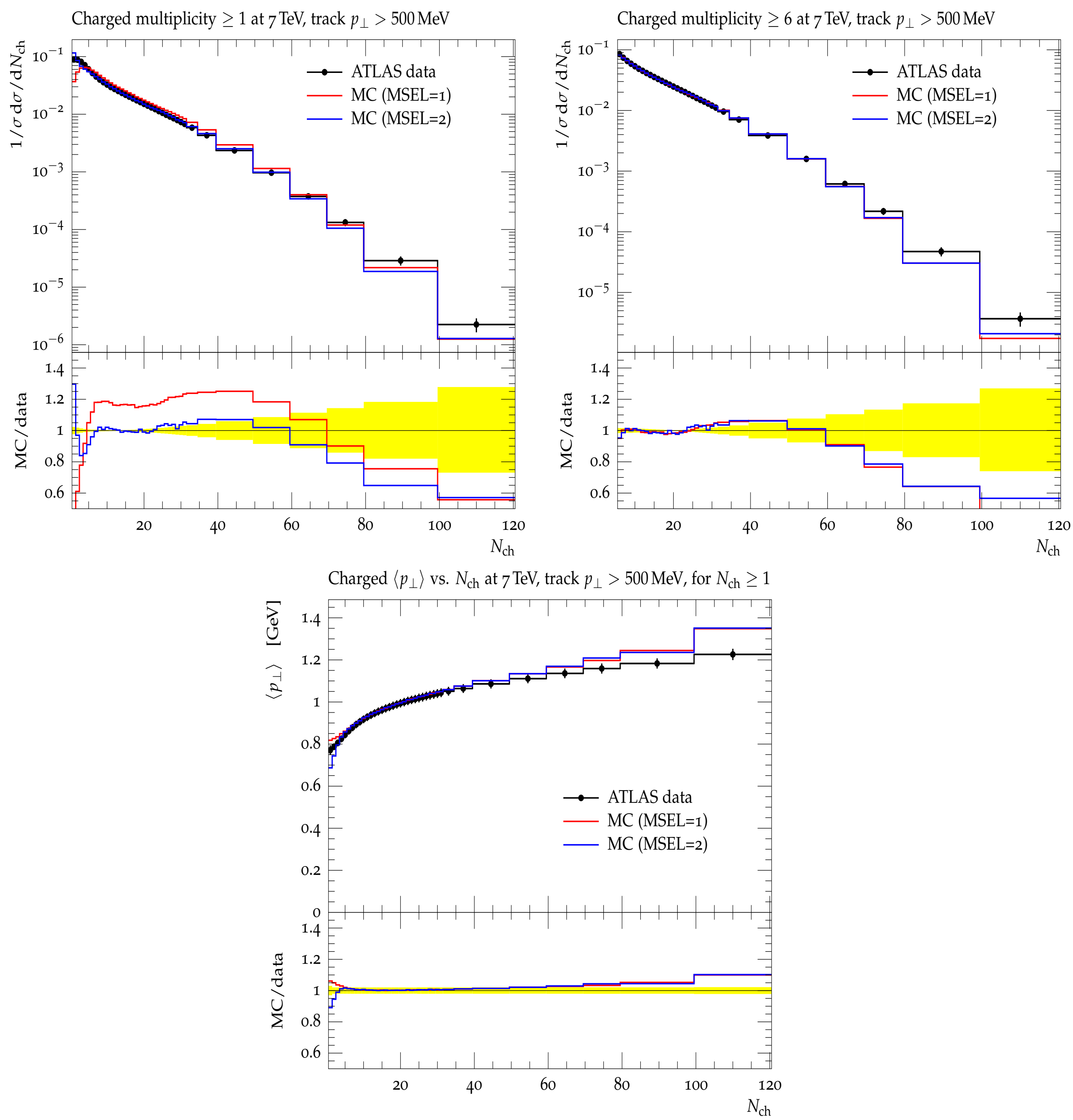

FIGURE 6.11: Comparison plots of tunes with two different options of MSEL to the ATLAS minimum bias data using CTEQ5L PDF set.

Chapter 7

Final Tunes

The set of data distributions chosen for the final fits has been discussed in Section 5.4 and is listed in Tables 5.6 and 5.7. We attempt a combined MB and UE tuning since the physics implemented in the MC event generator should describe the aspects of both the general inelastic processes (Minimum Bias) and the Underlying Event using a single set of parameter values. Six tuning parameters are selected for the final fits, including three parameters of the MPI model, one of the CR model and two Λ_{QCD} parameters. These were found to be very sensitive to the chosen data distributions, as discussed in Chapter 6. It is well known that Parton Density Functions (PDF) of LO, modLO and NLO type differ from each other, as well as PDF's of same type but from different collaborations. For example, in the kinematic region relevant for the generation of inelastic events (low-x, low-Q^2) the gluon density at NLO is lower than at LO. When combined with LO $2 \to 2$ scattering matrix elements, event properties are different. Therefore, the above six model parameters are tuned separately for each PDF.

The final tunes are the result of a long process, starting from previous knowledge, adding more data when becoming available, adding more parameters to the list of variable parameters and doing several iterations of the central points. The final results were checked by one or two more iterations depending on possible instabilities encountered.

7.1 Tuning Results and their PDF-dependence

The fitted parameter values and the overall $\chi^2/N_{dof}(N_{dof} = 1166)$ for nine PDF sets (listed in Table 5.2) are given in Tables 7.1 to 7.3. The overall fit quality is reasonably good for all the PDF-sets. In the following, the parameters are discussed one-by-one.

The values of MPI regularization parameter, p_{t0}, range between 2 and 3GeV with the lowest values coming from NLO PDF's. Non zero positive values are required for the energy power, ε, in order to fit the E_{cm}-dependence of particle multiplicities. As for p_{t0}, the lowest values of ε result from NLO PDF's. This clustering by PDF type is well visible from the PARP(90) vs PARP(82) plot, Figure 7.2.

The values for the matter overlap parameter, d_{MO}, are roughly in the range 1.8-1.9, and thus indicate that the matter overlap function is closer to a Gaussian than to an exponential.

The probabilities for color reconnection, P_{CR}, are large, between 0.4 and 0.6, but have to be seen in conjunction with the relatively large CR suppression parameter, PARP(77)=0.90 GeV^{-1}.

Rather large values are found for the Λ_{FSR} parameter, roughly in the range 400-700 MeV. This parameter should in principle be determined from jet properties of high-p_t jets in pp collisions. A fit to ATLAS jet shapes [6] yields 450 MeV, falling into the above range. In contrast, the value obtained from $e^+e^- \rightarrow$ jets, 260MeV, is too small and does not describe minimum bias data, as already demonstrated in Figure 6.7.

New and interesting results are obtained for the QCD parameter Λ_{ME}. While the fits with LO and NLO PDF's give reasonable values, 150-200 MeV, those with modLO PDF's are very low, about 60-80 MeV. As can be seen from the parameter errors in the Tables 7.1 to 7.3, the difference is very significant. These lower values must be related to the properties of the MC-adapted PDF's. This issue will be further discussed in Chapter 8. The two dimensional PARP(1) vs. PARP(82) plot, Figure 7.2, nicely shows this clustering by PDF type.

When attempting to perform separate fits to MB and UE data, it is observed that the errors on the parameters come out a factor 2-3 smaller in the MB fits compared to the UE fits, which shows that the combined fits are dominated by the MB data. This issue will be further discussed in Chapter 8.

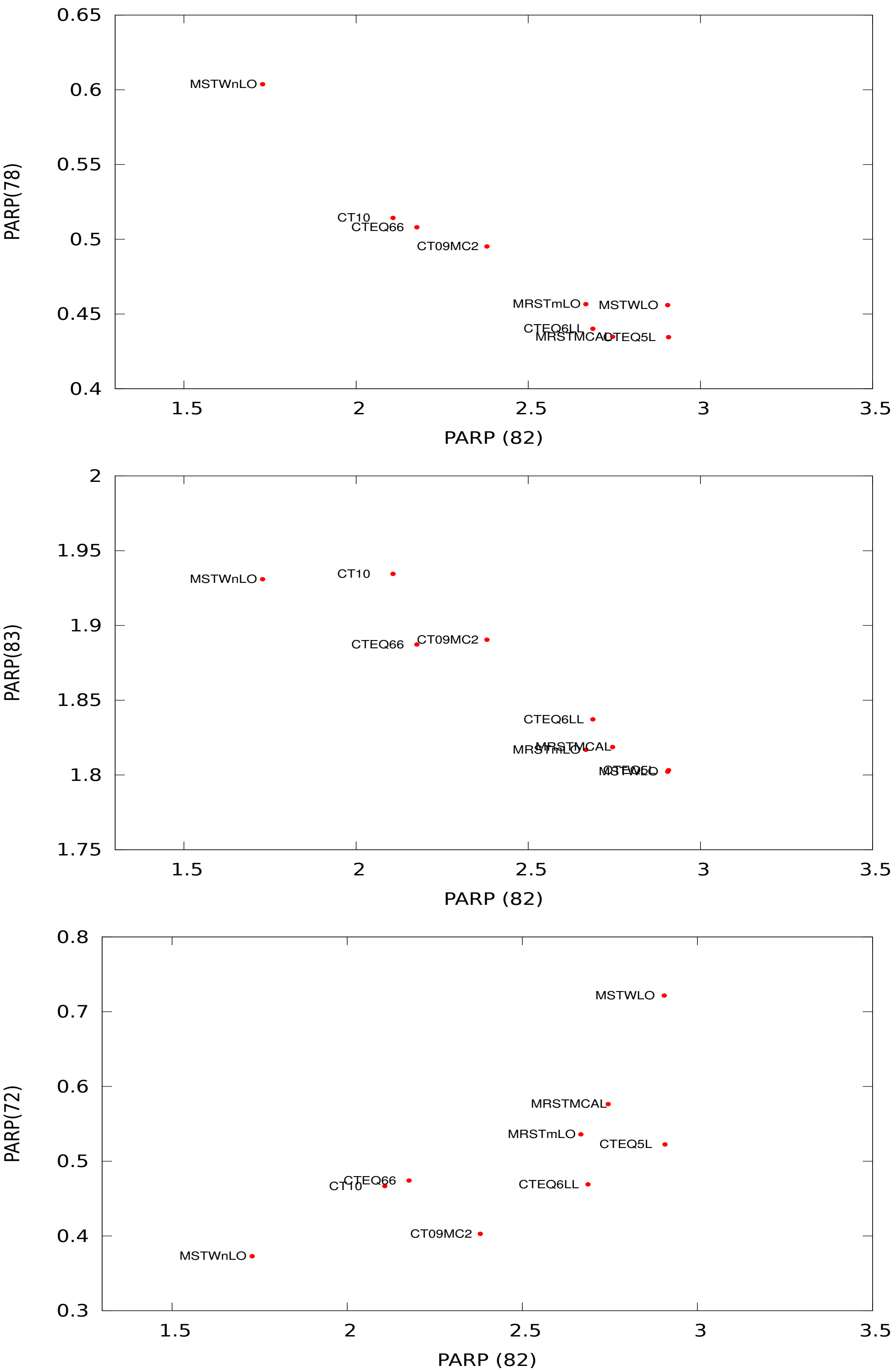

FIGURE 7.1: PDF dependence of PARP(78), PARP(78) and PARP(72) w.r.t PARP(82)

Parameter	Symbol	CTEQ5L	CTEQ6LL	MSTW2008
PARP(82)	pt_0	2.912 ±0.010	2.687 ±0.009	2.905 ±0.009
PARP(90)	ε	0.245 ±0.001	0.217 ±0.001	0.283 ±0.001
PARP(83)	d_{MO}	1.802 ±0.005	1.837 ±0.006	1.802 ±0.007
PARP(78)	P_{CR}	0.427 ±0.003	0.440 ±0.003	0.456 ±0.004
PARP(1)	Λ_{ME}	0.160 ±0.002	0.154 ±0.002	0.197 ±0.002
PARP(72)	Λ_{FSR}	0.524 ±0.006	0.476 ±0.006	0.721 ±0.01
χ^2/N_{dof}		1.17	1.29	1.23

TABLE 7.1: Tuning result of combined fit for three Leading order PDF sets

Parameter	Symbol	MRSTMLO	MRSTMCAL	CT09MC2
PARP(82)	pt_0	2.667 ±0.010	2.690 ±0.009	2.380 ±0.009
PARP(90)	ε	0.231 ±0.001	0.221 ±0.001	0.206 ±0.001
PARP(83)	d_{MO}	1.817 ±0.006	1.835 ±0.006	1.890 ± 0.007
PARP(78)	P_{CR}	0.457 ±0.003	0.446 ±0.003	0.495 ± 0.004
PARP(1)	Λ_{ME}	0.086 ±0.001	0.067 ±0.001	0.061 ± 0.001
PARP(72)	Λ_{FSR}	0.536 ±0.006	0.548 ± 0.006	0.402 ± 0.005
χ^2/N_{dof}		1.06	1.16	1.24

TABLE 7.2: Tuning result of combined fit for three Modified Leading order PDF sets

Parameter	Symbol	CTEQ66	CT10	MSTW2008NLO
PARP(82)	pt_0	2.176 ±0.008	2.107 ±0.010	1.728 ±0.009
PARP(90)	ε	0.178 ±0.001	0.170 ±0.001	0.177 ±0.001
PARP(83)	d_{MO}	1.887 ±0.006	1.934 ±0.006	1.931 ±0.006
PARP(78)	P_{CR}	0.508 ±0.004	0.514 ±0.003	0.604 ±0.005
PARP(1)	Λ_{ME}	0.177 ±0.002	0.178 ±0.002	0.153 ±0.002
PARP(72)	Λ_{FSR}	0.474 ±0.006	0.467 ±0.006	0.373 ±0.004
χ^2/N_{dof}		1.13	1.17	1.18

TABLE 7.3: Tuning result of combined fit for three Next-to-Leading order PDF sets

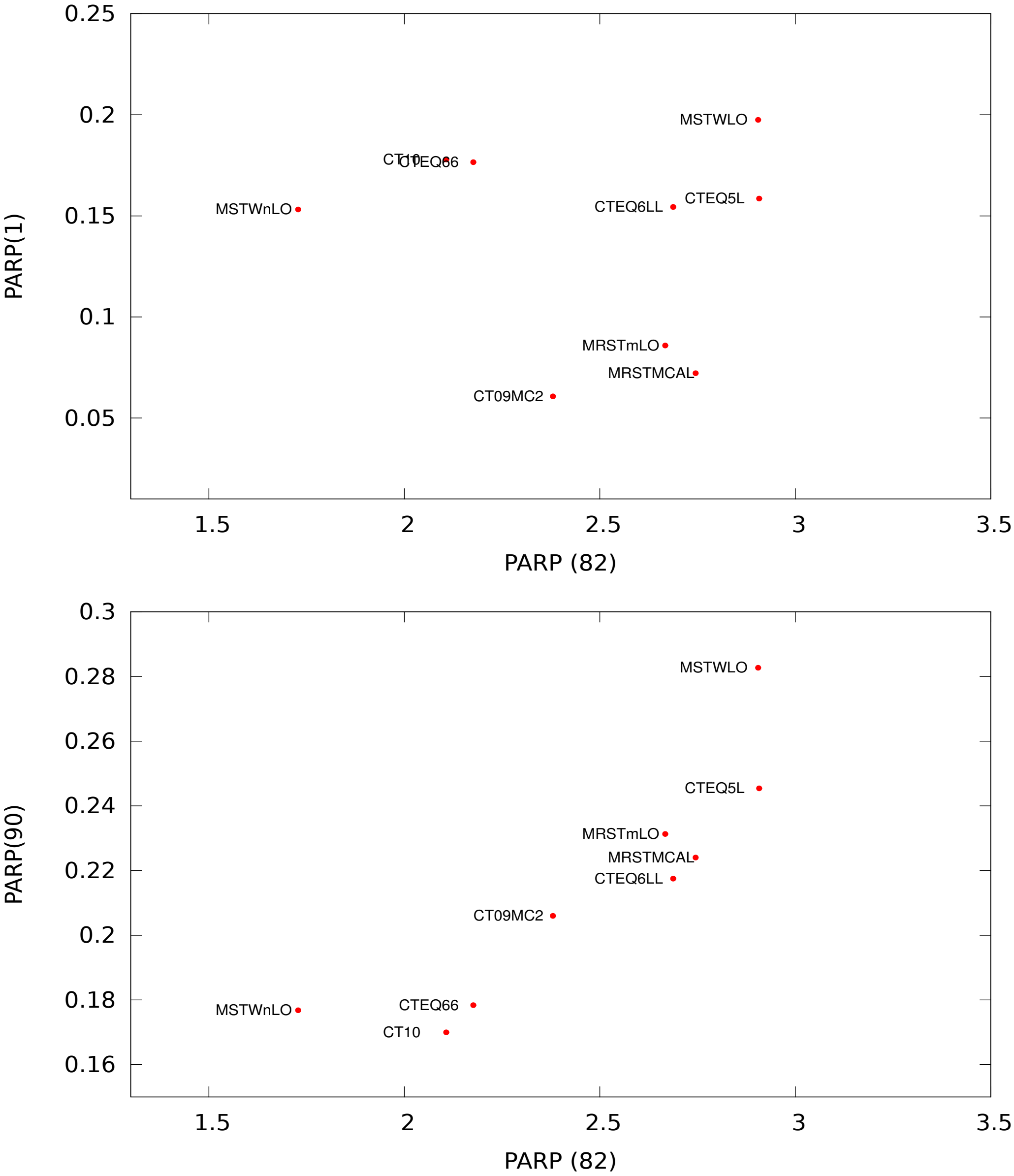

FIGURE 7.2: PDF dependence of PARP(1) and PARP(90) w.r.t PARP(82)

7.2 Comparison to Experimental Data (Used in Tuning)

In this section the combined tuning results are compared to the experimental data distributions which were used in the tuning. The plots are generated with RIVET software [28]. For better visibility, only one PDF set of each of the 3 classes (LO, modLO, NLO) is randomly selected.

7.2.1 ATLAS Minimum Bias Data, PS1

The pseudo-rapidity distribution as shown in Figure 7.3 agrees very well with data, both in shape and normalization. The central particle density around $\eta = 0$ shows the increase of average particle multiplicity with center-of-mass energy, E_{cm}, between 0.9 and 7TeV.

The MC models show good agreement with data over a wide range of charged particle multiplicities, Figure 7.4. The diffractive contribution, confined to low multiplicities, $1 \leq N_{ch} \leq 5$, is not well modeled by PYHTIA6. This region was thus excluded from the fits. Including it would only increase χ^2 , but not alter the fitted parameter values.

All three PDF's undershoot the high-N_{ch} tail, N_{ch} >60, at 7TeV, but this deviation is not very significant ($< 3\sigma$). The last bin (100-120) was not used in the fits.

The differential distribution of transverse momentum, $dn/(p_t.dp_t)$, is seen to be very well described by all 3 types of PDF, Figure 7.5, which is remarkable as the distribution falls by 7 orders of magnitude across the range 0.5 - 20 GeV. The data points above 20GeV, for 7 Tev, were not used in the fits. This good description, in particular for the modLO PDF, has not been achieved by any of the published ATLAS tunes [36, 34].

Figure 7.6 shows $< pt >$ as a function of N_{ch}. The rising trend is well reproduced by all three PDF's over a wide range , though slightly too much for the higher multiplicities, $N_{ch} > 60$. As for the N_{ch} distribution, the last bin (100-120) was not used in the fits, due to insufficient MC statistics.

7.2.2 ATLAS MB PS3: Diffraction Limited Phase space

This phase space differs from PS1 in that events with $N_{ch} < 6$ are removed. From the η, N_{ch} and p_t distributions, Figures 7.7, 7.8 and 7.9, it can be seen that the data are quite well described by all three PDF's apart from some discrepancies for p_t >3 GeV at 0.9TeV. The same holds what has been said about PS1 in the previous section.

7.2.3 ATLAS Underlying Event Data

ATLAS measurements of charged particle number (N_{ch}) and Σp_t densities as a function of the p_t of the leading track for three azimuthal angle regions (transverse, toward, away) and for both energies, 0.9 and 7TeV, are shown in Figures 7.10, 7.11, 7.12 and 7.13. While

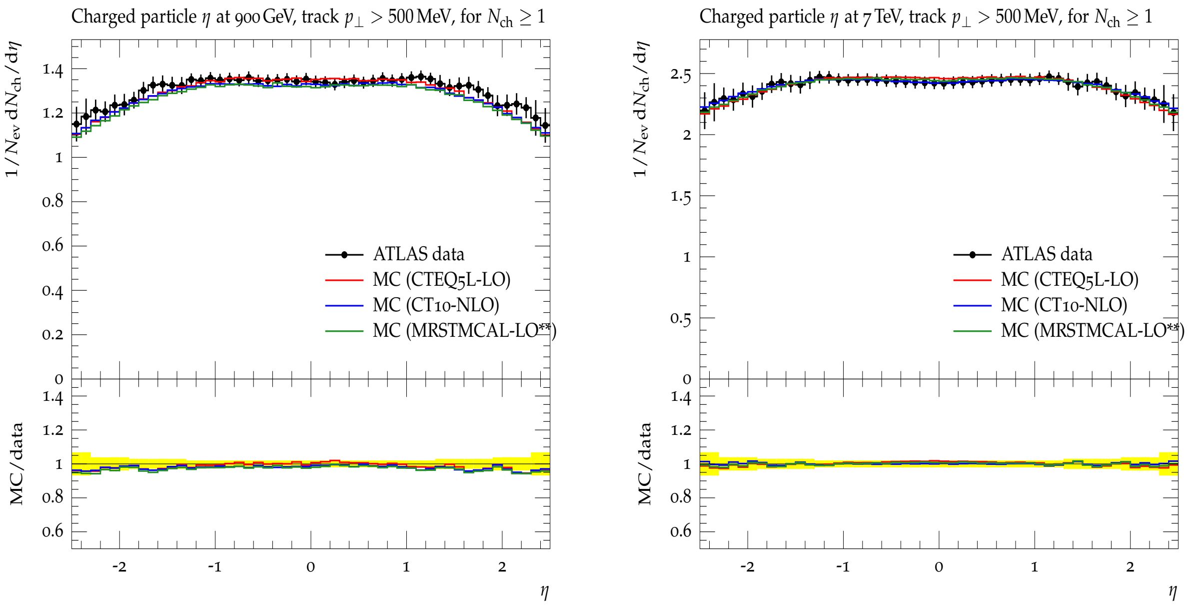

FIGURE 7.3: Comparison plots of PYTHIA6 tunes to the ATLAS pseudorapidity distribution for events with $N_{ch} \geq 1$, pt> $500MeV$, $|\ \eta\ | < 2.5$ at $\sqrt{s} = 0.9$ and 7TeV.

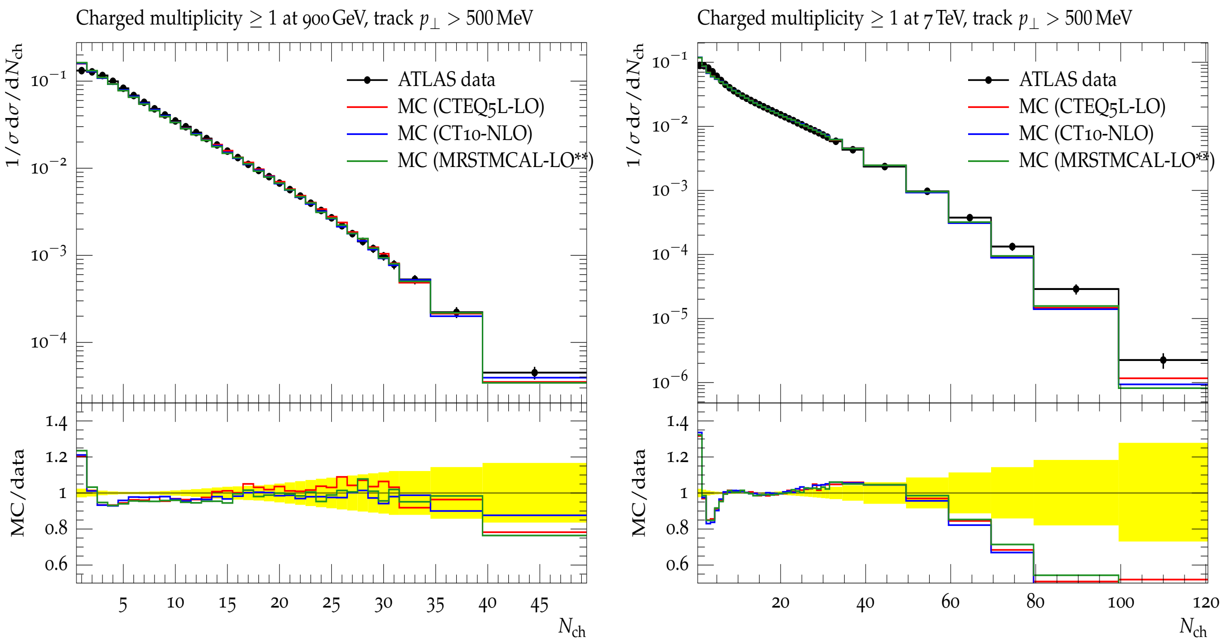

FIGURE 7.4: Comparison plots of PYTHIA 6.4 tunes to the ATLAS Charged-particle multiplicities for events with $N_{ch} \geq 1$, pt> $500MeV$, $|\ \eta\ | < 2.5$ at $\sqrt{s} = 0.9$ and 7TeV.

the turn-on region of the transverse densities is well described by the PYTHIA6 tunes, they are systematically low in the plateau region. The discrepancy is about 10% for 0.9 TeV. At 7TeV, the number density is low up to 7% and the Σp_t density is low by up to 10% in the $p_{t,lead}$ region 4-10 GeV.

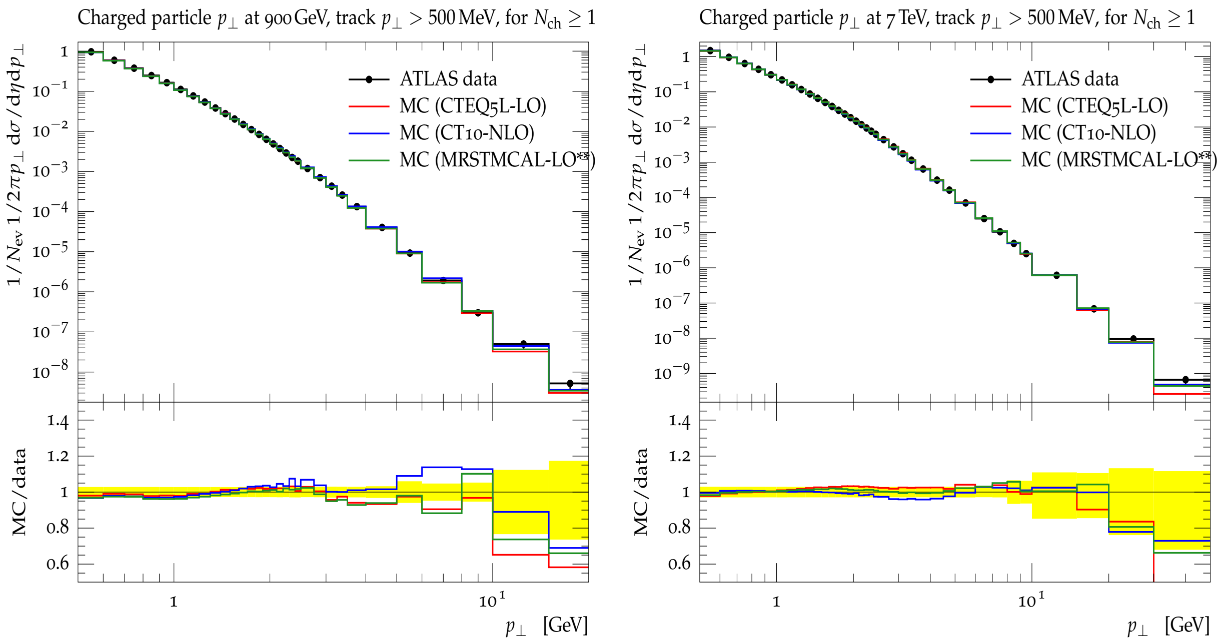

FIGURE 7.5: Comparison plots of PYTHIA 6.4 tunes to the ATLAS charged-particle multiplicities as a function of the transverse momentum for events with $N_{ch} \geq 1$, pt$> 500MeV$, $\mid \eta \mid < 2.5$ at $\sqrt{s} = 0.9$ and 7TeV.

7.2.4 CDF run II MB Data

This measurement of $< p_t >$ vs. N_{ch}, performed in $p\bar{p}$ collisions at $\sqrt{s}$=1.96 TeV is very well described by PYTHIA6 tunes as shown in Figure 7.18, and represents a third center-of-mass energy point in the tuning process. The data points above N_{ch} =30 were not included in the fits. The comparison between the tunes and the data is shown in Figure 7.18.

7.3 Predictions to Experimental Data (Not Used in Tuning)

In this section, the combined MB+UE tunes given in Section 7.1 are compared to measurements not used in tuning.

7.3.1 ATLAS MB Data: PS4

The η, N_{ch} and p_t distributions at 7TeV for the p_t >100 MeV analysis are shown in Figure 7.19, together with the MC predictions of three PDF's. The problematic region

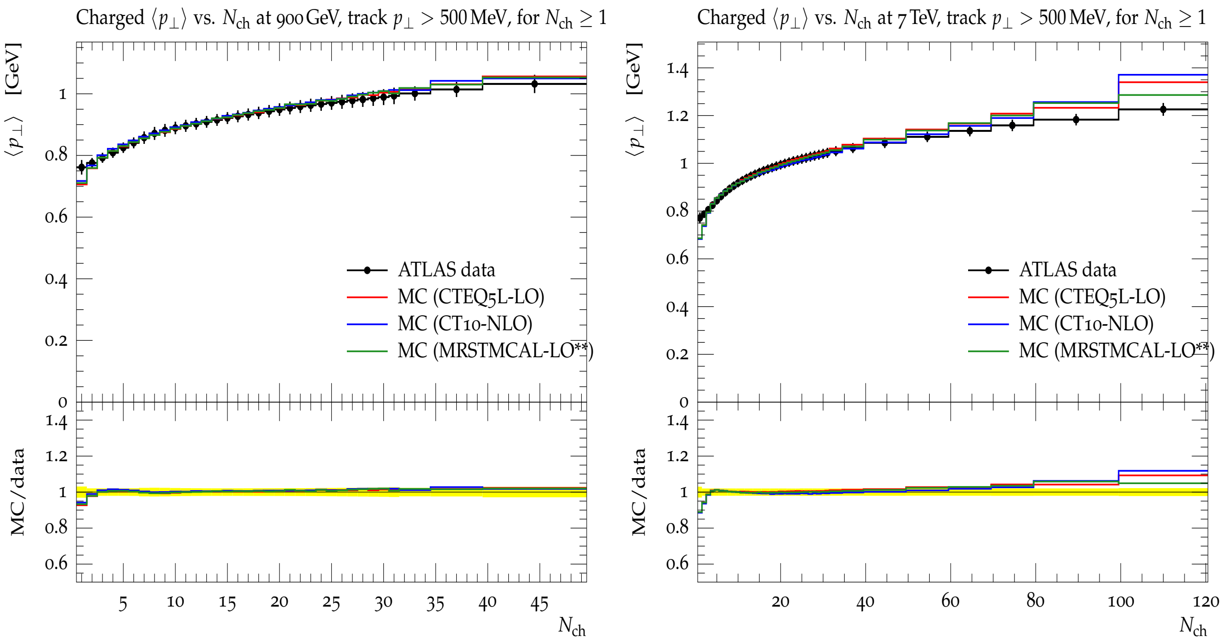

FIGURE 7.6: Comparison plots of PYTHIA6 tunes to the ATLAS average transverse momentum as a function of number of charged particles in the event for events with $N_{ch} \geq 1$, pt> $500MeV$, $\mid \eta \mid< 2.5$ at $\sqrt{s} = 0.9$ and 7TeV.

is 100< p_t <500 MeV where predicted charged particle rates are low by up to 30%. The overall multiplicity is too low by about 9%, and the MC models fail to describe the high-N_{ch} tail. These discrepancies, known already from [3], cannot be removed by parameter tuning and seem to be a property of the PYTHIA physics model. The region 0.5< p_t <20GeV is still quite well described.

7.3.2 ATLAS MB Data: PS5

Four distributions of phase space 5 at 7TeV, where only charged particles with p_t >2.5 GeV contribute, are shown in Figure 7.20. The MC predictions of three PDF's describe data relatively well, though multiplicity is slightly low.

7.3.3 CDF I MB Data

Figure 7.21 shows prediction for average p_t vs N_{ch} to CDFI MB data [14] at 0.630 TeV. Fit results show comparison between fit results using CDFI MB data alone to the fit results where both CDFI at 0.630 TeV and ATLAS MB data sets are used at 0.9 and 7TeV. Plot shows both tunes describe data quite well.

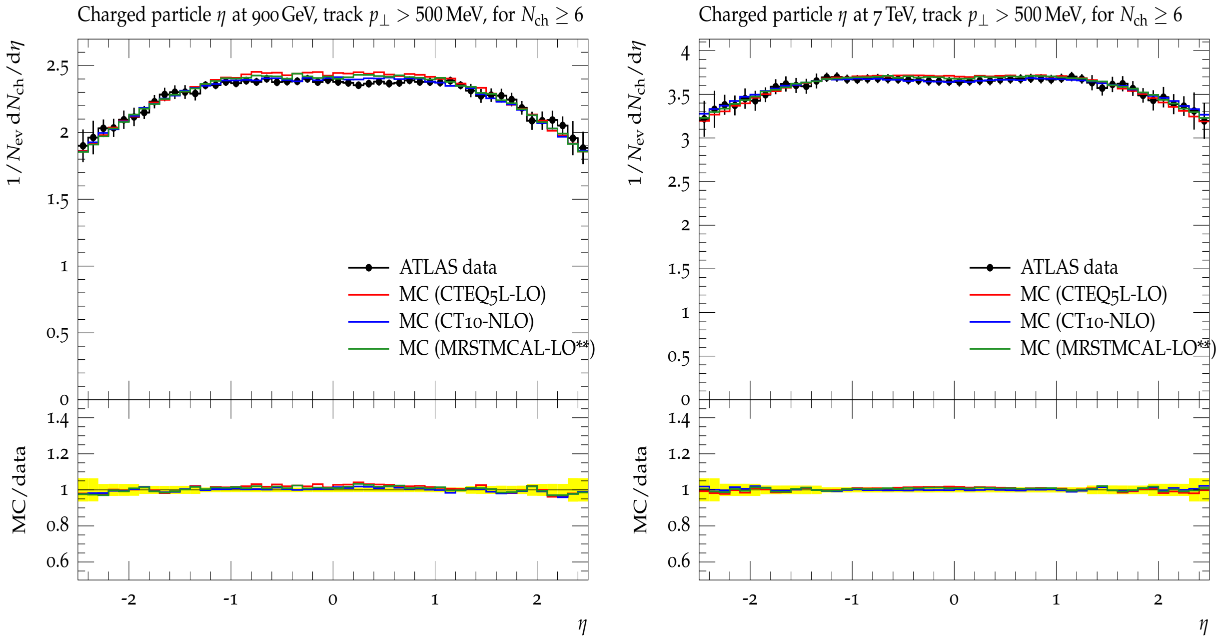

FIGURE 7.7: Comparison plots of PYTHIA 6.4 tunes to the ATLAS pseudorapidity distribution for events with $N_{ch} \geq 6$, pt> $500MeV$, $|\ \eta\ |< 2.5$ at $\sqrt{s} = 0.9$ and 7TeV.

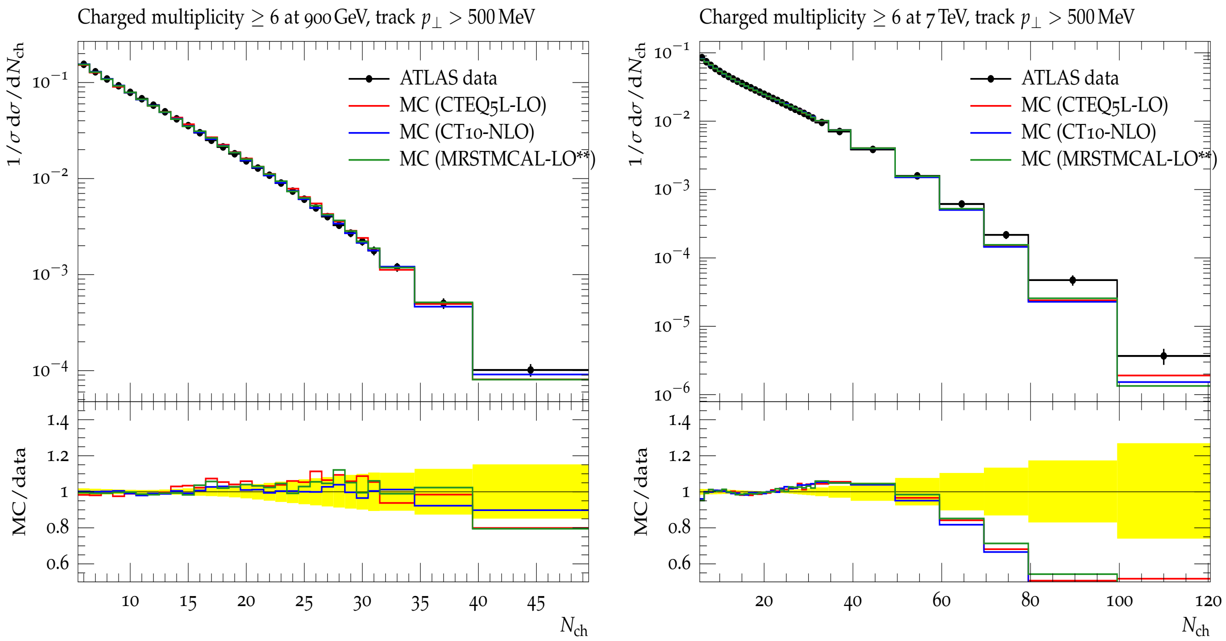

FIGURE 7.8: Comparison plots of PYTHIA 6.4 tunes to the ATLAS Charged-particle multiplicities for events with $N_{ch} \geq 6$, pt> $500MeV$, $|\ \eta\ |< 2.5$ at $\sqrt{s}$=0.9 and 7TeV.

7.3.4 CMS MB Data

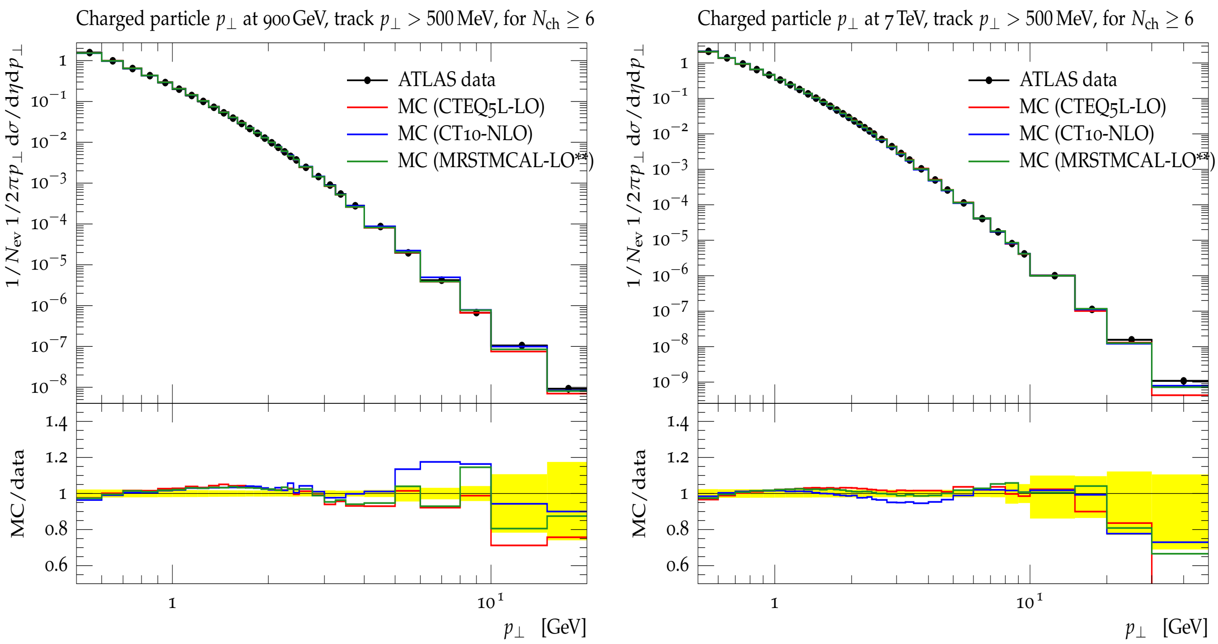

FIGURE 7.9: Comparison plots of PYTHIA 6.4 tunes to the ATLAS charged-particle multiplicities as a function of the transverse momentum for events with $N_{ch} \geq 6$, pt$> 500 MeV$, $| \eta | < 2.5$ at $\sqrt{s} = 0.9$ and 7TeV.

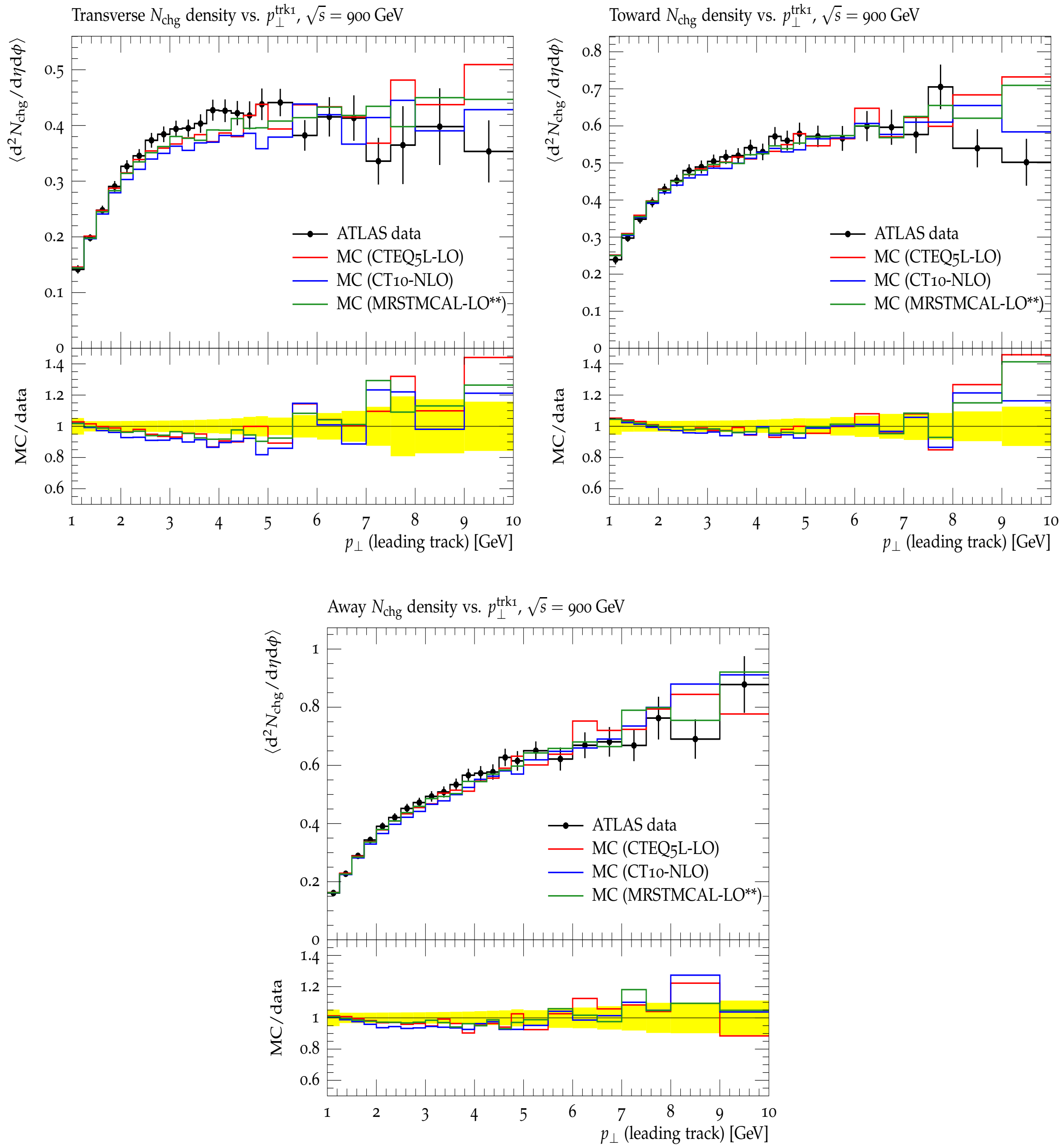

FIGURE 7.10: Comparison plots of PYTHIA6 tunes to the ATLAS UE distribution, charged particle densities vs p_t lead for three regions at $\sqrt{s} = 0.9TeV$.

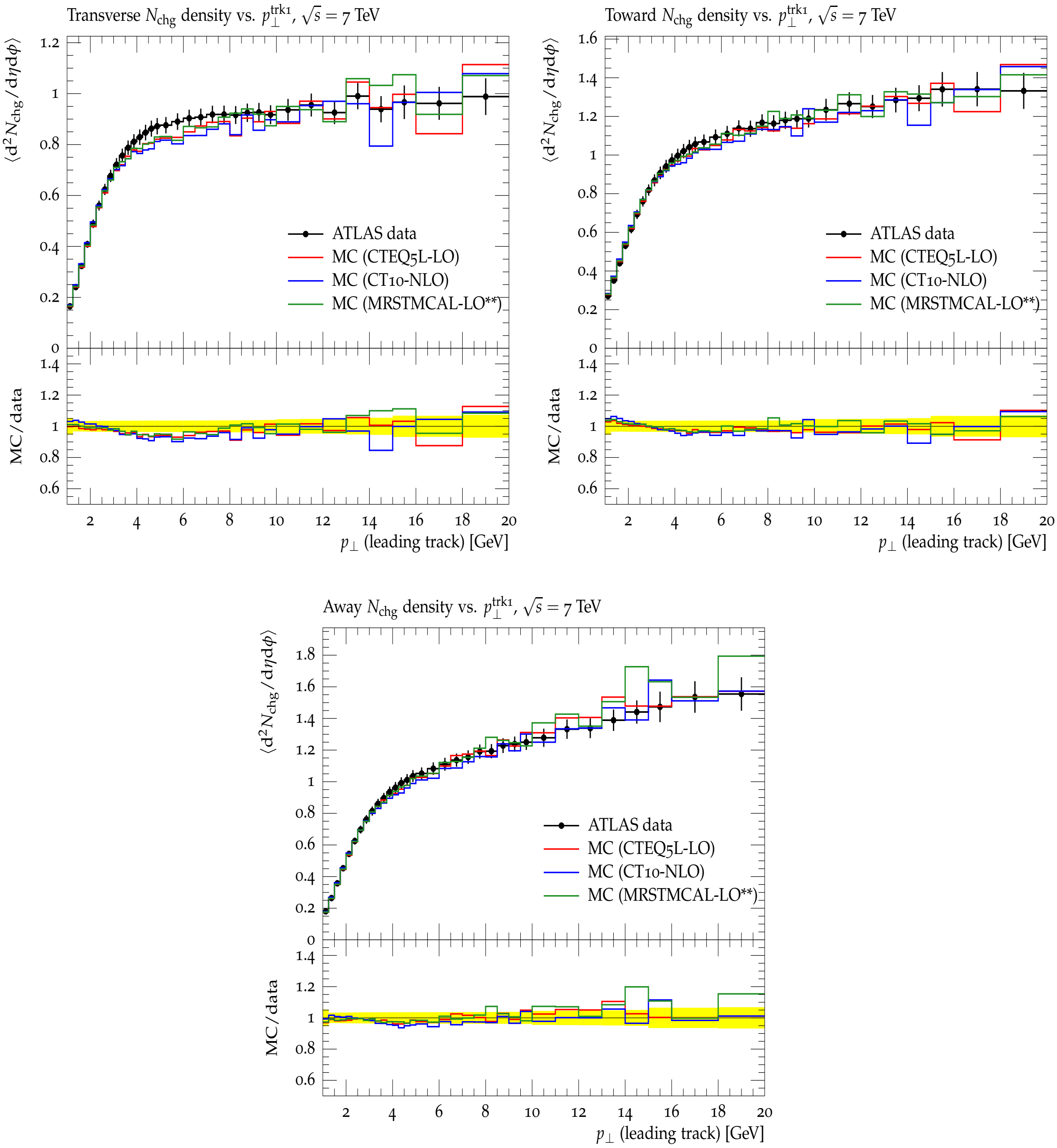

FIGURE 7.11: Comparison plots of PYTHIA6 tunes to the ATLAS UE distribution, N_{ch} densities vs$p_{t,lead}$ for three regions at $\sqrt{s} = 7TeV$.

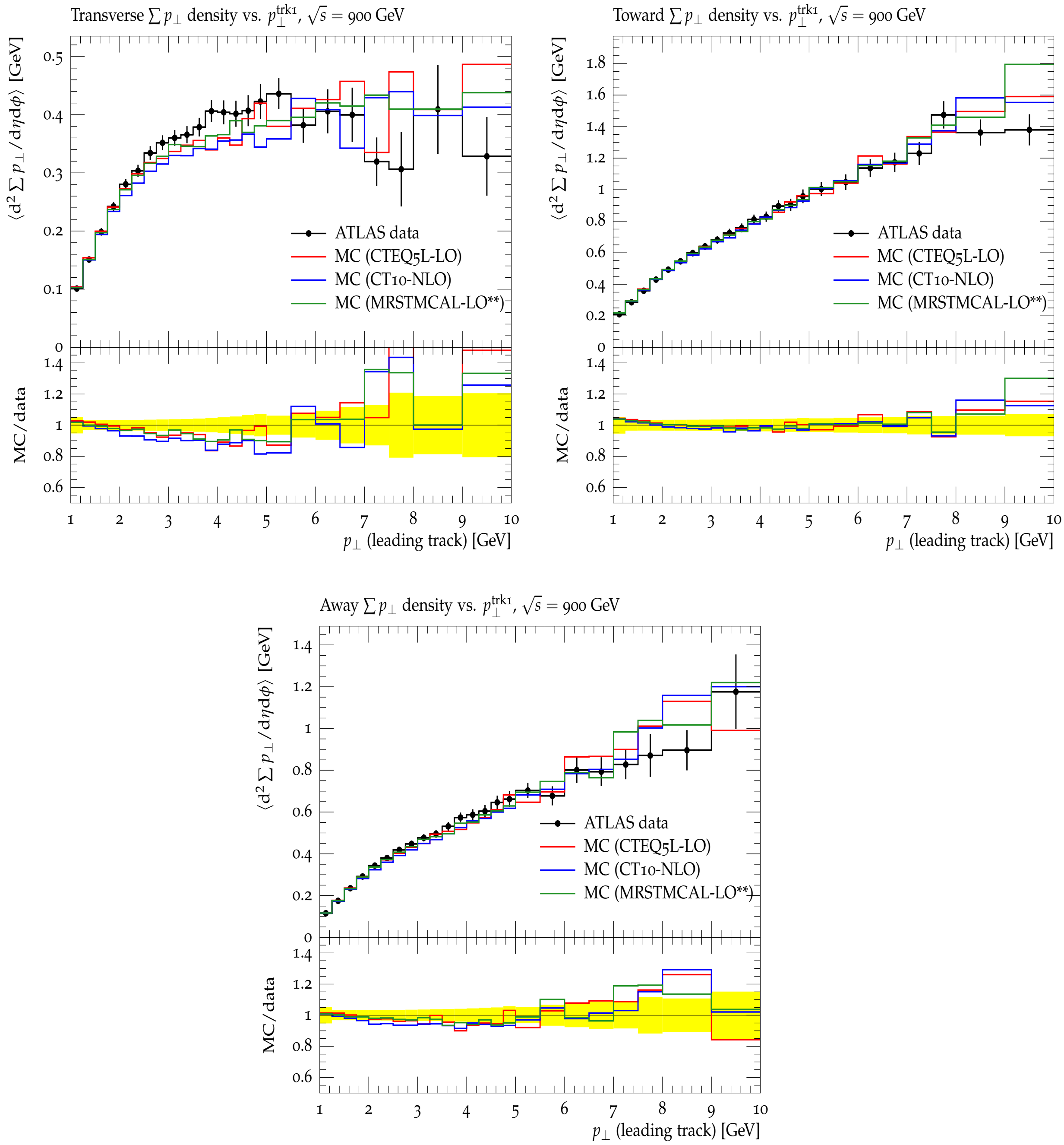

FIGURE 7.12: Comparison plots of PYTHIA6 tunes to the ATLAS UE distribution, Σp_t *vs* $p_{t,lead}$, of three regions at $\sqrt{s} = 0.9TeV$.

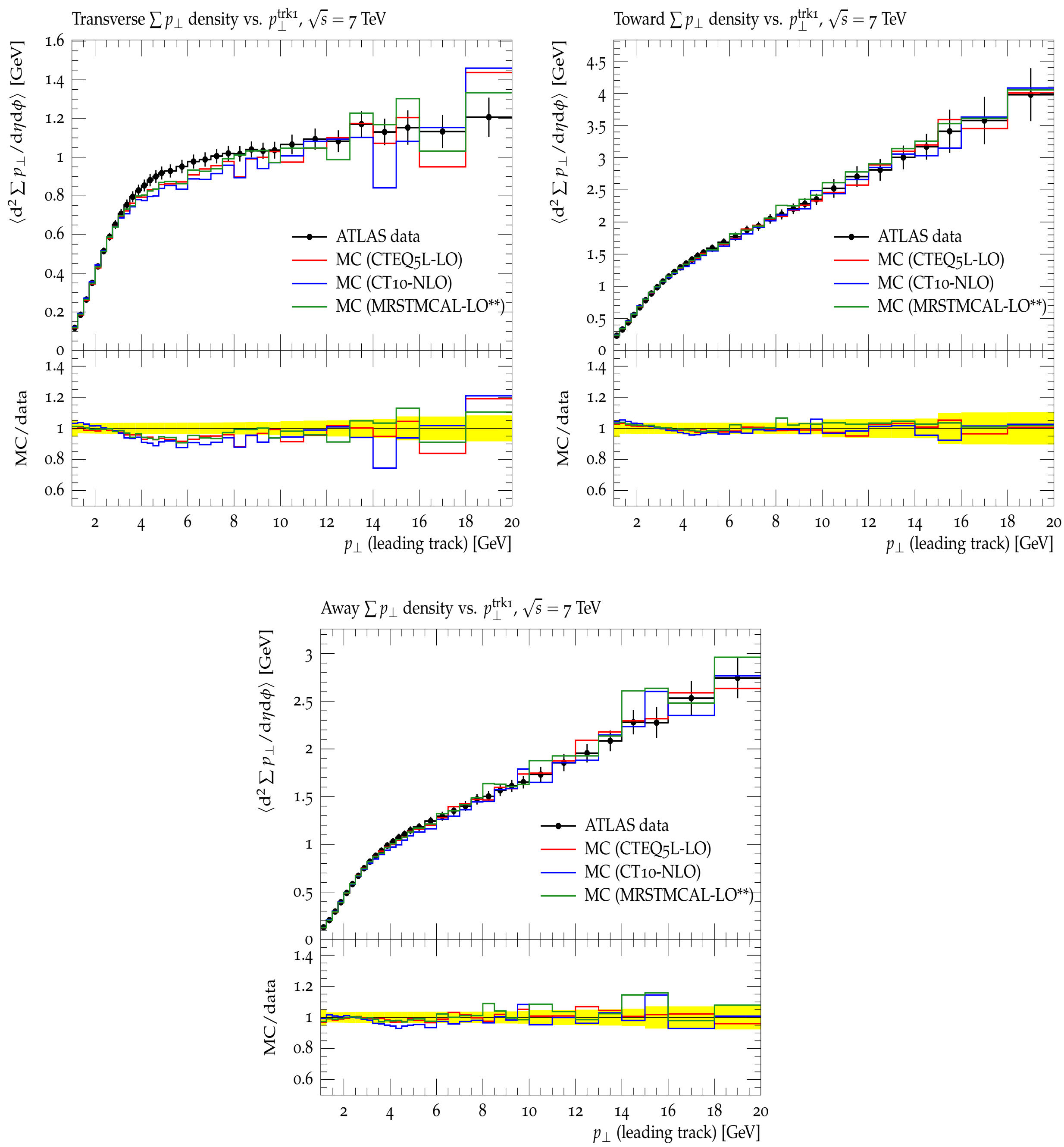

FIGURE 7.13: Comparison plots of PYTHIA6 tunes to the ATLAS UE distribution, Σp_t *vs* $p_{t,lead}$, of three regions at $\sqrt{s} = 7TeV$.

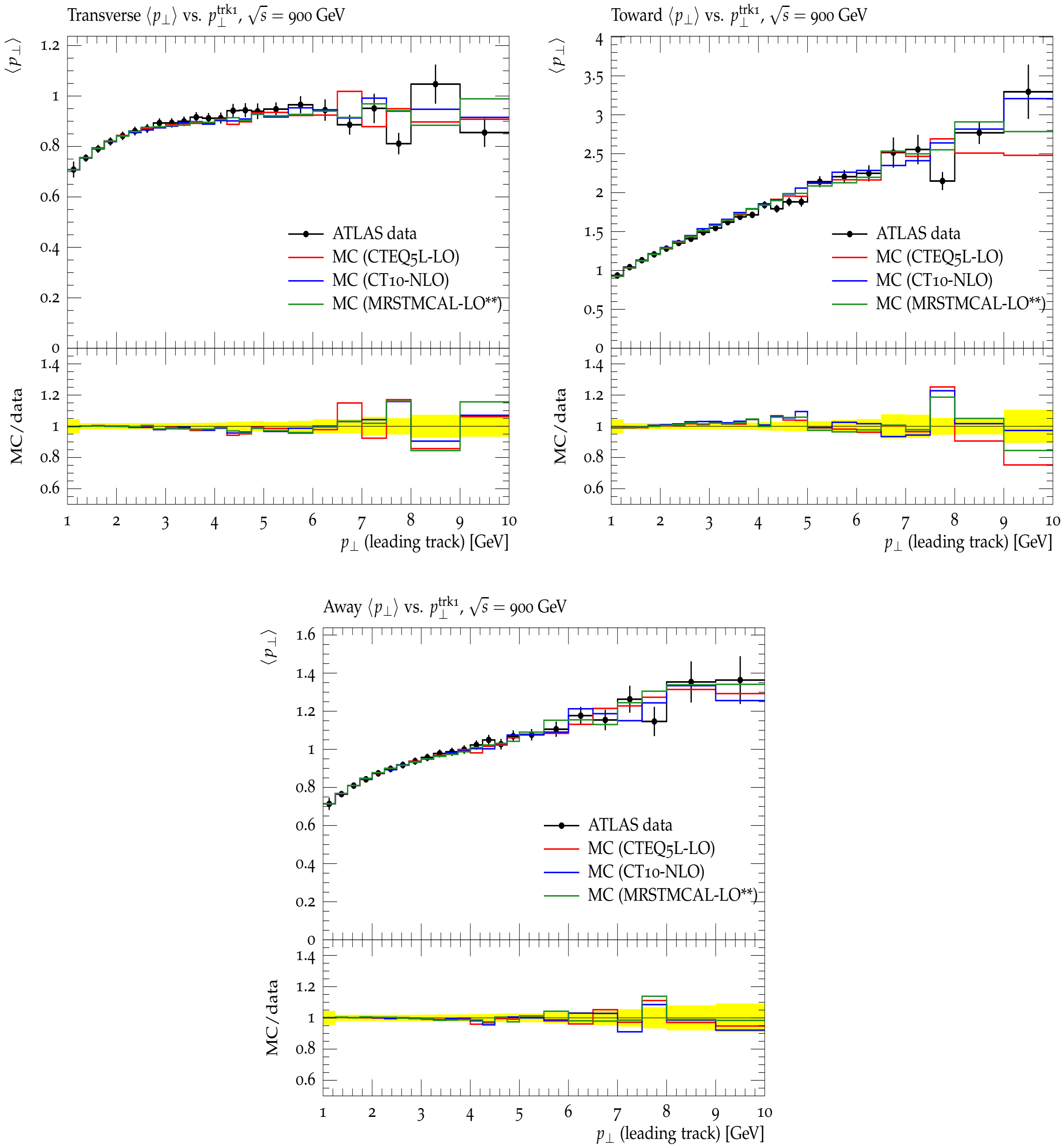

FIGURE 7.14: Comparison plots of PYTHIA6 tunes to the ATLAS UE distribution, $< p_t > \ vs \ p_{t,lead}$, of three regions at $\sqrt{s} = 0.9TeV$.

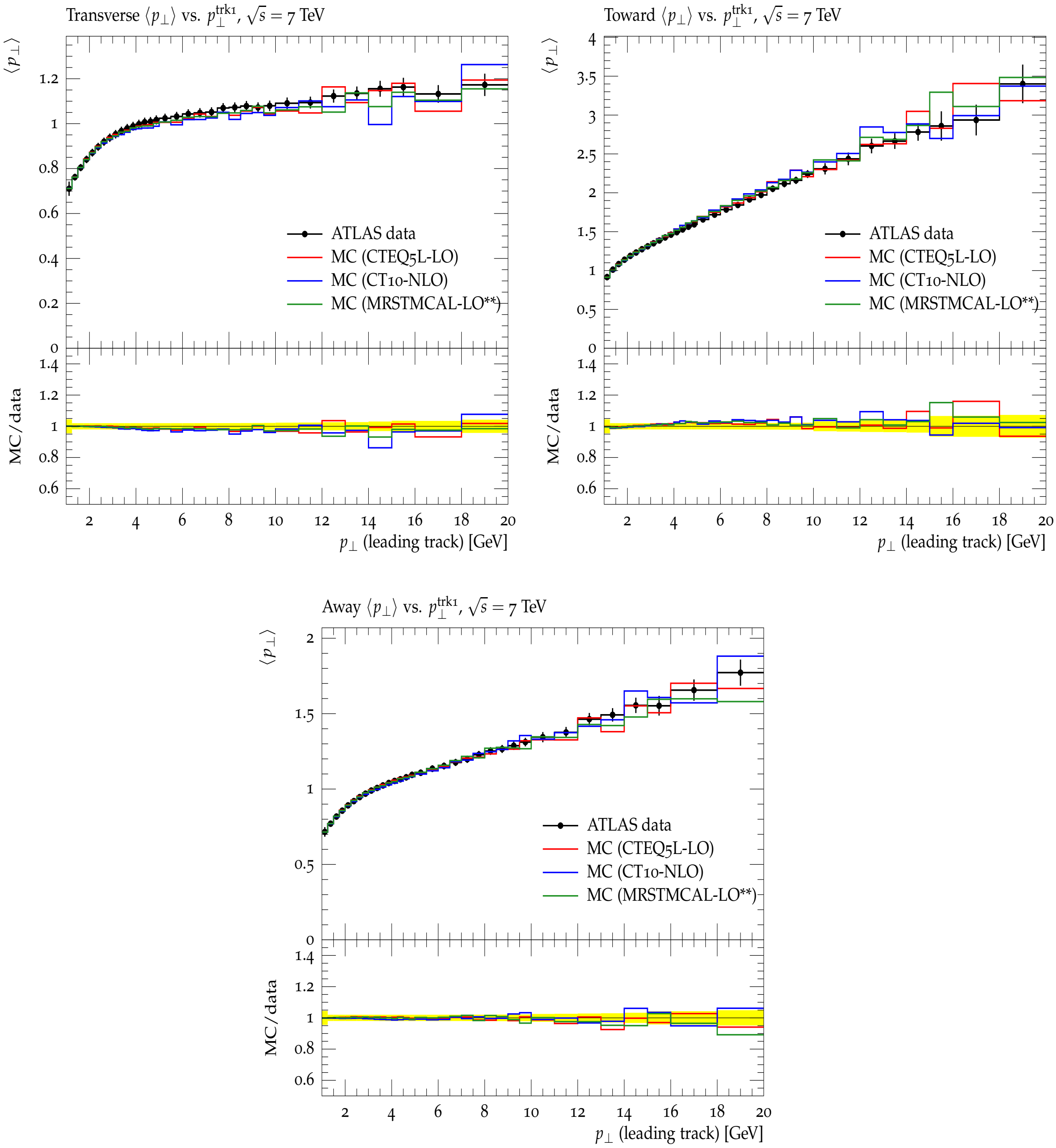

FIGURE 7.15: Comparison plots of PYTHIA6 tunes to the ATLAS UE distribution, $< p_t > \ vs \ p_{t,lead}$, of three regions at $\sqrt{s} = 7TeV$.

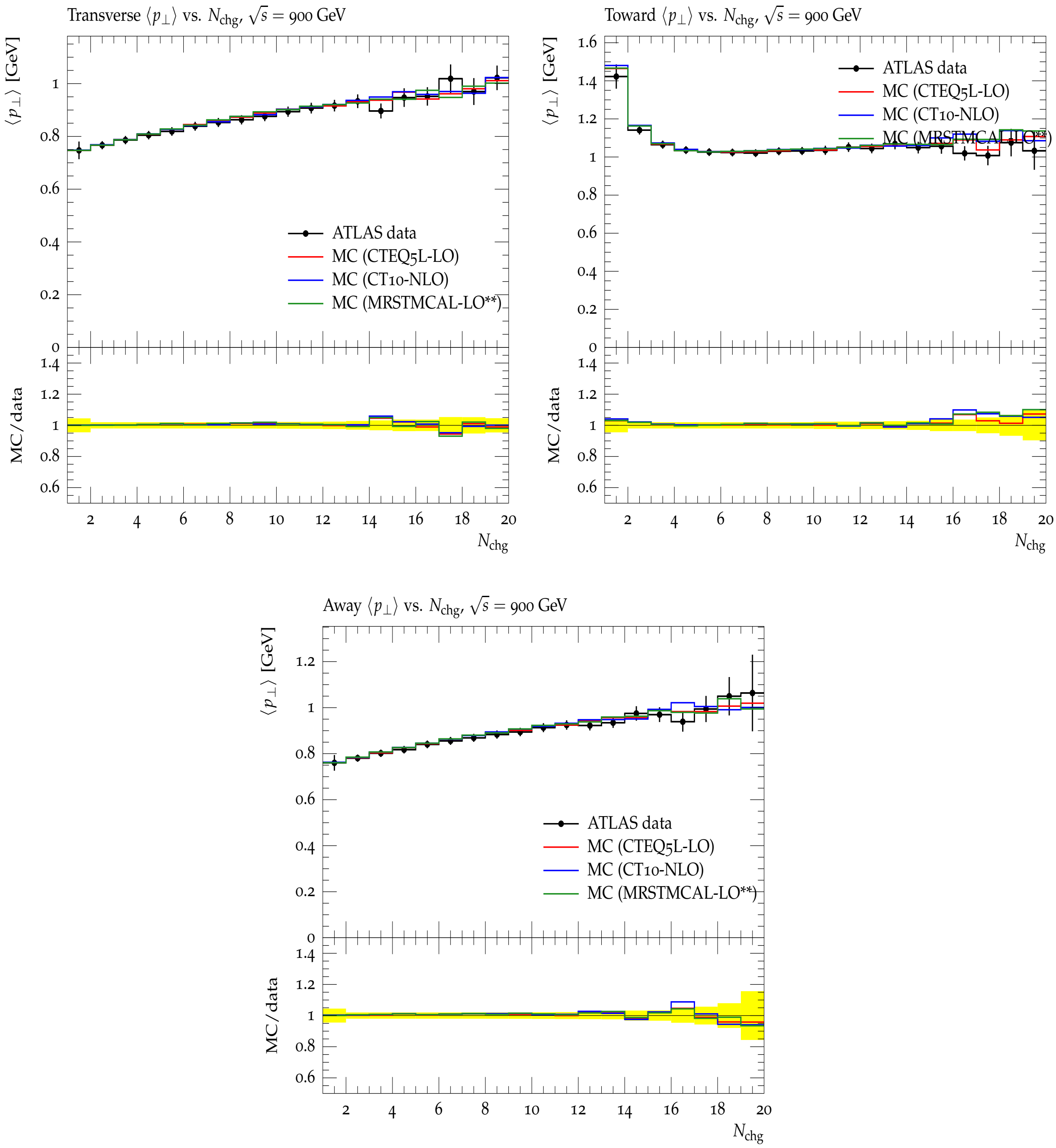

FIGURE 7.16: Comparison plots of PYTHIA6 tunes to the ATLAS UE distribution, $< p_t >$ vs N_{ch}, of three regions at $\sqrt{s} = 0.9TeV$ using three different PDF sets.

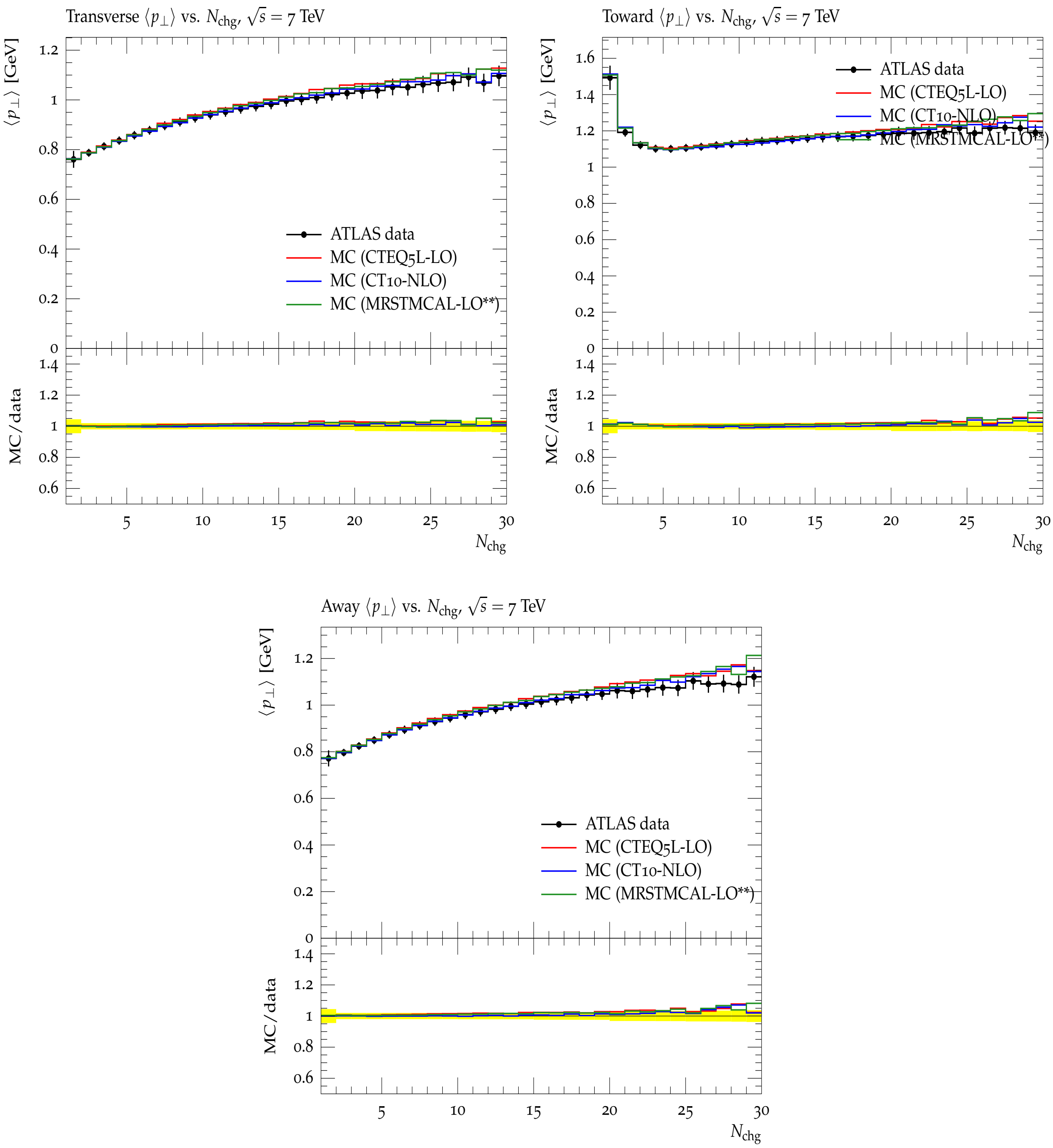

FIGURE 7.17: Comparison plots of PYTHIA6 tunes to the ATLAS UE distribution, average Pt vs N_{ch}, of three regions at $\sqrt{s} = 7TeV$ using three different PDF sets.. The bottom plot shows the ratio of the MC over the data.

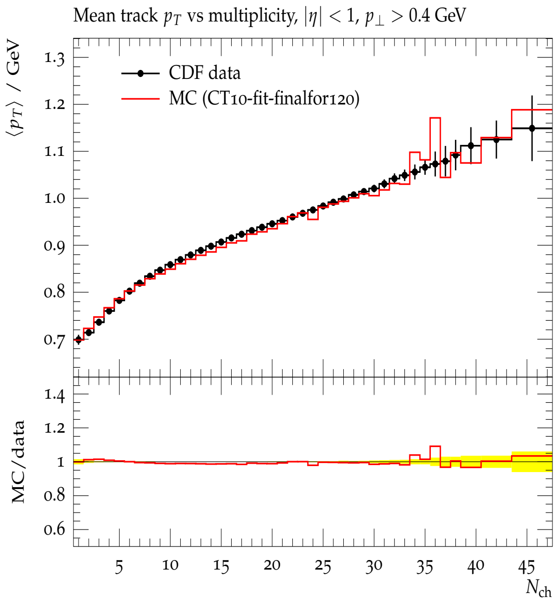

FIGURE 7.18: Tunes of PYTHIA6 to the CDF II MB distribution, average Pt vs N_{ch}, at$\sqrt{s} = 1.96TeV$.

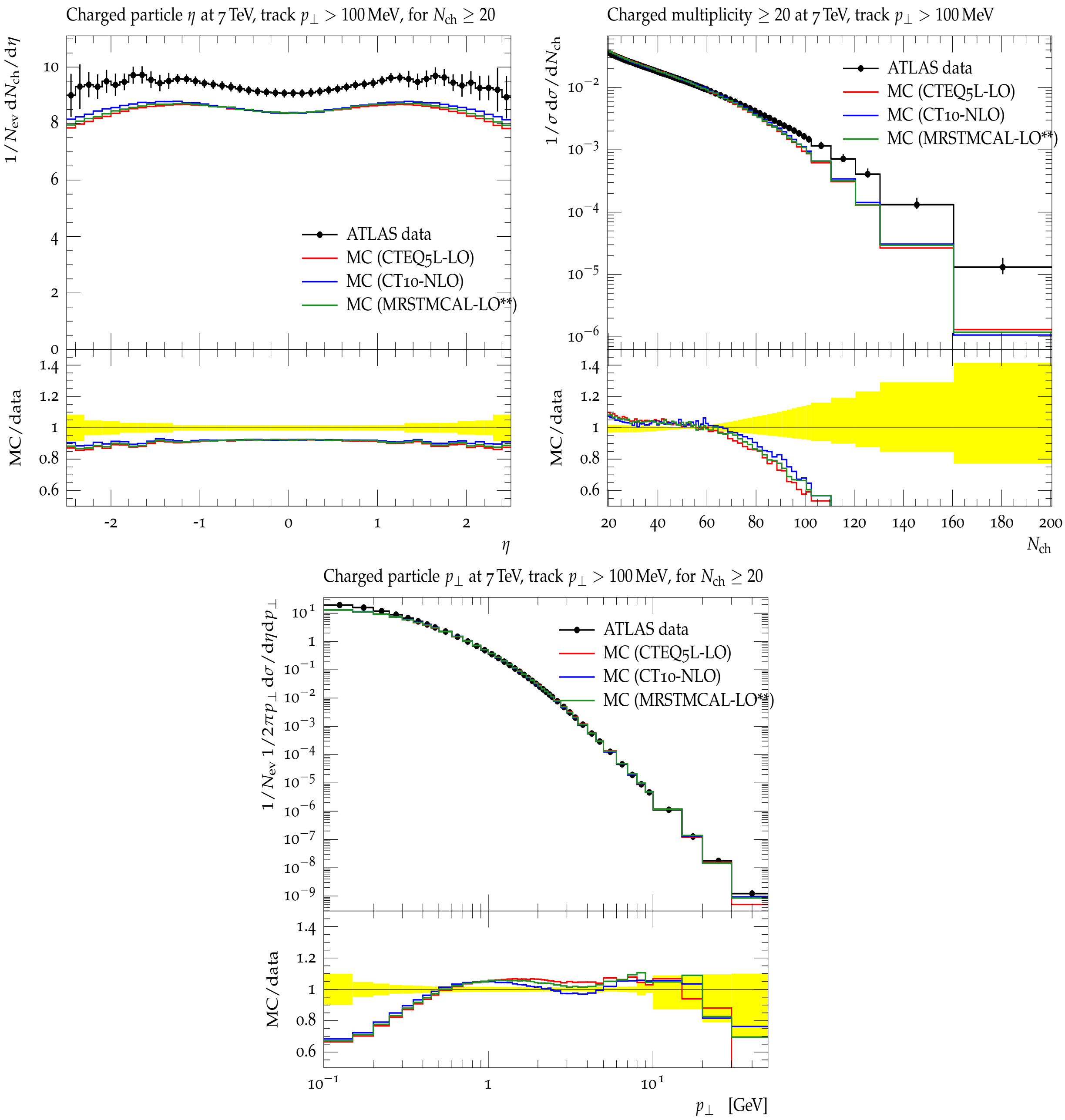

FIGURE 7.19: Prediction plots of PYTHIA6 tunes to the ATLAS MB distribution: PS4 at $\sqrt{s} = 7TeV$.

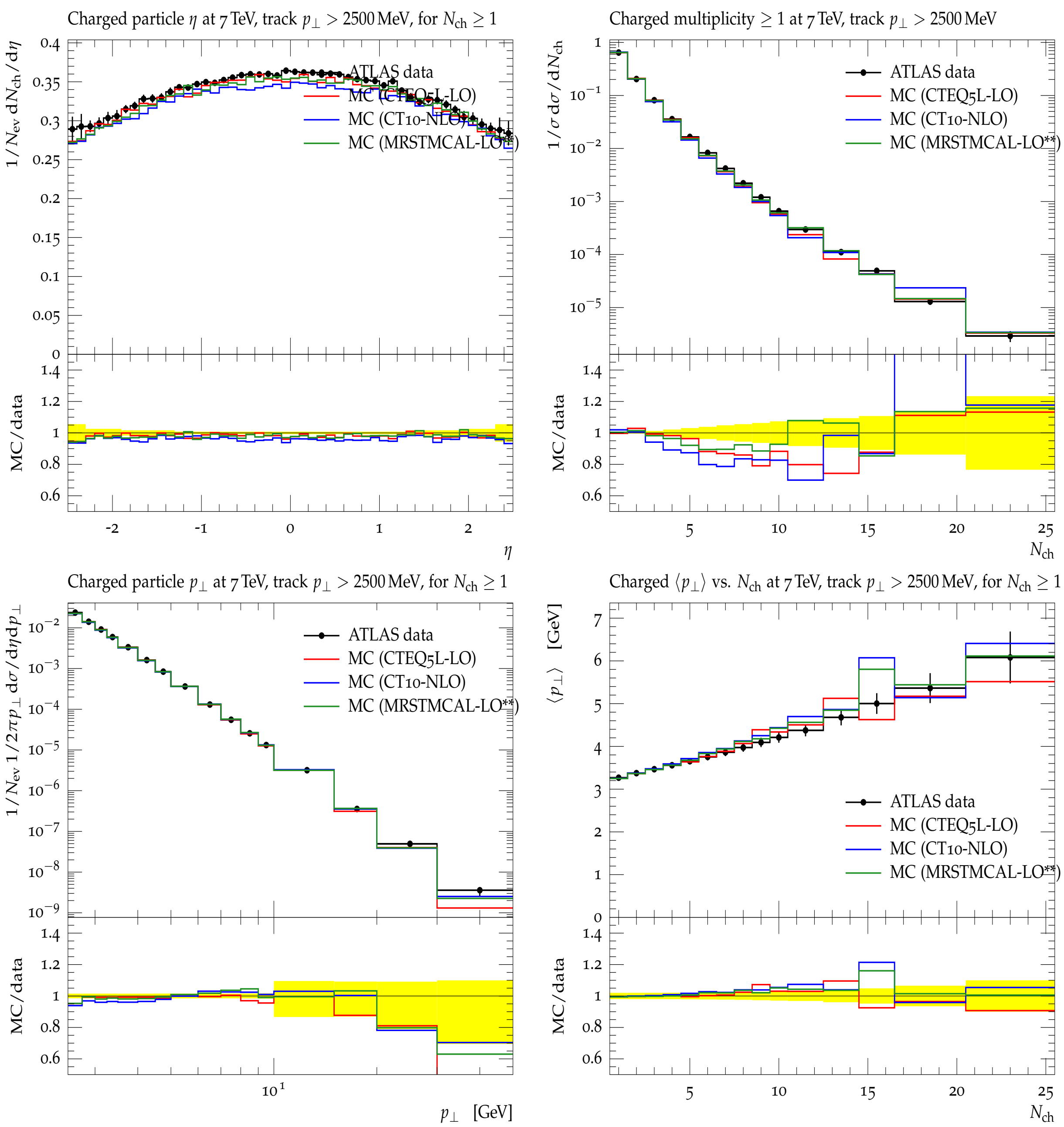

FIGURE 7.20: Prediction plots of PYTHIA6 tunes to the ATLAS MB distribution: PS5 at $\sqrt{s} = 7TeV$.

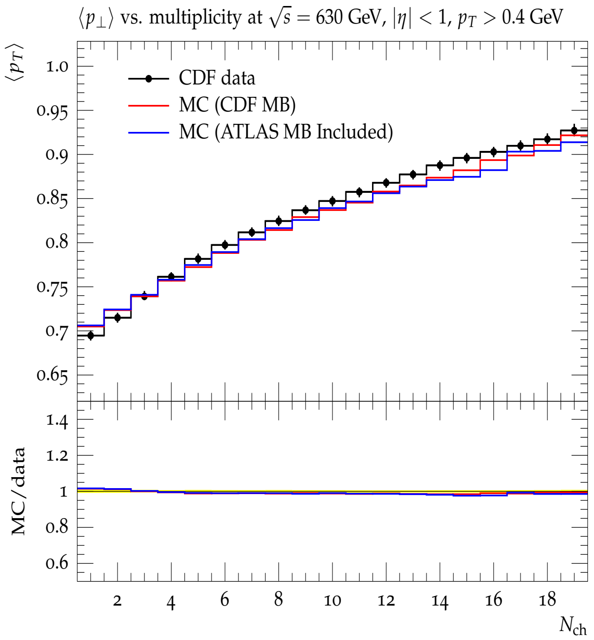

FIGURE 7.21: Prediction of PYTHIA6 tunes to the CDF I MB distribution, average Pt vs N_{ch}, at $\sqrt{s} = 0.63 TeV$.

Chapter 8

Alternative Tunes

Motivated by the systematic deviations observed in the underlying event distributions for the combined MB and UE tunes, discussed in Chapter 7, we investigate the option of separate tunes to MB and UE data in the following two sections. Such separate tunes have previously been performed by the ATLAS collaboration, named AMBT2B and AUET2B [36], to which we compare in sections 8.2 and 8.3.

8.1 Minimum Bias Tunes

The set of observables and weights has been chosen to be very very close to the one used by ATLAS in their AMBT2B tunes and is given in Table 8.1. More weight is given to 7TeV data and to the $p_t > 500$ MeV analyses. This allows a more meaningful comparison. The included phase spaces are all diffraction-suppressed. With this procedure the influence of the ATLAS PS4 distributions can be studied where significant discrepancies were seen, see Section 7.3.1.

The tuning results for three PDF's are given in Table 8.2. Compared to the combined tunes for each PDF, Tables 7.1-7.3, the following pattern can be seen: Both PARP(82) and PARP(1) change in a correlated way. Their values are now larger for LO and MC-adapted PDF's. Note that the correlation coefficient between these two parameters is large and positive, see Chapter 6. While PARP(83) and PARP(78) become smaller, PARP(72) becomes larger. Less changes are seen for the NLO case. The best χ^2 is found for the MC-adapted PDF.

Observable	$\sqrt{s}$	Weights
Track-based minimum bias in ATLAS [3]		
N_{ch}, $track\ p_\perp >\ 500 MeV, N_{ch,} \geq 6, \mid \eta \mid \leq 2.5$	7 TeV	1
$p_\perp$, $track\ p_\perp\ >\ 500\ MeV, N_{ch} \geq 6, \mid \eta \mid \leq 2.5$	7 TeV	1
η, $track\ p_\perp > 500\ MeV,\ N_{ch} \geq 6, \mid \eta \mid \leq 2.5$	7 TeV	1
$\langle p_\perp \rangle\ vs.\ N_{ch}, trackp_\perp > 500\ MeV, N_{ch} \geq 1, \mid \eta \mid \leq 2.5$	7 TeV	1
N_{ch}, $track\ p_\perp >\ 2500 MeV, N_{ch,} \geq 1, \mid \eta \mid \leq 2.5$	7 TeV	1/2
$p_\perp$, $track\ p_\perp\ >\ 2500\ MeV, N_{ch} \geq 1, \mid \eta \mid \leq 2.5$	7 TeV	1/2
η, $track\ p_\perp > 2500\ MeV,\ N_{ch} \geq 1, \mid \eta \mid \leq 2.5$	7 TeV	1/2
N_{ch}, $track\ p_\perp >\ 100 MeV, N_{ch,} \geq 20, \mid \eta \mid \leq 2.5$	7 TeV	1/4
$p_\perp$, $track\ p_\perp\ >\ 100\ MeV, N_{ch} \geq 20, \mid \eta \mid \leq 2.5$	7 TeV	1/4
η, $track\ p_\perp > 100\ MeV,\ N_{ch} \geq 20, \mid \eta \mid \leq 2.5$	7 TeV	1/4
N_{ch}, $track\ p_\perp > 500 MeV,\ N_{ch,}\ \geq\ 6, \mid \eta \mid \leq 2.5$	0.9TeV	1/2
$p_\perp$, $track\ p_\perp >\ 500\ MeV,\ N_{ch}\ \geq\ 6, \mid \eta \mid \leq 2.5$	0.9TeV	1/2
η, $track\ p_\perp\ >\ 500\ MeV,\ N_{ch}\ \geq\ 6, \mid \eta \mid \leq 2.5$	0.9TeV	1/2
$\langle p_\perp \rangle\ vs.\ N_{ch}, trackp_\perp > 500\ MeV,\ N_{ch} \geq 1, \mid \eta \mid \leq 2.5$	0.9TeV	1/2
N_{ch}, $track\ p_\perp > 2500 MeV,\ N_{ch,}\ \geq\ 1, \mid \eta \mid \leq 2.5$	0.9TeV	1/4
$p_\perp$, $track\ p_\perp >\ 2500\ MeV,\ N_{ch}\ \geq\ 1, \mid \eta \mid \leq 2.5$	0.9TeV	1/4
η, $track\ p_\perp\ >\ 2500\ MeV,\ N_{ch}\ \geq\ 1, \mid \eta \mid \leq 2.5$	0.9TeV	1/4
N_{ch}, $track\ p_\perp > 100 MeV,\ N_{ch,}\ \geq\ 20, \mid \eta \mid \leq 2.5$	0.9TeV	1/8
$p_\perp$, $track\ p_\perp >\ 100\ MeV,\ N_{ch}\ \geq\ 20, \mid \eta \mid \leq 2.5$	0.9TeV	1/8
η, $track\ p_\perp\ >\ 100\ MeV,\ N_{ch}\ \geq\ 20, \mid \eta \mid \leq 2.5$	0.9TeV	1/8
CDF Run II minimum bias [8]		
$p_\perp\ vs.\ N_{ch}, track\ p_\perp >\ 400 MeV, \mid \eta \mid < 1$	1.96TeV	1/2

Table 8.1: Minimum Bias observables with weights used in the alternative tunes to minimum bias data from ATLAS and CDF II.

Comparison plots of ATLAS PS3, PS4 and PS5 data at 7TeV with the MB tunes overlaid are shown in Figures 8.1, 8.2 and 8.3. The last bin (160-200) of the N_{ch} distribution in Figure 8.2 has not been used in the tuning because of too low MC statistics.

The MC histograms are almost identical to those shown in Chapter 7 for the combined tunes. Despite the parameter changes, the level of average multiplicity remain almost the same with only a little increase (1%) in the case of PS4. This proves that the MC-data discrepancies for the $p_t > 100$ MeV selection can not be removed by mere parameter tuning.

Parameter	Symbol	CTEQ5L	MRSTMCAL	CT10
PARP(82)	pt_0	2.992 ±0.013	2.791 ±0.012	2.143 ±0.014
PARP(90)	ε	0.241 ±0.001	0.218 ±0.001	0.161 ±0.001
PARP(83)	d_{MO}	1.767 ±0.006	1.768 ±0.006	1.888 ±0.007
PARP(78)	P_{CR}	0.385 ±0.004	0.397 ±0.003	0.479 ±0.004
PARP(1)	Λ_{ME}	0.175 ±0.002	0.078 ±0.001	0.188 ±0.003
PARP(72)	Λ_{FSR}	0.535 ±0.010	0.595 ±0.008	0.453 ±0.009
χ^2/N_{DOF}		1.78	1.63	2.17

TABLE 8.2: Tuning result of separate minimum bias tunes for three different PDF types

8.1.1 Underlying Event Tunes

The set of observables for these tunes is the same as used in Chapter 7 and is listed in Table 5.7. The results of six parameter fits for three PDF's are given in Table 8.3 and comparison plots are shown in Figures 7.10 to 7.15 for 7TeV only. Given the larger errors, the parameter values are not very different from those of MB tunes. The fits are seen to be excellent, even too good from a statistical point of view. The previously seen discrepancies in the transverse densities are reduced or even vanished.

Parameter	Symbol	CTEQ5L	MRSTMCAL	CT10
PARP(82)	pt_0	2.917 ±0.024	2.667 ±0.026	2.102 ±0.022
PARP(90)	ε	0.247 ±0.002	0.223 ±0.001	0.177 ±0.002
PARP(83)	d_{MO}	1.749 ±0.026	1.722 ±0.034	1.835 ±0.030
PARP(78)	P_{CR}	0.424 ±0.007	0.434 ±0.008	0.552 ±0.009
PARP(1)	Λ_{ME}	0.168 ±0.005	0.068 ±0.004	0.185 ±0.005
PARP(72)	Λ_{FSR}	0.519 ±0.017	0.502 ±0.015	0.489 ±0.018
χ^2/N_{DOF}		0.51	0.52	0.58

TABLE 8.3: Tuning result of separate UE fit for three PDF types.

8.2 Comparison to AMBT2B

The ATLAS Collaboration has published separate MB and UE tunes, named AMBT2 and AUET2 [36], because of difficulties describing all features of the MPI-sensitive observables with one tune. Improved versions are named AMBT2B and AUET2B [34]. In this section we compare our MB tune with AMBT2B using MRSTMCAL (LO**) PDF set. The fitted

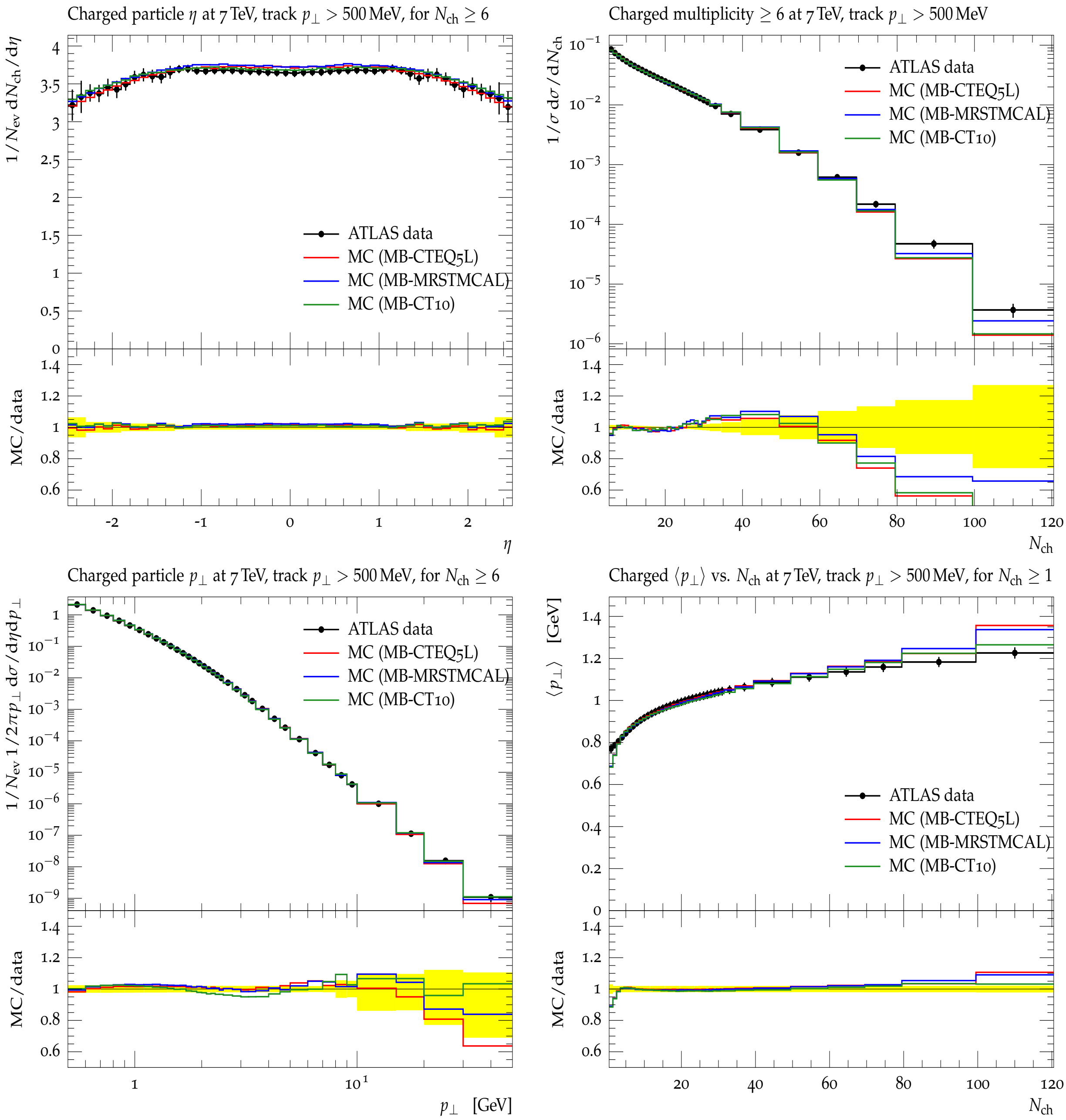

FIGURE 8.1: Comparison plots of PYTHIA 6.4 tunes to the ATLAS eta, charged-particle multiplicities and pt distributions for events with $N_{ch} \geq 6$, pt$> 500MeV$, $\mid \eta \mid < 2.5$ at $\sqrt{s} = 7TeV$

.

model parameters can not directly be compared because of several important differences in the tuning set-up and tuning strategy. What can be compared are the predictions for the observables used in the tuning. This is shown in Figures 8.8, 8.9 and 8.10. From the plot of ATLAS PS3, Figure 8.8, it can be seen that AMBT2B tune has slightly higher mean multiplicity and that the high-N_{ch} tail is better described. Whereas the charged particle

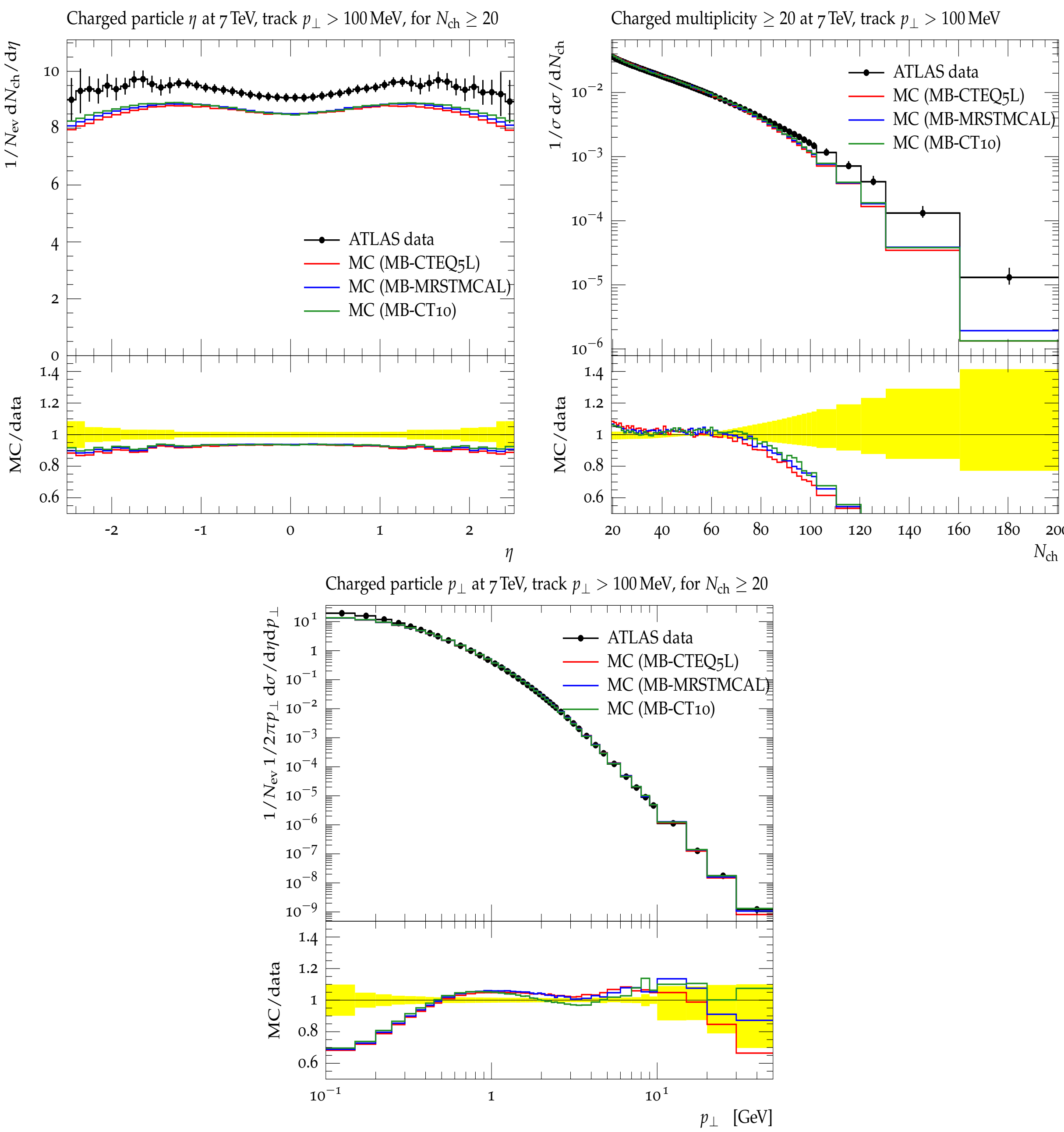

FIGURE 8.2: Comparison plots of PYTHIA6 tunes to the ATLAS Charged-particle multiplicities for events with $N_{ch} \geq 20$, pt$> 100MeV$, $\mid \eta \mid< 2.5$ at$\sqrt{s} = 7TeV$.

p_t spectrum is perfectly described by our tune, AMBT2B exhibits large and significant deviations from the data: the MC is above data around 0.5GeV, changes to below data around 2GeV and overshoots the data in the high-p_t region by up to 40% around $p_t = 10$ GeV.

From our studies we conclude that this large excess at high-p_t is directly related to the value of the PARP(1)=Λ_{ME} parameter which was left at its default value of 0.19 GeV in

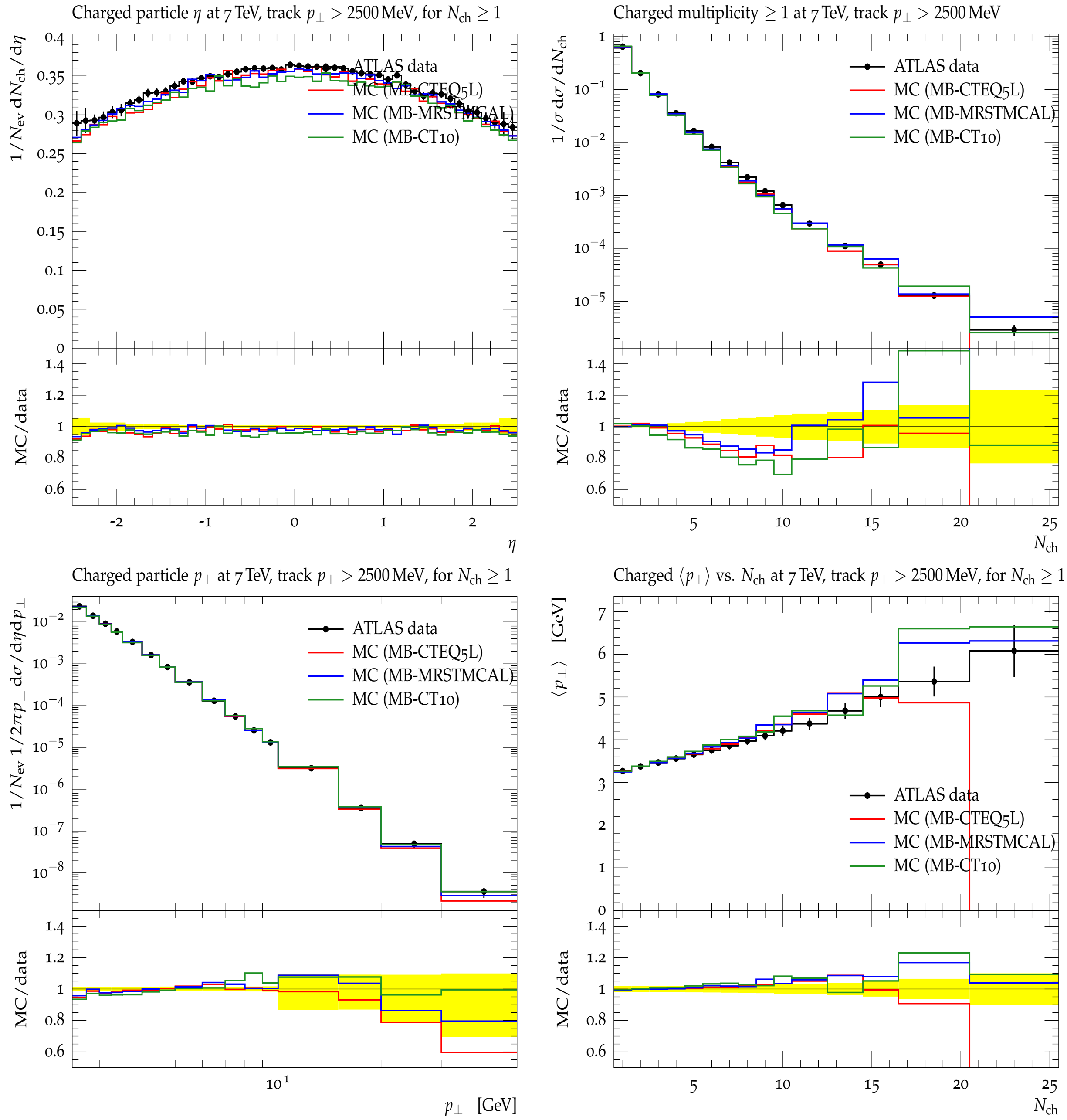

FIGURE 8.3: Comparison plots of PYTHIA6 tunes to the ATLAS eta,charged-particle multiplicities and pt distributions for events with $N_{ch} \geq 1$, pt> $2500 MeV$, $\mid \eta \mid < 2.5$ at $\sqrt{s} = 7TeV$.

AMBT2B, while it was treated as a free parameter in our tunes. Note the surprisingly low values obtained for this parameter for the case of MC-adapted PDF's, see Table 8.2 and 7.2. The trend of $< p_t >$ vs. N_{ch} is relatively well described by both tunes. The plots for ATLAS PS4 in Figure 8.9 show the already known defect at low $p_t <$ 500 MeV, but otherwise the features are similar to those for ATLAS PS3 and also PS5, Figure 8.10. For completeness, Appendix A shows this comparison for the case of an LO PDF which is not affected by the problem in the high-p_t region discussed above.

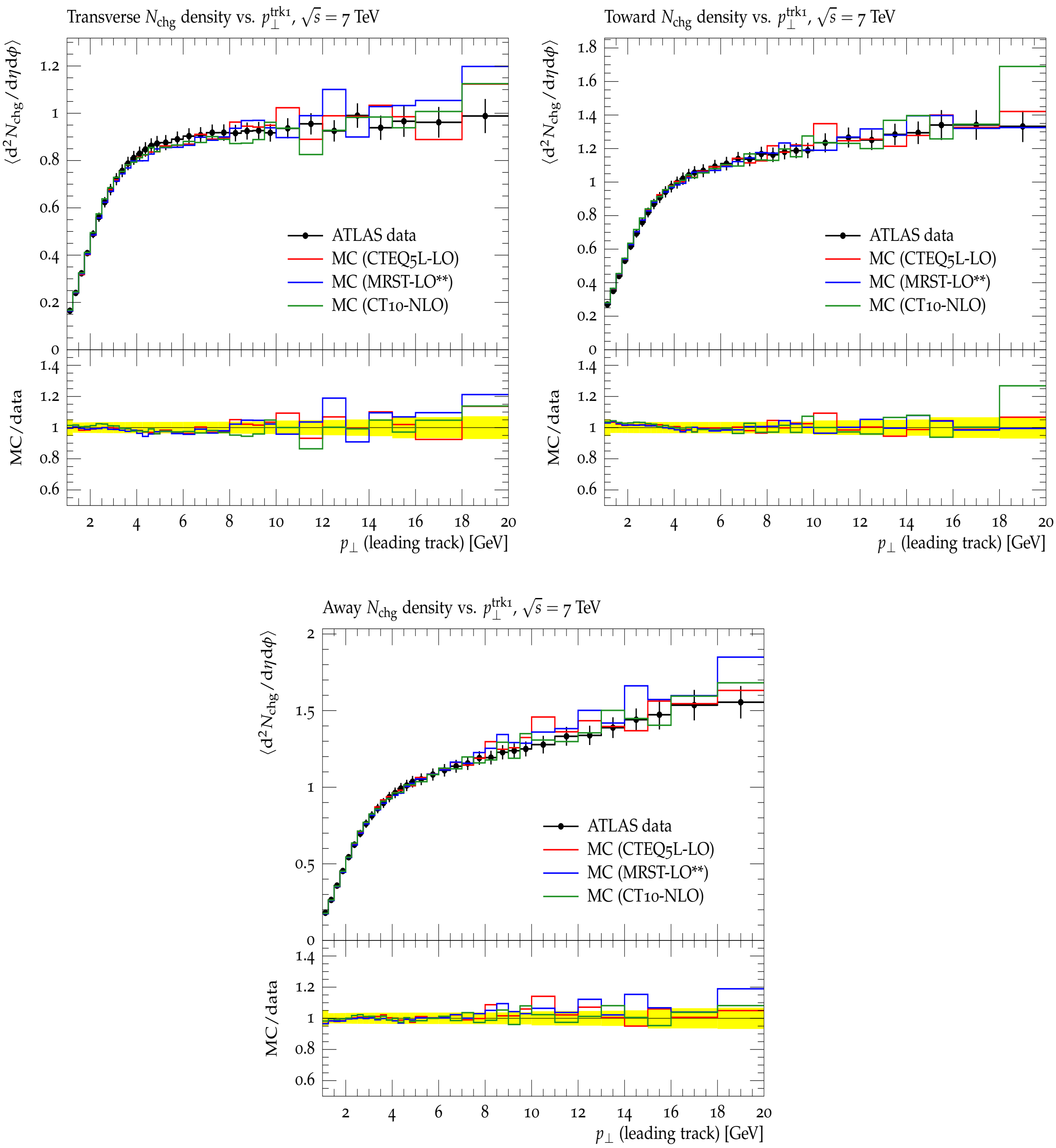

FIGURE 8.4: Comparison plots of PYTHIA6 tunes to the ATLAS UE distribution, charged particle densities vs pt lead for three regions at $\sqrt{s} = 7TeV$.

8.3 Comparison to AUET2B

Figures 8.11 to 8.14 show comparison plots of our UE tunes with AUET2B to ATLAS UE data at 7TeV. The LO** PDF set was used for both cases. It can be seen from Figures 8.11 and 8.12 that AUET2B provides a bad description of the N_{ch} and Σp_t densities with levels being systematically too high by around 10% everywhere. In contrast, our UE tunes

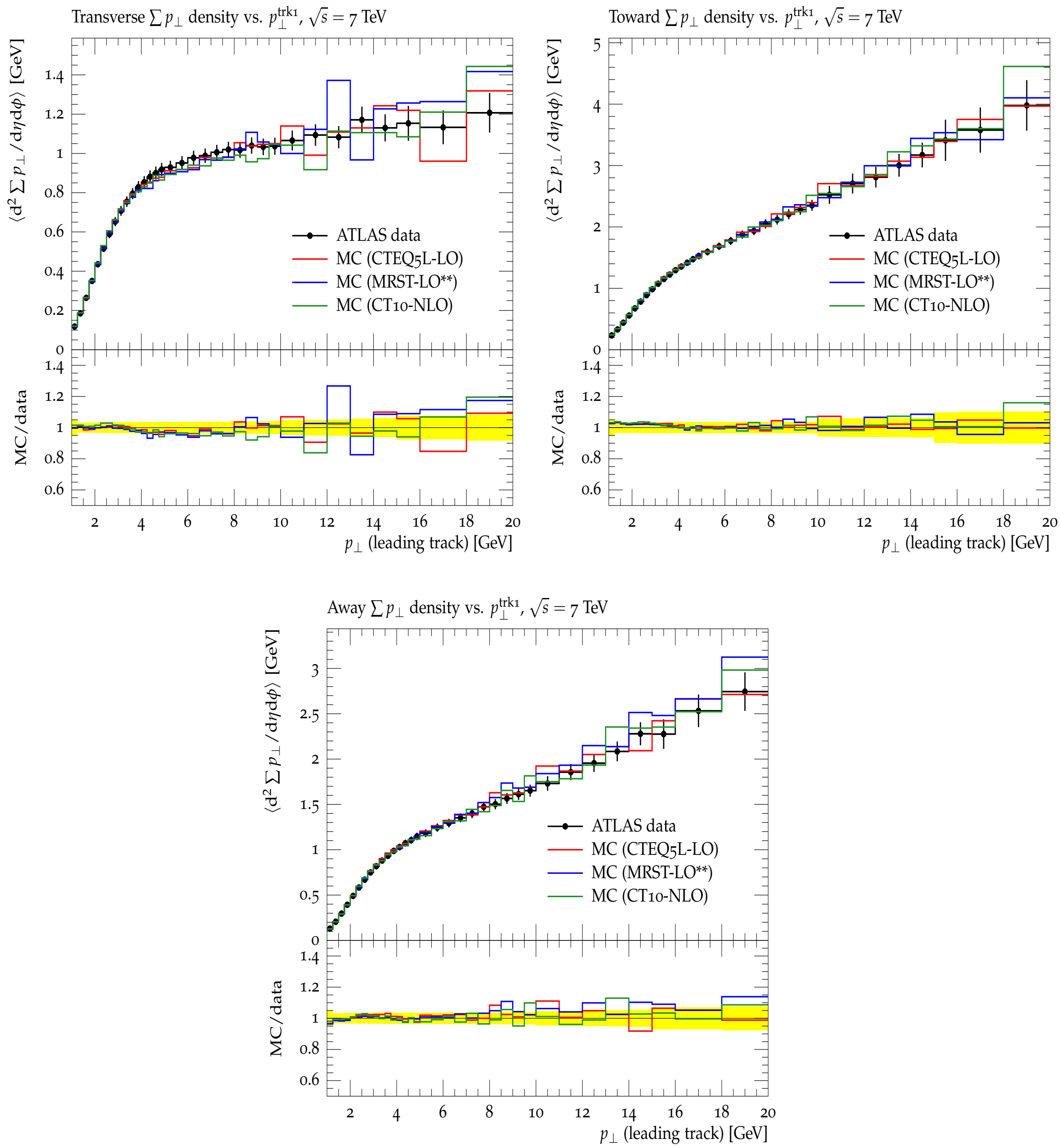

FIGURE 8.5: Comparison plots of PYTHIA6 tunes to the ATLAS UE distribution, sum pt densities vs pt lead for three regions at $\sqrt{s} = 7TeV$

.

fits the data quite well. No problems are seen in Figures 8.13 and 8.14 for the $< p_t >$ distributions.

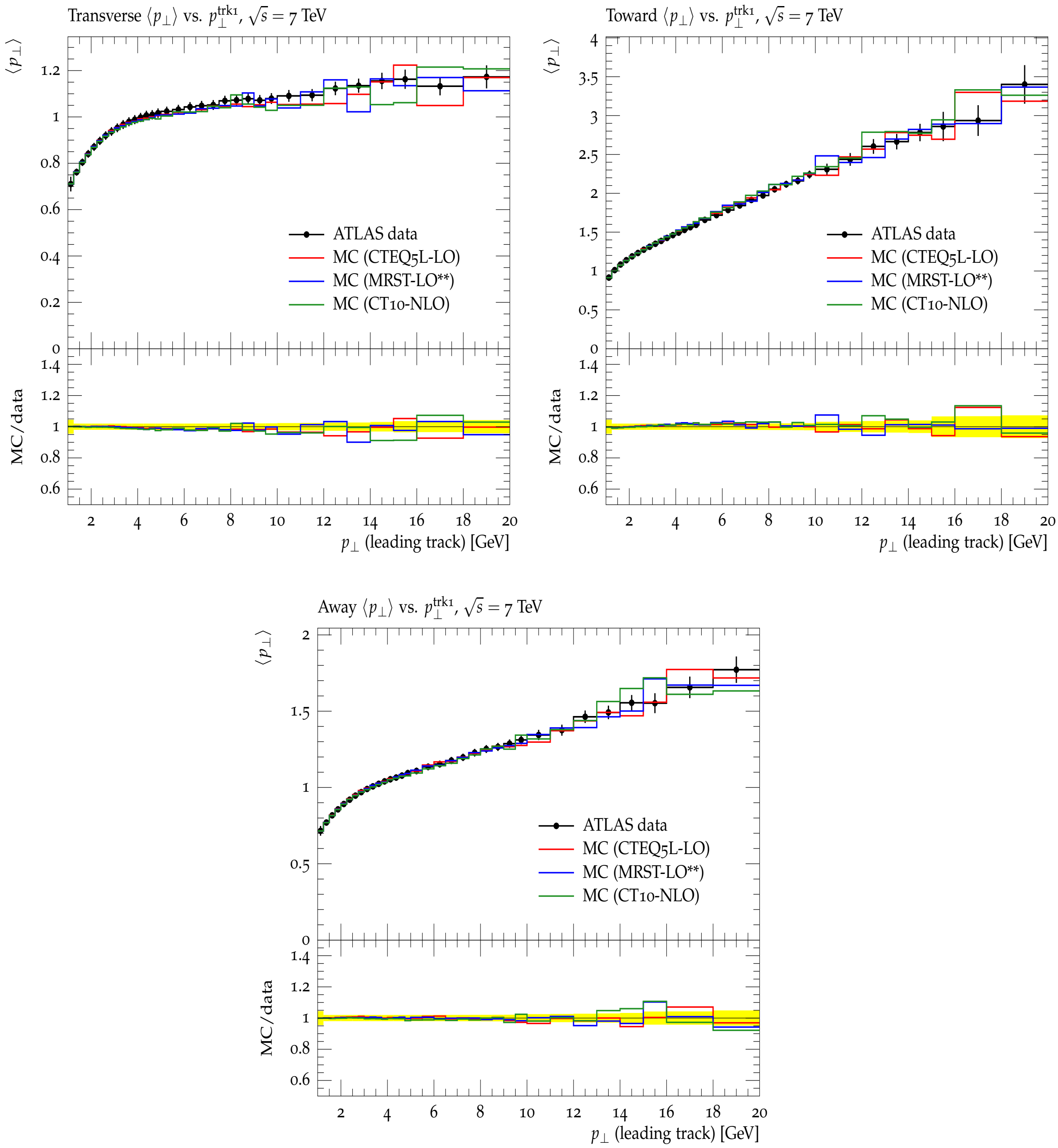

FIGURE 8.6: Comparison plots of PYTHIA6 tunes to the ATLAS UE distribution, average Pt vs Pt lead, of three regions at $\sqrt{s} = 7TeV$

.

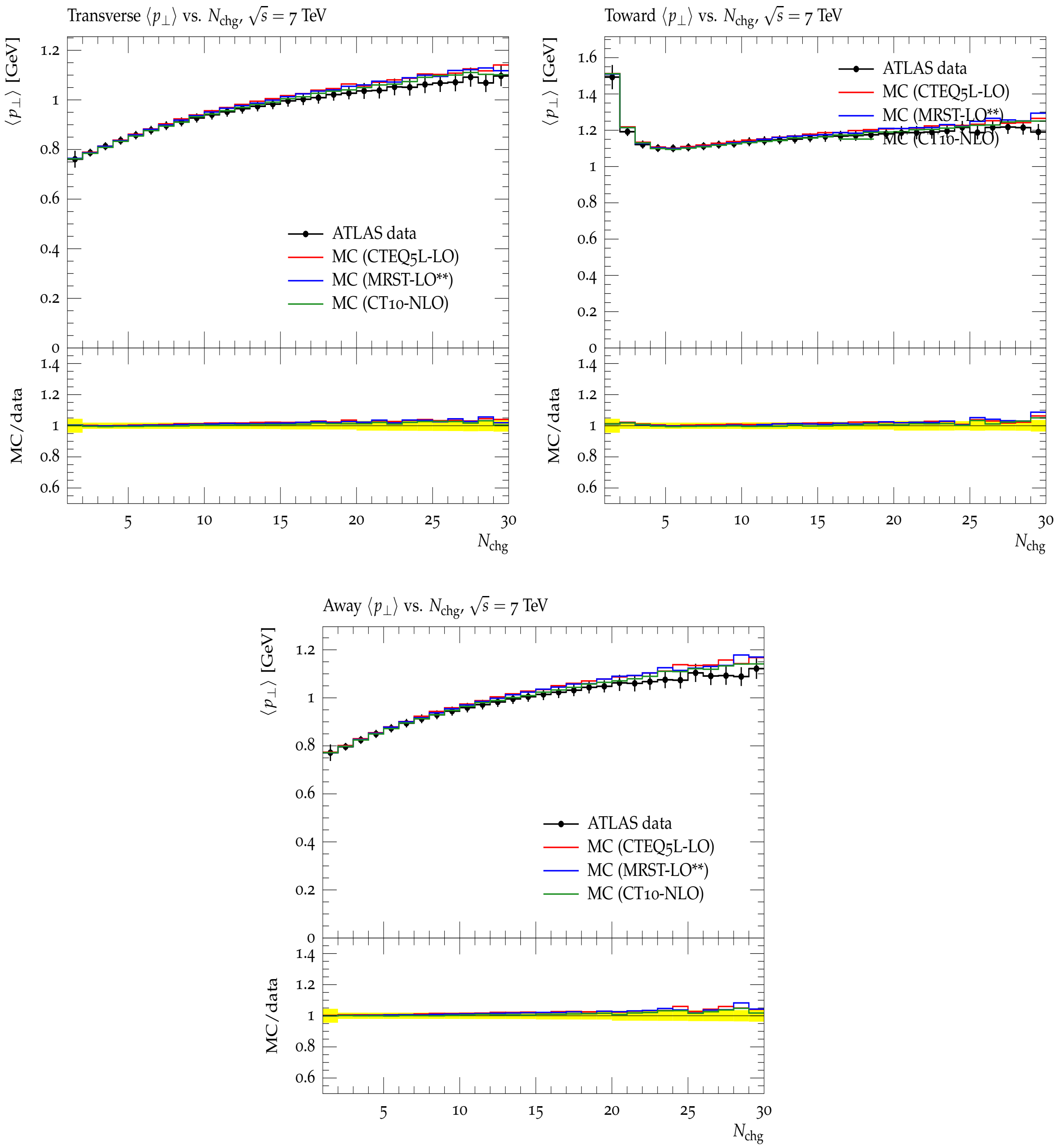

FIGURE 8.7: Comparison plots of PYTHIA6 tunes to the ATLAS UE distribution, average Pt vs Nch, of three regions at $\sqrt{s} = 7TeV$

.

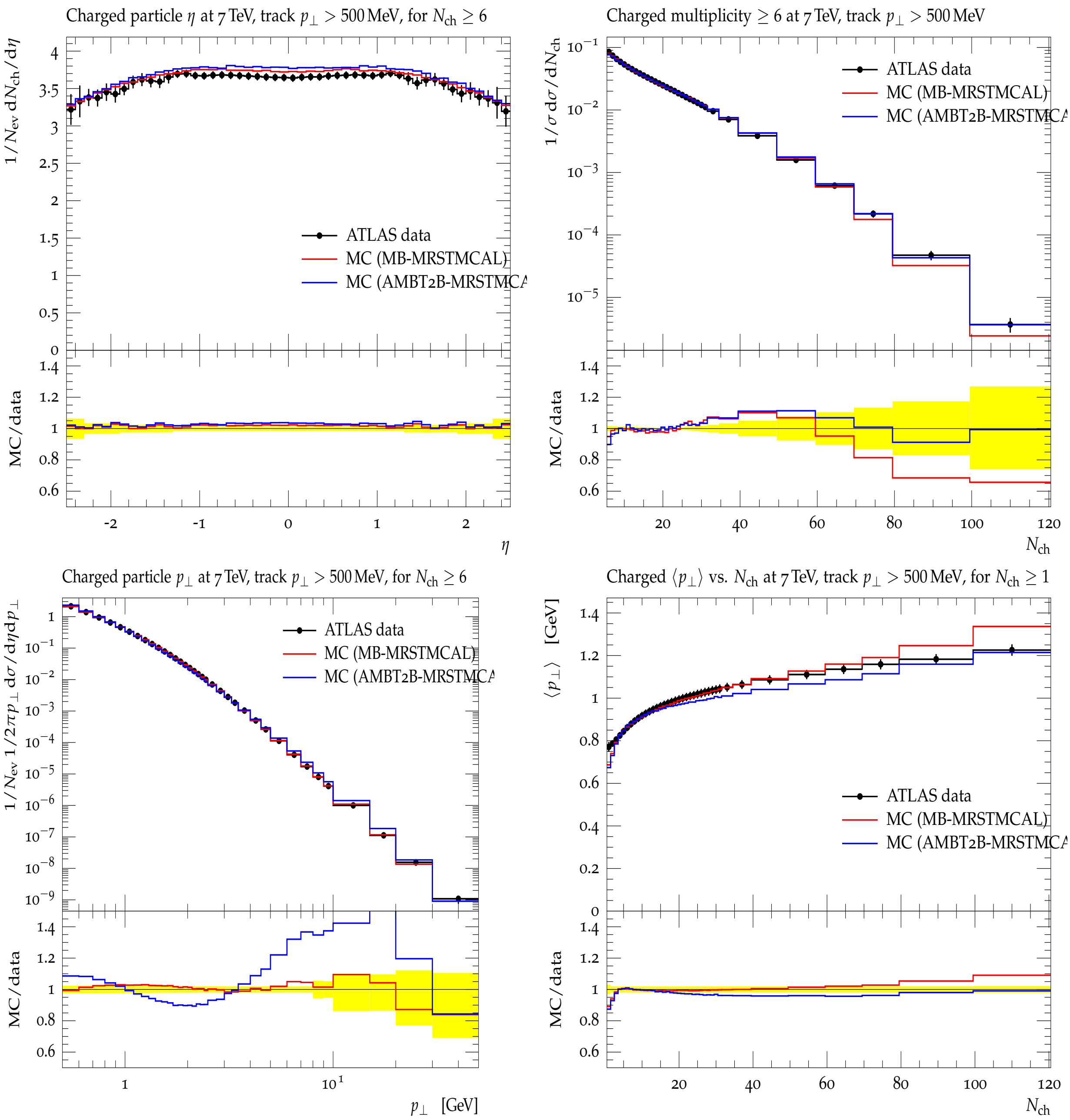

FIGURE 8.8: Comparison plots of PYTHIA6 tunes to the ATLAS eta Nch and pt distributions for events with $N_{ch} \geq 6$, $p_t > 500MeV$, $\mid \eta \mid < 2.5$ at $\sqrt{s} = 7TeV$ only average pt vs Nch distribution is for events with $N_{ch} \geq 1$.

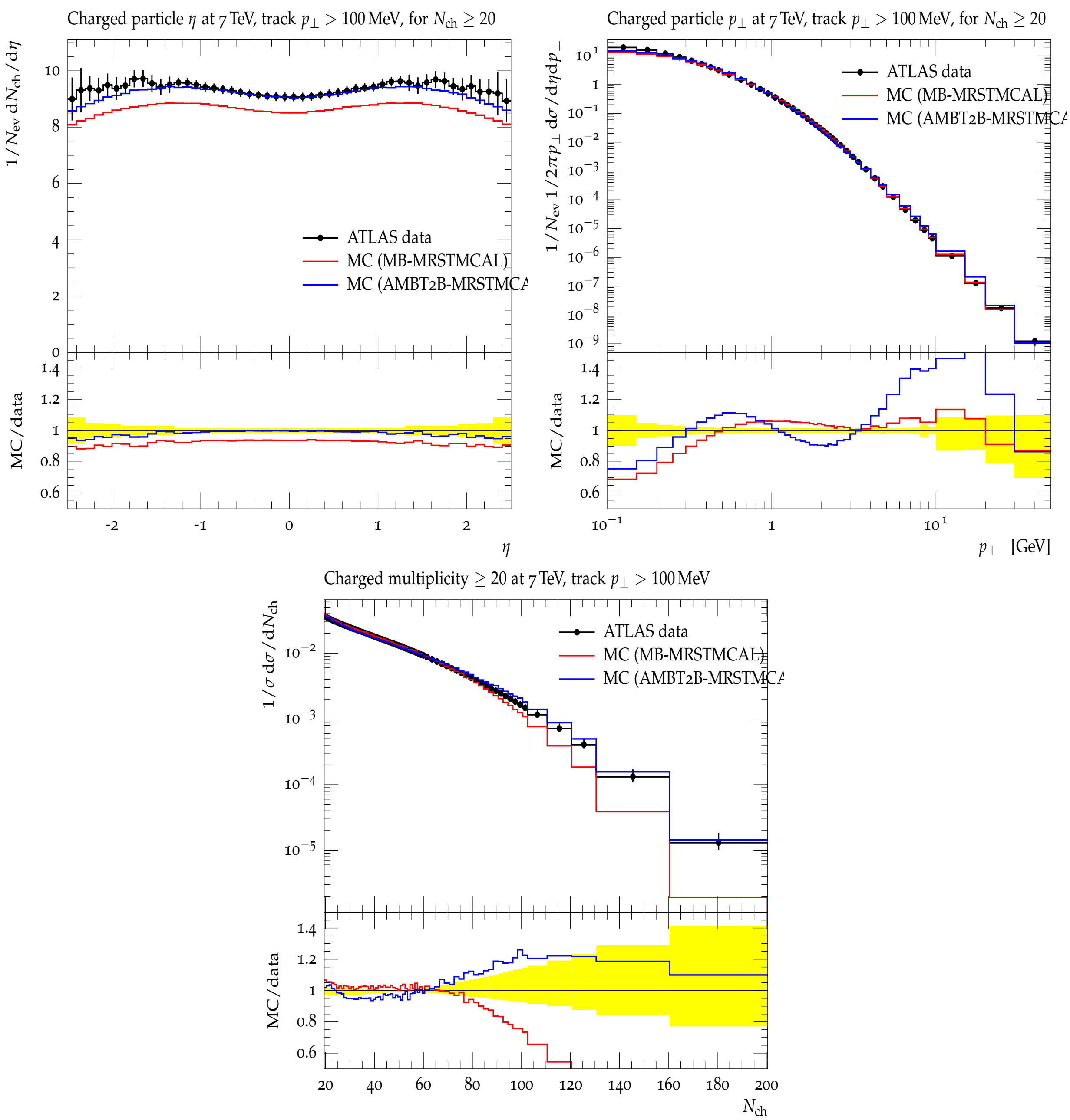

FIGURE 8.9: Comparison plots of PYTHIA6 tunes to the ATLAS η ,N_{ch} and p_t distributions for events with $N_{ch} \geq 20$, $p_t > 100MeV$, $\mid \eta \mid < 2.5$ at $\sqrt{s} = 7TeV$.

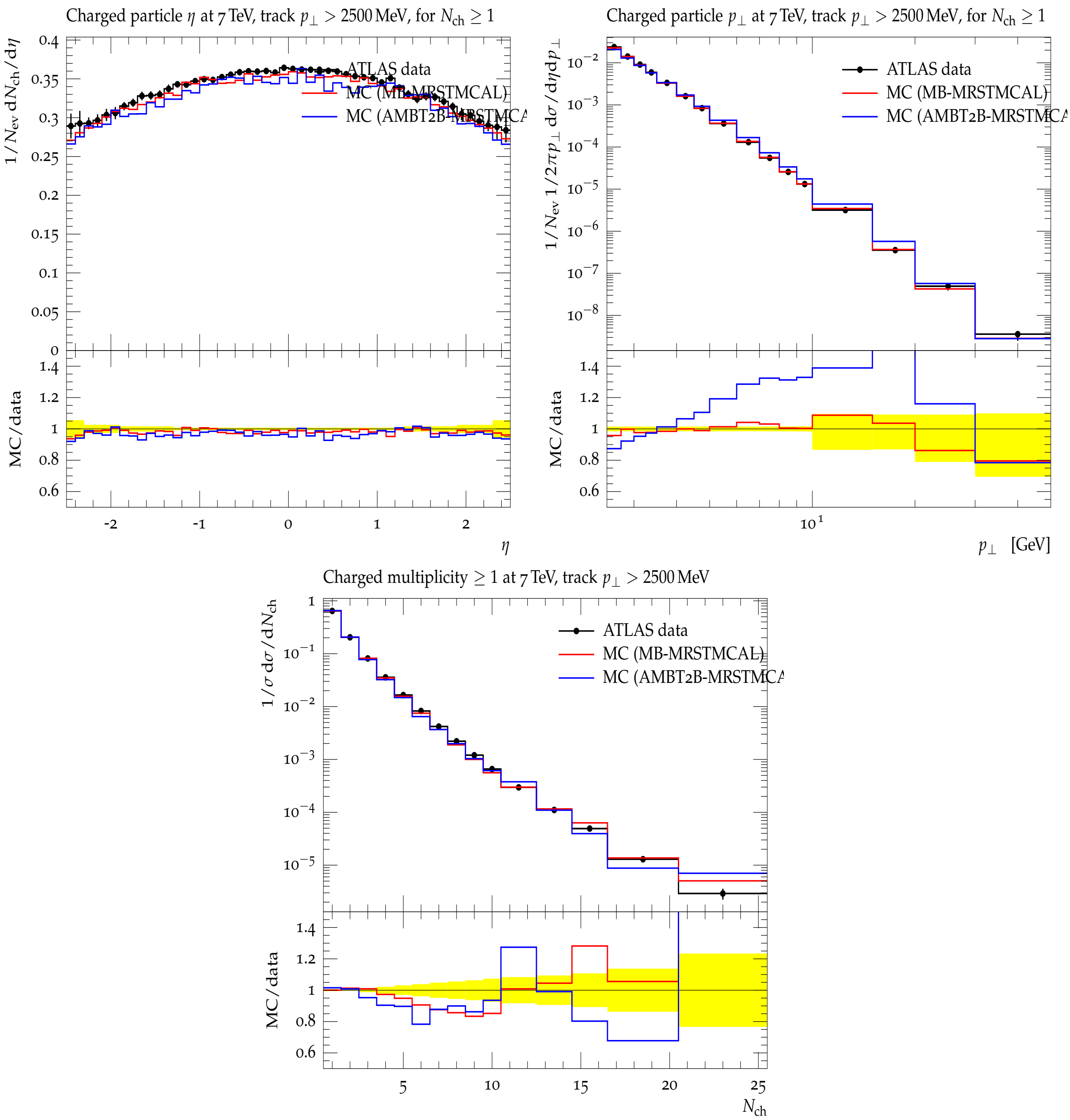

FIGURE 8.10: Comparison plots of PYTHIA6 tunes to the ATLAS eta ,charged-particle multiplicities (N_{ch}),and p_t distributions for events with $N_{ch} \geq 1$, $p_t > 2500MeV$, $\mid \eta \mid < 2.5$ at $\sqrt{s} = 7TeV$.

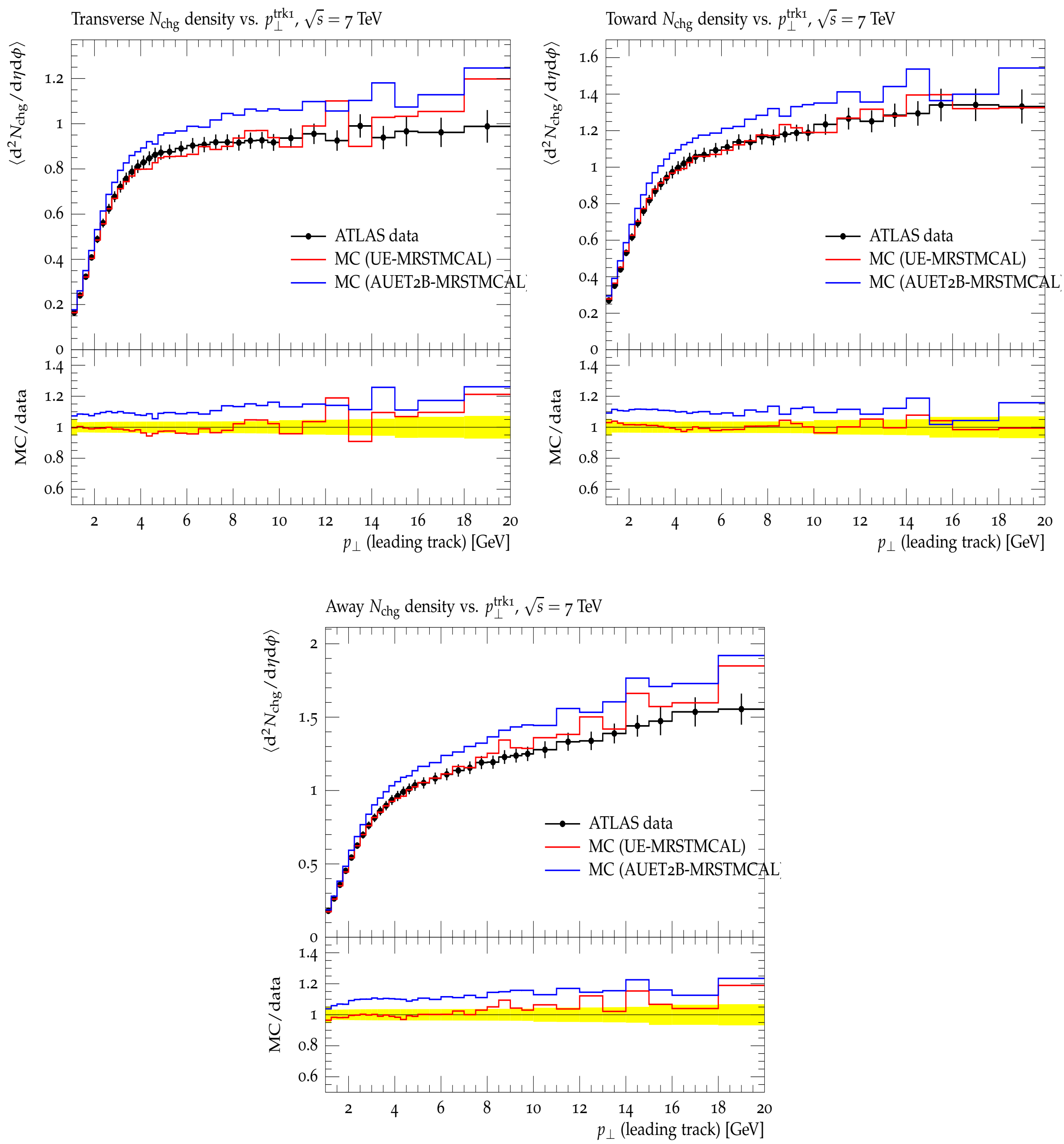

FIGURE 8.11: Comparison plots of PYTHIA6 tunes to the ATLAS UE distribution, charged particle densities vs pt lead for three regions at $\sqrt{s} = 7TeV$.

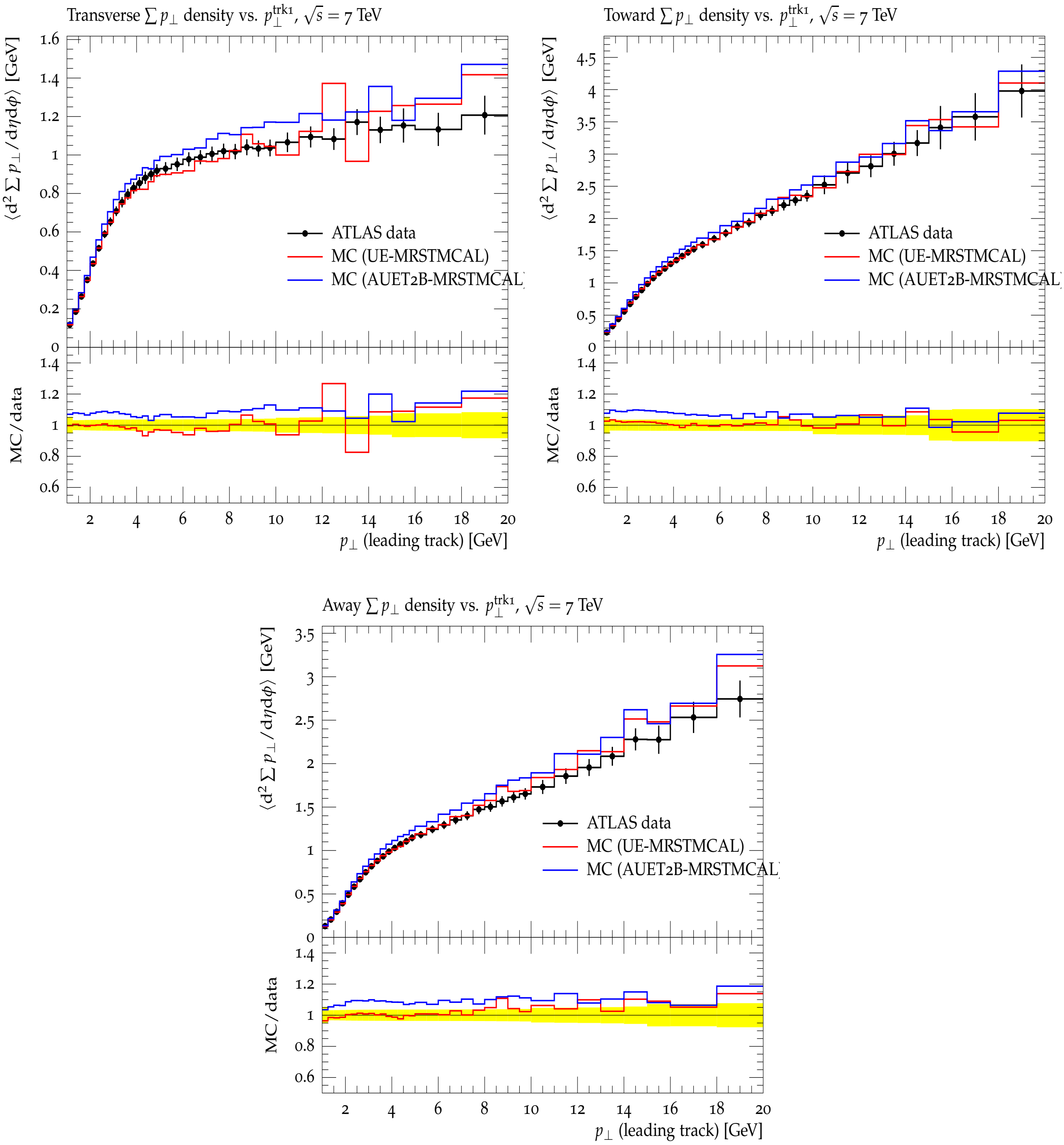

FIGURE 8.12: Comparison plots of PYTHIA6 tunes to the ATLAS UE distribution, sum pt vs pt lead for three regions at $\sqrt{s} = 7TeV$.

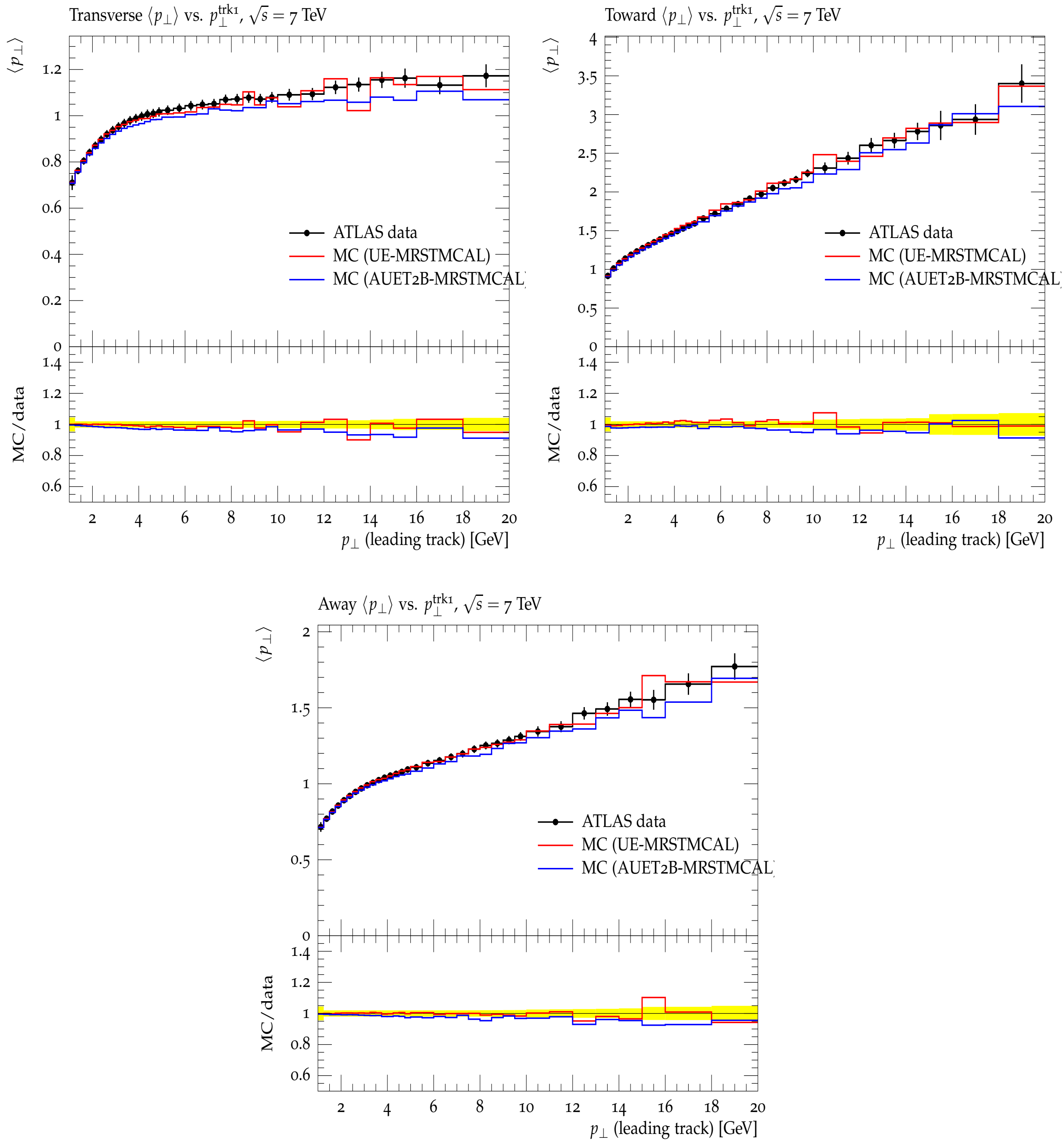

FIGURE 8.13: Comparison plots of PYTHIA6 tunes to the ATLAS UE distribution, average pt vs pt lead, of three regions at $\sqrt{s} = 7TeV$.

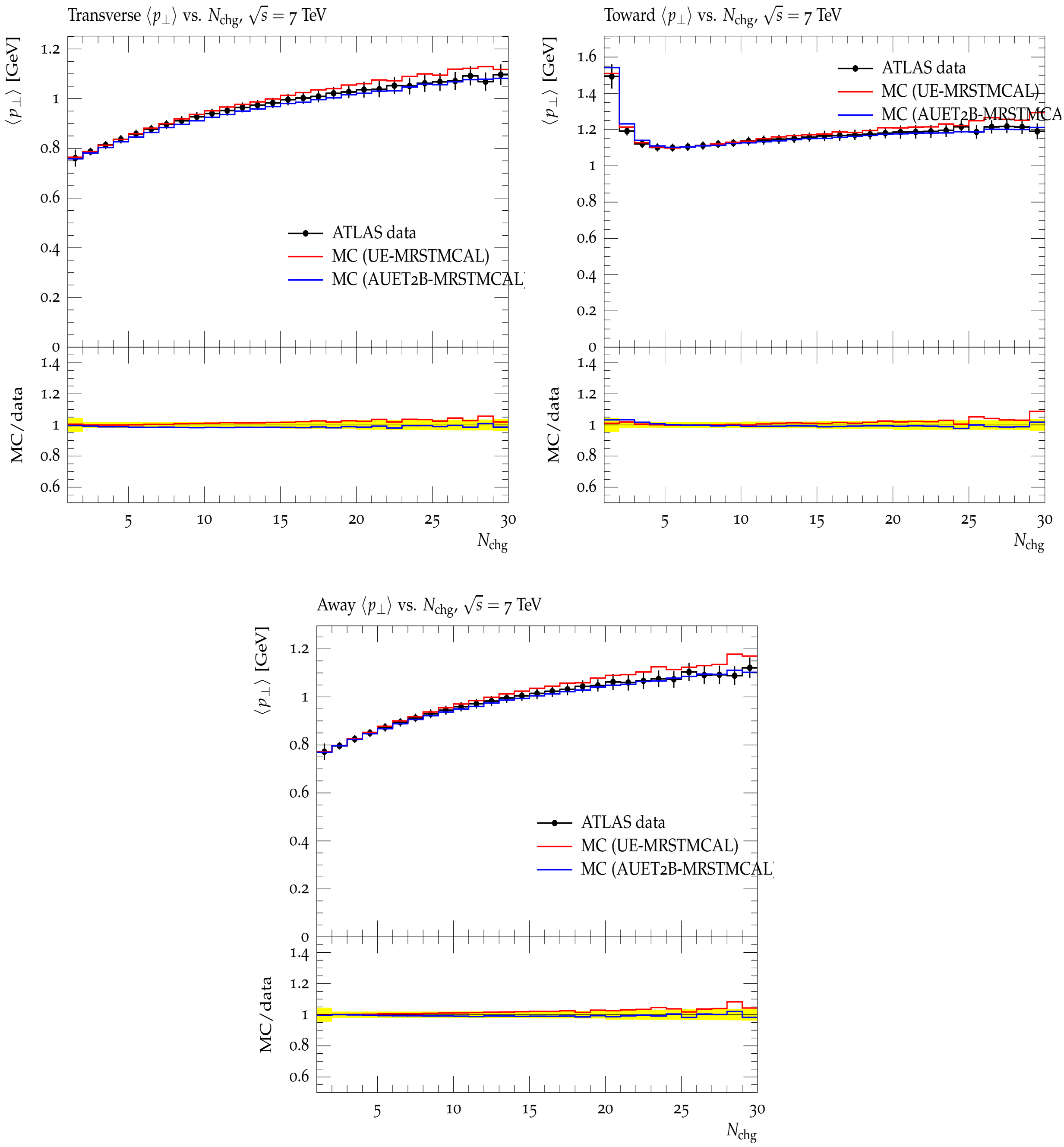

FIGURE 8.14: Comparison plots of PYTHIA6 tunes to the ATLAS UE distribution, average pt vs Nch, of three regions at $\sqrt{s} = 7TeV$.

Chapter 9

Conclusion

Current models of high-energy hadron collisions typically combine perturbative QCD to explain parton interactions (high-pt scatterings) and phenomenological approach to describe soft processes. These models have free parameters which need to be tuned to describe data well.

In this thesis thirteen MPI parameters of PYTHIA6 event generator are studied and finally six parameters are tuned to the minimum bias and underlying event published data by ATLAS Collaboration at 0.9 and 7TeV and from CDF II at 1.96TeV using nine PDFs of three different types: Leading order, MC-adapted and Next-to-leading order. These parameters includes three parameters of the MPI model, one of the CR model and two Λ_{QCD} parameters using nine different PDF sets. The overall fit quality is reasonably good for all PDF-sets.

We observed a significant connection between the PDF being used and the parameter values obtained. It is seen that tuning results are clustered by PDF type in p_{t0}. New and interesting results are obtained for the QCD parameter Λ_{ME} for MC-adapted PDF's, the fits with these PDF's give very low values, 60-80 MeV. This observation could point to an inherent characteristic of these MC-adapted PDF's.

The p_t distribution is seen to be very well described by all PDF sets inclusing MC-adapted PDF's which was not possible in the latest ATLA tunes. We investigate the option of separate tunes to MB and UE data and compare them to the ATLAS tunes named AMBT2B AUET2B and showed that our tunes describe data better than ATLAS tunes almost everywhere in all distributions. The reason for this difference in data description for same model using same PDF type can be associated to the Λ_{QCD} treatment.

Our conclusions are that reasonably good fits can be obtained using all three PDF types provided p_t >500 MeV, but the modeling of diffractive processes is not well defined. It should be noted that in the current tunes lowest multilicity bins are excluded due to their relatively stronger sensitivity to diffractive physics which was beyond the scope of this thesis. Another finding is that it is not possible to describe ATLAS distributions with the lowered track p_t cut of 100 MeV reasonably well. We included these data sets in alternative tunes to study model behavior in this kinematic range. These data sets require quite high activity as compared to the data sets with p_t cut of 500 MeV. So both data can not be described by the selected model simultaneously.

We hope these new tunes will be helpful to the LHC communities.

In the future it will be important to continue this effort with PYTHIA8 and including more data from the LHC. It is also impotant to consider other Monte-Carlo programs for tuning, e.g, Herwig++ and SHERPA. Herwig event generator plays an important role in ATLAS as a systematic cross check for PYTHIA in the unfolding procedure. A corresponding tuning of PYTHIA8 and HERWIG gen- erator including the JIMMY MPI model has already been done within the ATLAS MC group [35].

Appendix A

A*T2B Tunes

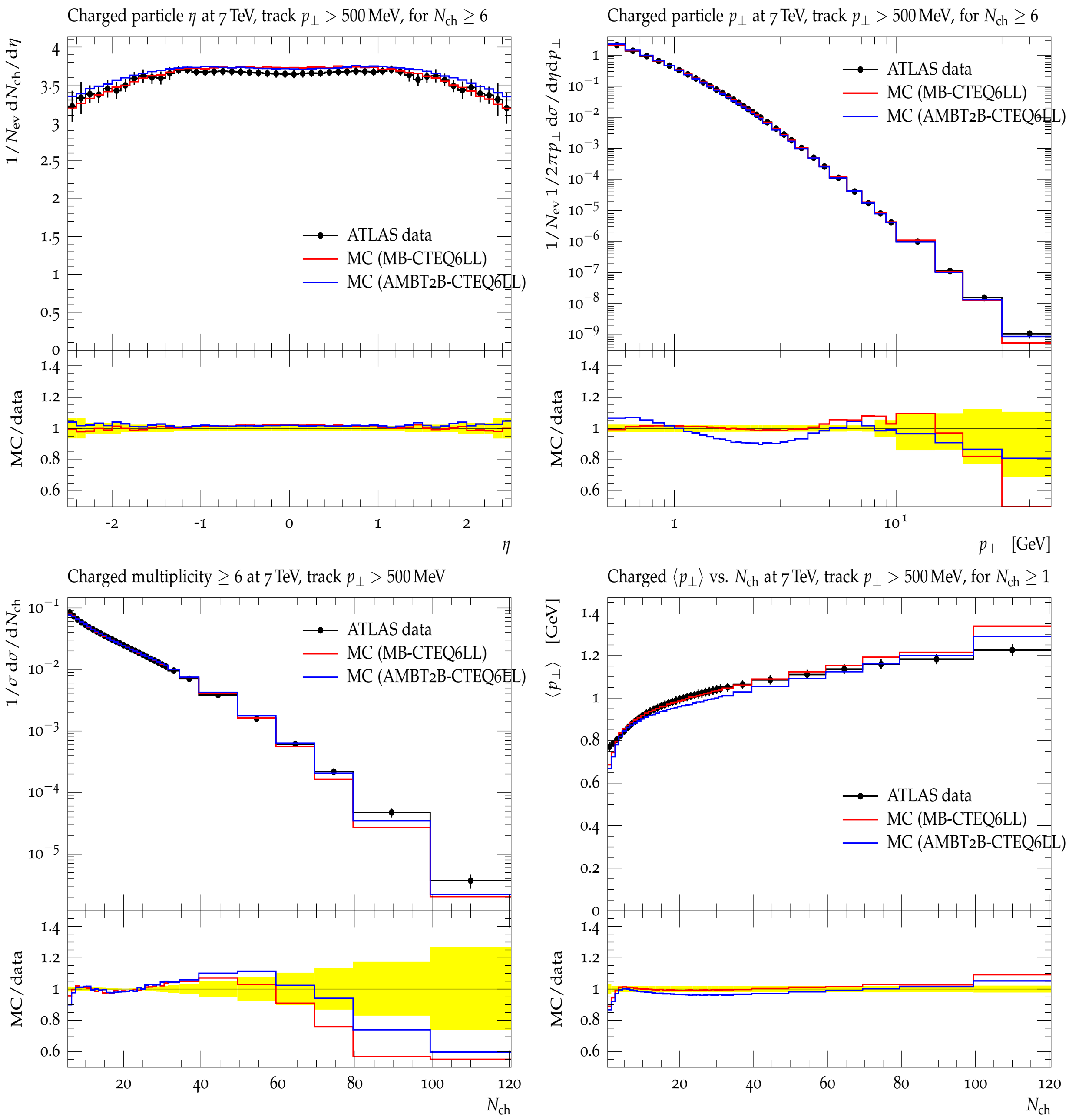

FIGURE A.1: Comparison plots of PYTHIA6 tunes to the ATLAS eta Nch and pt distributions for events with $N_{ch} \geq 6$, $p_t > 500MeV$, $\mid \eta \mid< 2.5$ at$\sqrt{s} = 7TeV$ only average pt vs Nch distribution is for events with $N_{ch} \geq 1$.

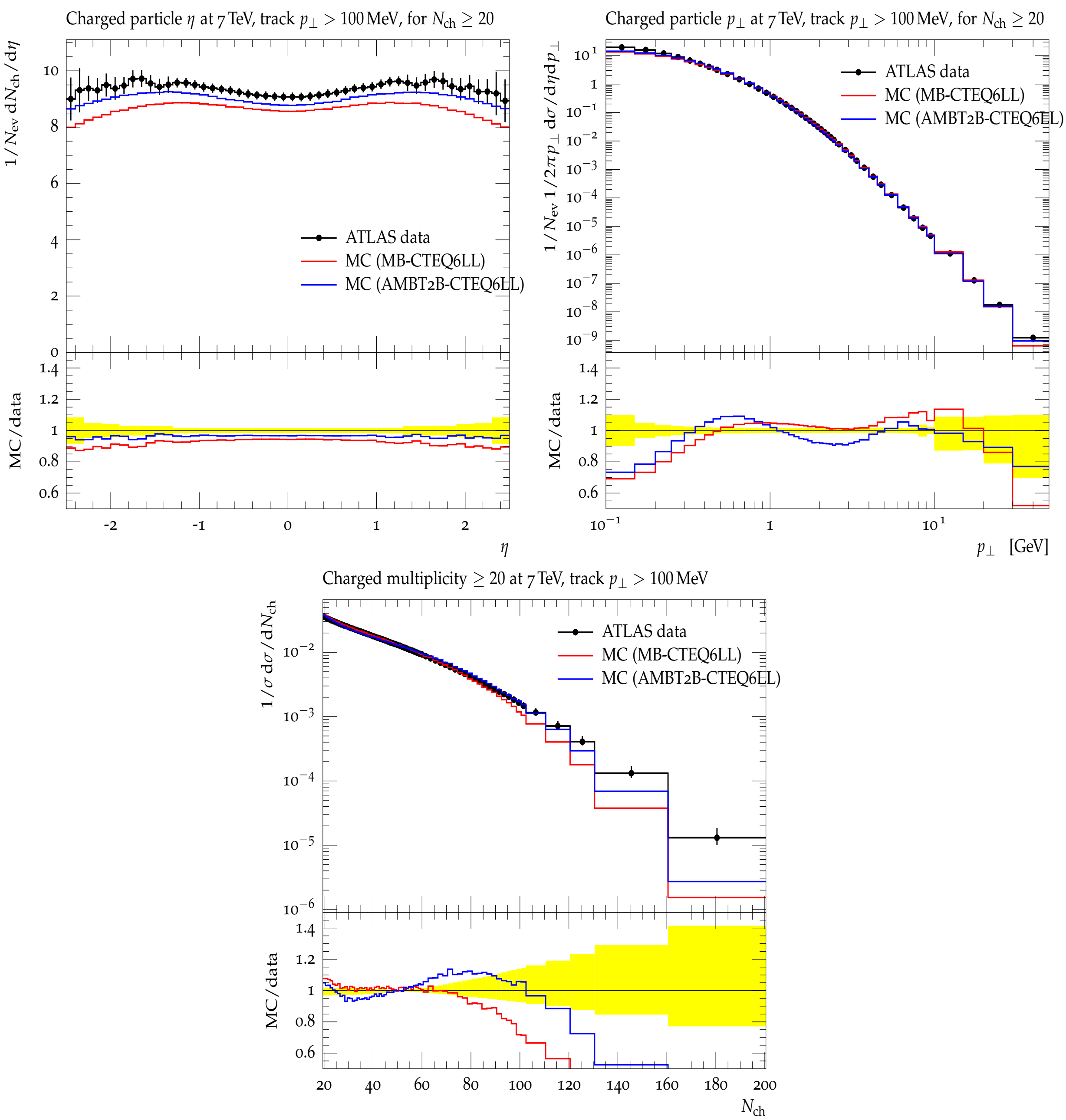

FIGURE A.2: Comparison plots of PYTHIA6 tunes to the ATLAS η ,N_{ch} and p_t distributions for events with $N_{ch} \geq 20$, $p_t > 100MeV$, $\mid \eta \mid < 2.5$ at $\sqrt{s} = 7TeV$.

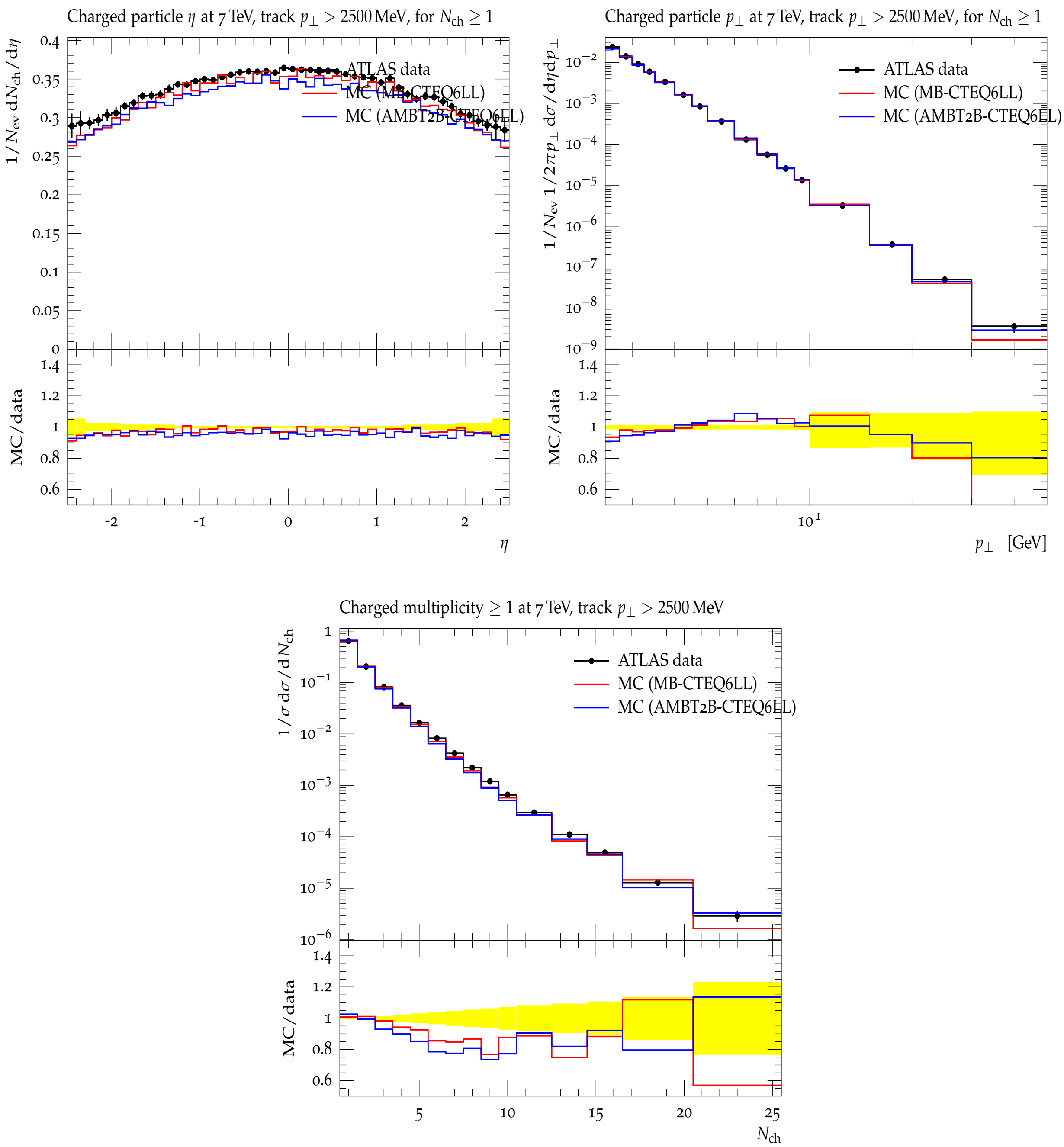

FIGURE A.3: Comparison plots of PYTHIA6 tunes to the ATLAS eta ,charged-particle multiplicities (Nch),and pt distributions for events with $N_{ch} \geq 1$, pt> $2500 MeV$, $\mid \eta \mid <$ 2.5 at$\sqrt{s} = 7TeV$.

vi

Bibliography

[1] G. Aad et al. The ATLAS Experiment at the CERN Large Hadron Collider. *JINST*, 3:S08003, 2008.

[2] G. Aad et al. Expected performance of the atlas experiment - detector, trigger and physics, arxiv:hep-ex/0901.0512, 2009.

[3] G. Aad et al. Charged-particle multiplicities in pp interactions measured with the ATLAS detector at the LHC. *New J.Phys.*, 13:053033, 2011.

[4] G. Aad et al. Measurement of underlying event characteristics using charged particles in pp collisions at $\sqrt{s} = 900 GeV$ and 7 TeV with the ATLAS detector. *Phys.Rev.*, D83:112001, 2011.

[5] G. Aad et al. Measurements of underlying-event properties using neutral and charged particles in *pp* collisions at 900 GeV and 7 TeV with the ATLAS detector at the LHC. *Eur.Phys.J.*, C71:1636, 2011.

[6] G. Aad et al. Study of Jet Shapes in Inclusive Jet Production in *pp* Collisions at $\sqrt{s} = 7$ TeV using the ATLAS Detector. *Phys.Rev.*, D83:052003, 2011.

[7] Georges Aad et al. Measurement of the Inelastic Proton-Proton Cross-Section at $\sqrt{s} = 7$ TeV with the ATLAS Detector. *Nature Commun.*, 2:463, 2011.

[8] T. Aaltonen et al. Measurement of Particle Production and Inclusive Differential Cross Sections in p anti-p Collisions at s**(1/2) = 1.96-TeV. *Phys.Rev.*, D79:112005, 2009.

[9] K. Aamodt et al. The ALICE experiment at the CERN LHC. *JINST*, 3:S08002, 2008.

[10] F.D. Aaron et al. Combined Measurement and QCD Analysis of the Inclusive e+- p Scattering Cross Sections at HERA. *JHEP*, 1001:109, 2010.

[11] E. Abat et al. The ATLAS Transition Radiation Tracker (TRT) proportional drift tube: Design and performance. *JINST*, 3:P02013, 2008.

[12] F. Abe et al. Transverse momentum distributions of charged particles produced in $\bar{p}p$ interactions at $\sqrt{s} = 630$ GeV and 1800 GeV. *Phys.Rev.Lett.*, 61:1819, 1988.

[13] P. Abreu et al. Tuning and test of fragmentation models based on identified particles and precision event shape data. *Z.Phys.*, C73:11–60, 1996.

[14] D. Acosta et al. Soft and hard interactions in $p\overline{p}$ collisions at $\sqrt{s} = 1800$ and 630 gev. *Phys. Rev. D*, 65:072005, Apr 2002.

[15] Anthony A. Affolder et al. Intermediate silicon layers detector for the CDF experiment. *Nucl.Instrum.Meth.*, A453:84–88, 2000.

[16] Guido Altarelli and G. Parisi. Asymptotic Freedom in Parton Language. *Nucl.Phys.*, B126:298, 1977.

[17] M. Althoff et al. Determination of alpha-s in first and second order qcd from e+ e- annihilation into hadrons. *Z.Phys.*, C26:157, 1984.

[18] A. Augusto Alves et al. The LHCb Detector at the LHC. *JINST*, 3:S08005, 2008.

[19] B. Andersson, G. Gustafson, G. Ingelman, and Torbjörn Sjöstrand. Parton fragmentation and string dynamics. *Physics Reports*, 97(2-3):31 – 145, 1983.

[20] G. Arnison et al. Transverse Momentum Spectra for Charged Particles at the CERN Proton anti-Proton Collider. *Phys.Lett.*, B118:167, 1982.

[21] ATL-COM-PHYS-2010-033 ATLAS Collaboration, ATL-PHYS-PUB-2010-002. Atlas monte carlo tunes for mc09, 2010.

[22] Emil Avsar. On the High Energy Behaviour of The Total Cross Section in the QCD Dipole Model. *JHEP*, 0804:033, 2008.

[23] R. Barate et al. Studies of quantum chromodynamics with the ALEPH detector. *Phys.Rept.*, 294:1–165, 1998.

[24] (ed.) Bartalini, Paolo and (ed.) Fano, Livio. Multiple partonic interactions at the LHC. Proceedings, 1st International Workshop, MPI'08, Perugia, Italy, October 27-31, 2008, 2010.

[25] Siegfried Bethke. Experimental tests of asymptotic freedom. *Prog.Part.Nucl.Phys.*, 58:351–386, 2007.

[26] A. Bettini. *Introduction to elementary particle physics /*. Cambridge Univ. Press,, Cambridge :, 2008.

[27] Andy Buckley, Jonathan Butterworth, Stefan Gieseke, David Grellscheid, Stefan Hoche, et al. General-purpose event generators for LHC physics. *Phys.Rept.*, 504:145–233, 2011.

[28] Andy Buckley, Jonathan Butterworth, Leif Lonnblad, Hendrik Hoeth, James Monk, et al. Rivet user manual. 2010.

[29] Andy Buckley, Hendrik Hoeth, Heiko Lacker, Holger Schulz, and Jan Eike von Seggern. Systematic event generator tuning for the LHC. *Eur.Phys.J.*, C65:331–357, 2010.

[30] D. Buskulic et al. Properties of hadronic Z decays and test of QCD generators. *Z.Phys.*, C55:209–234, 1992.

[31] John M. Campbell, J.W. Huston, and W.J. Stirling. Hard Interactions of Quarks and Gluons: A Primer for LHC Physics. *Rept.Prog.Phys.*, 70:89, 2007.

[32] S. Chatrchyan et al. The CMS experiment at the CERN LHC. *JINST*, 3:S08004, 2008.

[33] ATLAS Collaboration. Atlas detector and physics performance: Technical design report, 1999.

[34] ATLAS Collaboration. Atlas tunes of pythia 6 and pythia 8 for mc11. Technical Report ATL-PHYS-PUB-2011-009, CERN, Geneva, Jul 2011.

[35] ATLAS Collaboration. Further atlas tunes of pythia6 and pythia 8. Technical Report ATL-PHYS-PUB-2011-014, CERN, Geneva, Nov 2011.

[36] ATLAS Collaboration. New atlas event generator tunes to 2010 data. Technical Report ATL-PHYS-PUB-2011-008, CERN, Geneva, Apr 2011.

[37] T Cornelissen, M Elsing, S Fleischmann, W Liebig, E Moyse, and A Salzburger. Concepts, design and implementation of the atlas new tracking (newt). Technical Report ATL-SOFT-PUB-2007-007. ATL-COM-SOFT-2007-002, CERN, Geneva, Mar 2007.

[38] T Cornelissen, M Elsing, I Gavrilenko, W Liebig, E Moyse, and A Salzburger. The new atlas track reconstruction (newt). *Journal of Physics: Conference Series*, 119(3):032014, 2008.

[39] Yuri L. Dokshitzer. Calculation of the Structure Functions for Deep Inelastic Scattering and e^+e^- Annihilation by Perturbation Theory in Quantum Chromodynamics. *Sov. Phys. JETP*, 46:641–653, 1977.

[40] S.D. Drell and Tung-Mow Yan. Partons and their Applications at High-Energies. *Annals Phys.*, 66:578, 1971.

[41] A.Abulencia et al. (CDF Collaboration). *Journal of Physics G: Nuclear and Particle Physics*, 34(12):2457, 2007.

[42] Evans and Bryant. LHC Machine. *JINST*, 3:S08001, 2008.

[43] Rick D. Field. The Underlying event in hard scattering processes. *eConf*, C010630:P501, 2001.

[44] Agnes Grau, Rohini M. Godbole, Giulia Pancheri, and Yogendra N. Srivastava. Soft Gluon k(t)-Resummation and the Froissart bound. *Phys.Lett.*, B682:55–60, 2009.

[45] V. N. Gribov and L. N. Lipatov. Deep inelastic e p scattering in perturbation theory. *Sov. J. Nucl. Phys.*, 15:438–450, 1972.

[46] G.Rudolph. Private communication.

[47] Gosta Gustafson. Multiple scattering, underlying event and minimum bias, arxiv: hep-ph/0712.1941, 2007.

[48] Francis. Halzen and Alan D. Martin. Quarks and leptons. Wiley, 1985.

[49] Christopher S. Hill. Operational experience and performance of the CDFII silicon detector. *Nucl.Instrum.Meth.*, A530:1–6, 2004.

[50] F. James and M. Roos. Minuit: A System for Function Minimization and Analysis of the Parameter Errors and Correlations. *Comput.Phys.Commun.*, 10:343–367, 1975.

[51] Vardan Khachatryan et al. Transverse momentum and pseudorapidity distributions of charged hadrons in pp collisions at $\sqrt(s) = 0.9$ and 2.36 TeV. *JHEP*, 1002:041, 2010.

[52] Vardan Khachatryan et al. Transverse-momentum and pseudorapidity distributions of charged hadrons in *pp* collisions at $\sqrt{s} = 7$ TeV. *Phys.Rev.Lett.*, 105:022002, 2010.

[53] H.L. Lai et al. Global QCD analysis of parton structure of the nucleon: CTEQ5 parton distributions. *Eur.Phys.J.*, C12:375–392, 2000.

[54] Hung-Liang Lai, Marco Guzzi, Joey Huston, Zhao Li, Pavel M. Nadolsky, et al. New parton distributions for collider physics. *Phys.Rev.*, D82:074024, 2010.

[55] A.D. Martin, W.J. Stirling, R.S. Thorne, and G. Watt. Parton distributions for the LHC. *Eur.Phys.J.*, C63:189–285, 2009.

[56] B. Martin and G. P. Shaw. *Particle Physics/.* John Wiley and Sons,, Manchester:, 2008.

[57] A. Moraes, C. Buttar, and I. Dawson. Prediction for minimum bias and the underlying event at LHC energies. *The European Physical Journal C - Particles and Fields*, 50(2):435–466, apr 2007.

[58] Sparsh Navin. Diffraction in pythia, 2010 , arXiv:1005.3894, LUTP-09-23, MCNET-10-09.

[59] Skands Peter. Introduction to QCD, arXiv:1207.2389, CERN-PH-TH-2012-196, 2012.

[60] Gerhard A. Schuler and Torbjörn Sjöstrand. Hadronic diffractive cross-sections and the rise of the total cross-section. *Phys.Rev.*, D49:2257–2267, 1994.

[61] A. Sherstnev and R.S. Thorne. Different PDF approximations useful for LO Monte Carlo generators. *Eur.Phys.J.*, page 149, 2008.

[62] A. Sherstnev and R.S. Thorne. Parton Distributions for LO Generators. *Eur.Phys.J.*, C55:553–575, 2008.

[63] A. Sill. CDF Run II silicon tracking projects. *Nucl.Instrum.Meth.*, A447:1–8, 2000.

[64] Torbjörn Sjöstrand. New showers with transverse-momentum-ordering, arxiv:hep-ph/0401061,. 2004.

[65] Torbjörn Sjöstrand. Monte Carlo Tools, arXiv:0911.5286,LU-TP-09-31, MCNET-09-17, 2009 , 2009.

[66] Torbjörn Sjöstrand and Albert de Roeck. Monte carlo generators for the lhc, 2005. CERN, Geneva, 4 - 7 Apr 2005.

[67] Torbjörn Sjöstrand, Stephen Mrenna, and Peter Z. Skands. PYTHIA 6.4 Physics and Manual. *JHEP*, 05:026, 2006.

[68] Torbjörn Sjöstrand and Peter Z. Skands. Multiple interactions and the structure of beam remnants. *JHEP*, 0403:053, 2004.

[69] Torbjörn Sjöstrand and Peter Z. Skands. Transverse-momentum-ordered showers and interleaved multiple interactions. *Eur.Phys.J.*, C39:129–154, 2005.

[70] Torbjörn Sjöstrand and Maria van Zijl. A Multiple Interaction Model for the Event Structure in Hadron Collisions. *Phys.Rev.*, D36:2019, 1987.

[71] Peter Zeiler Skands. Tuning Monte Carlo Generators: The Perugia Tunes. *Phys.Rev.*, D82:074018, 2010.

[72] M. Deile et al. TOTEM Collaboration. Diffraction and total cross-section at the tevatron and the lhc, arxiv:hep-ex/0602021, Feb 2006.

[73] M.R. Whalley, D. Bourilkov, and R.C. Group. The Les Houches accord PDFs (LHAPDF) and LHAGLUE, 2005.